Title
Microfluidic Reactors for the Controlled Synthesis of Monodisperse Nanoparticles

Author
Erdem, Emine Yegan

Publication Date
2013

Peer reviewed|Thesis/dissertation

Microfluidic Reactors for the Controlled Synthesis of Nanoparticles

By

Emine Yegan Erdem

A dissertation submitted in partial satisfaction of the

requirements for the degree of

Doctor of Philosophy

in

Engineering - Mechanical Engineering

in the

Graduate Division

of the

University of California, Berkeley

Committee in charge:

Professor Albert P. Pisano, Co-Chair

Professor Fiona M. Doyle, Co-Chair

Professor Liwei Lin

Professor Tsu-Jae King Liu

Spring, 2013

Abstract

Microfluidic Reactors for the Controlled Synthesis of Nanoparticles

by

Emine Yegân Erdem

Doctor of Philosophy in Engineering - Mechanical Engineering

University of California, Berkeley

Professor Albert P. Pisano, Co-Chair

Professor Fiona M. Doyle, Co-Chair

Nanoparticles have attracted a lot of attention in the past few decades due to their unique, size-dependent properties. In order to use these nanoparticles in devices or sensors effectively, it is important to maintain uniform properties throughout the system; therefore nanoparticles need to have uniform sizes – or monodisperse. In order to achieve monodispersity, an extreme control over the reaction conditions is required during their synthesis. These reaction conditions such as temperature, concentration of reagents, residence times, etc. affect the structure of nanoparticles dramatically; therefore when the conditions vary locally in the reaction vessel, different sized nanoparticles form, causing polydispersity.

In widely-used batch wise synthesis techniques, large sized reaction vessels are used to mix and heat reagents. In these types of systems, it is very hard to avoid thermal gradients and to achieve rapid mixing times as well as to control residence times. Also it is not possible to make rapid changes in the reaction parameters during the synthesis. The other drawback of conventional methods is that it is not possible to separate the nucleation of nanoparticles from their growth; this leads to combined nucleation and growth and subsequently results in polydisperse size distributions.

Microfluidics is an alternative method by which the limitations of conventional techniques can be addressed. Due to the small size, it is possible to control temperature and concentration of reagents precisely as well as to make rapid changes in mixing ratios of reagents or temperature of the reaction zones. There have been several microfluidic reactors – (microreactors) in literature that were designed to improve the size distribution of nanoparticles.

In this work, two novel microfluidic systems were developed for achieving controlled synthesis of nanoparticles. The first microreactor was made out of a chemically robust polymer, polyurethane, and it was used for low temperature nanoparticle synthesis. This microreactor was fabricated by using a CO_2-laser printer, which is an inexpensive method

for fabricating microfluidic devices and it is a relatively fast way compared to other fabrication techniques. Iron oxide nanoparticle synthesis was demonstrated using this reactor and size distributions with a standard deviation of 10% was obtained.

The second microreactor presented in this work was designed to produce monodisperse nanoparticles by utilizing thermally isolated heated and cooled regions for separating nucleation and growth processes. This microreactor was made out of silicon and it was used to demonstrate the synthesis of TiO_2 nanoparticles. Size distributions with less than 10% standard deviation were achieved. This microreactor also provides a platform for studying the effects of temperature and residence times which is very important to understand the reaction kinetics of nanoparticle synthesis.

In this work, two microfluidic techniques for retrieving nanoparticles from the microreactors were also discussed. The first method was based on trapping the aqueous droplet phase inside the microchannel and the second method was utilizing a micropost array to direct droplets from the oil solution to the pure water.

As a final step, a printing technique was used to print nanoparticles synthesized inside the microreactors for future applications. This ability is important for achieving smart surfaces that can utilize the properties of nanoparticles for sensing applications in the future.

Dedicated to my parents, Sema and Vahit Erdem.

TABLE OF CONTENTS

LIST OF FIGURES

LIST OF TABLES

ACKNOWLEDGEMENTS

This work would not have been possible without the various contributions of many valuable people. First, I am very grateful for having Prof. Albert P. Pisano and Prof. Fiona M. Doyle as my advisors whose guidance was invaluable. Prof. Pisano was very supportive of my ideas and Prof. Doyle always encouraged me to learn new fields and pursue my ideas. I am very pleased for their support in the planning of my future academic career. I am also very thankful to my thesis committee members, Prof. Liwei Lin and Prof. Tsu-Jae King Liu for reading my thesis and sharing their valuable comments as well as Prof. Samuel Mao for serving in my qualification exam committee. Advice given by Prof. Ömer Savaş has been a great help in planning my future research path.

Discussions with Dr. Jim Cheng and his advice and contributions were very important for this research. I am very pleased for his assistance with the TEM imaging. I am also grateful for Prof. Debbie Senesky's help with reviewing my papers and research statements. Discussions with Dr. Gabriele Vigevani, Dr. Michael Demko, Dr. Tim Brackbill, Dr. Chris Hogue, Dr. Navdeep Dhillon, Dr. Trey Cauley, Dr. Yolanda Zhang and Dr. Sun Choi were also very valuable. I would also like to thank Dr. Jodi Iwata and Dr. Julie Karel for their help with the magnetometer measurements.

During this work, I got the chance to collaborate with Dr. Il Doh on a research project related to the droplet trapping and with Mr. Kosuke Iwai on the droplet lysis project. It was a great opportunity to work together with them.

I wish to acknowledge the practical guidance provided by the staff of Berkeley Marvell Nanofabrication Laboratory as well as by Dr. Paul Lum in the Biomolecular Nanotechnology Center (BNC).

I very much appreciate the support and encouragement given by the members of Berkeley Micromechanical Analysis and Design (BMAD) Lab. Their friendship was also very special. Especially I will miss our discussions over the coffee breaks with Debbie Senesky, Gabriele Vigevani, Wei-Cheng Lien, Sarah Wodin-Schwartz, Fabian Goericke and Matt Chan.

I am also thankful to the members of Prof. Doyle's Lab for their feedback during the group meetings and their collaboration and kindness in sharing the same laboratory environment.

I would like to offer my special thanks to Aydın Gündüz for being in my life; his support and encouragement was very valuable to me.

Finally, I greatly appreciate and value the support, encouragement and patience of my family during my PhD work and throughout my life. My siblings Gülşah Erdem Efe and Kerem Erdem and my brother-in-law Murat Efe and sister-in-law Neslihan Erdem always shared my stress and helped me calm down. My parents, Sema and Vahit Erdem have always encouraged me and became great role models for me. Without their support and prayers, this work would not have been possible; therefore it is dedicated to them.

Chapter 1

INTRODUCTION

Nanoparticles have attracted a great deal of attention in the past few decades due to their unique structural, mechanical, thermal, optical and chemical properties [1]. Their small size and large surface–to–volume ratio make them valuable candidates for several applications in electronics, sensor technologies as well as biological detection/separation applications. For example semiconductor nanoparticles transmit light at different wavelengths depending on their size and there is a dramatic change in the color they transmit as their size changes. Therefore when these nanoparticles are needed to be used in a specific application, their size and shape should be uniform, or monodisperse.

In order to synthesize monodisperse nanoparticles, the reaction conditions during the synthesis must be very well controlled. However it is difficult to maintain uniform conditions without any thermal gradients simultaneously with rapid mixing times in batch wise synthesis methods due to their large scale. In comparison, microfluidic reactors - or microreactors – show promise for commercial-scale synthesis of nanoparticles. Handling small volumes of liquid gives the ability to control the amount of reagents precisely and to mix them uniformly. In the case of reactions that require heating, reagents can be heated and cooled rapidly and uniformly, avoiding the large thermal gradients that are problematic in conventional batch techniques.

This chapter specifically discusses the importance of monodispersity in nanoparticle synthesis and the motivation for using microfluidics to achieve this goal. First the size dependence of nanoparticle properties will be described, and then synthesis metrics to achieve monodispersity will be discussed. As a next step the limitations of batch methods for synthesis of nanoparticles will be described. Finally, a brief review of existing microreactors will be given followed by the outline of the research described in this thesis.

1.1. Size and Shape Dependence of Nanoparticle Properties

Some physical properties of nanoparticles are different than their bulk form due to their small size. As their size decreases, their surface–to–volume ratio increases and therefore surface effects dominate the material properties. We can classify these properties as electrical, magnetic, optical, mechanical, structural and thermal properties [1]. All of these properties are highly dependent on the size and shape of nanoparticles. In this section some of the size dependent properties of nanoparticles will be discussed.

1.1.1. Electrical Properties

Unique electrical properties of nanoparticles attract a lot of attention in electronics for the purpose of making faster, smaller and thinner electronic products. As the material size decreases, the density of energy states also decreases [2]. At the nanoscale these states change from being continuous to discrete, which is named as quantum confinement effect. This effect changes the electrical properties of nanoparticles such as their dielectric constant.

1.1.2. Magnetic Properties

Magnetic nanoparticles have a large variety of applications in drug delivery, biotagging, bioseparation and imaging [3]. Due to their small size, nanoparticles behave as single domain materials and therefore when there is an applied external magnetic field, they behave like a paramagnet. This effect is named as 'superparamagnetism' and the difference from paramagnetism is that there is that there is saturation magnetization. That is to say, there is a magnetic field at which all domains (nanoparticles) align themselves with the applied field. This superparamagnetic property is mainly useful in magnetic resonance imaging.

As an example of the effect of size on magnetic property, the dependence of saturation magnetization on the size of particles can be given. As the size of nanoparticles increases, the saturation magnetization decreases as well and this is due to the 'surface canting' effect [4]. Karaağaç *et al.* showed that iron oxide nanoparticles with different diameters showed different magnetization curves and had different saturation magnetization [5].

1.1.3. Optical Properties

Optical properties of nanoparticles are also dependent on their size and shape. A very good example of this phenomenon is the case of semiconductor nanoparticles. Due to the quantum confinement effect, the energy band gap of nanoparticles becomes wider and this leads to tunable optical properties based on their size [6]. This results in transmission of light with different colors at different nanoparticle sizes; within less than 1nm of change in diameter colors change dramatically; as the size of nanoparticles increase from 2.3 nm to 5.5nm, color changes from blue to red as demonstrated by Dabbousi *et al.* [7] This property of semiconductor nanoparticles make them very popular candidates as building blocks of chemical and biological sensors [8], especially in labeling, imaging and detection of biological entities [9].

1.1.4. Mechanical Properties

Nanoparticles also have unique mechanical properties due to their small size. Their smaller crystalline size leads them to have higher mechanical strength [1]. Their deformation mechanism shows difference compared to their bulk form, for instance ceramic materials become more ductile when their sizes are in the nanometer range [10]. Specifically these properties are useful for making new type of ceramic materials with decreased brittleness [11].

1.1.5. Thermal Properties

The increased surface energy of nanoparticles due to their large surface-to-volume ratio affects their chemical potential such that their melting point is decreased compared to that of the bulk material. For example Castro *et al.* studied this effect with gold and silver nanoparticles and demonstrated that their melting temperature decreases with the size of nanoparticles [12].

1.2. Synthesis Conditions for Monodispersity

The synthesis metrics required for monodisperse nanoparticle production were described by LaMer and Dinegar [13]. According to LaMer *et al.*, in order to obtain monodisperse size and shape, the nucleation and growth of nanoparticles should be separated from each other. That is to say, nucleation and growth should not occur concurrently. Otherwise particles that were nucleated at an earlier stage will grow to a larger size compared to the ones nucleated at a later time.

Nanoparticle formation is a process where first nuclei are formed when the free-precursor concentration in the reaction solution reaches a critical concentration for nucleation. This is followed with the growth of these nuclei above the solubility limit [1]. In closed systems, where there is no continuous supply of reagents, free-precursors are formed as a result of a chemical reaction [14]. (In this context free precursors refer to the dissolved feed-stock for nanoparticles [15]). These reactions can be decomposition (for e.g. in the formation of quantum dots) or hydrolysis reactions (as in the case for metal oxide nanoparticles). In order to separate nucleation and growth, the concentration of free-precursors in the system needs to be controlled such that during the growth stage they are above the solubility limit but below the critical concentration for nucleation. This can be achieved by controlling the precursor formation. The change of concentration in a monodisperse nanoparticle formation is shown by a LaMer diagram in Figure 1.1. This diagram shows the three stages of nanoparticle formation. In stage I, free precursors are formed. When the concentration reaches the nucleation threshold (or critical concentration for nucleation), self-nucleation starts to occur (stage II). This stage lasts until the concentration drops below the threshold as a result of being consumed during the process of nucleation. In the final stage the existing nuclei grows by consuming the precursors in the solution. Eventually the concentration becomes close to the saturation of the solution and growth ends. In order to obtain monodisperse particles, the precursor formation needs to be controlled. Specifically, during the growth stage, the concentration should not reach the nucleation threshold. This would create new nuclei that had less time to grow compared to the nuclei formed at an earlier time.

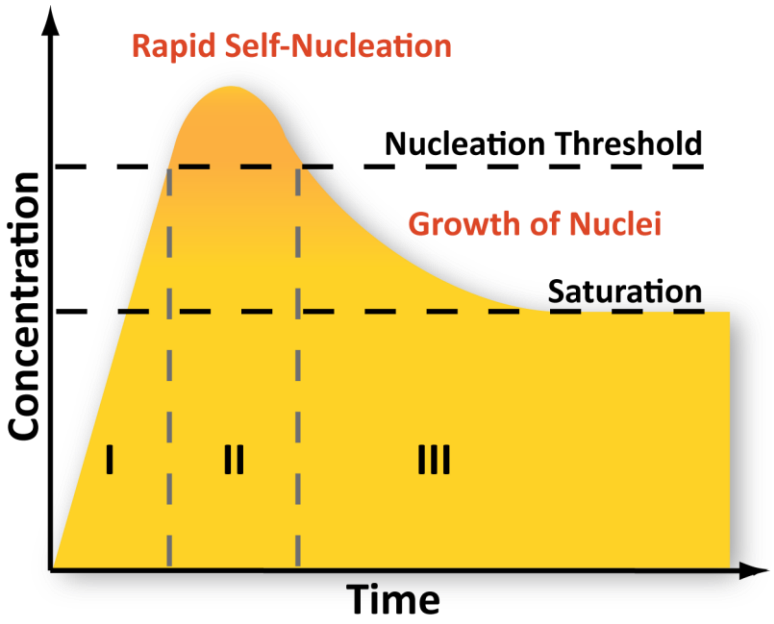

Figure 1.1: LaMer diagram showing the concentration profile necessary for the formation of monodisperse nanoparticles. After LaMer and Dinegar [13].

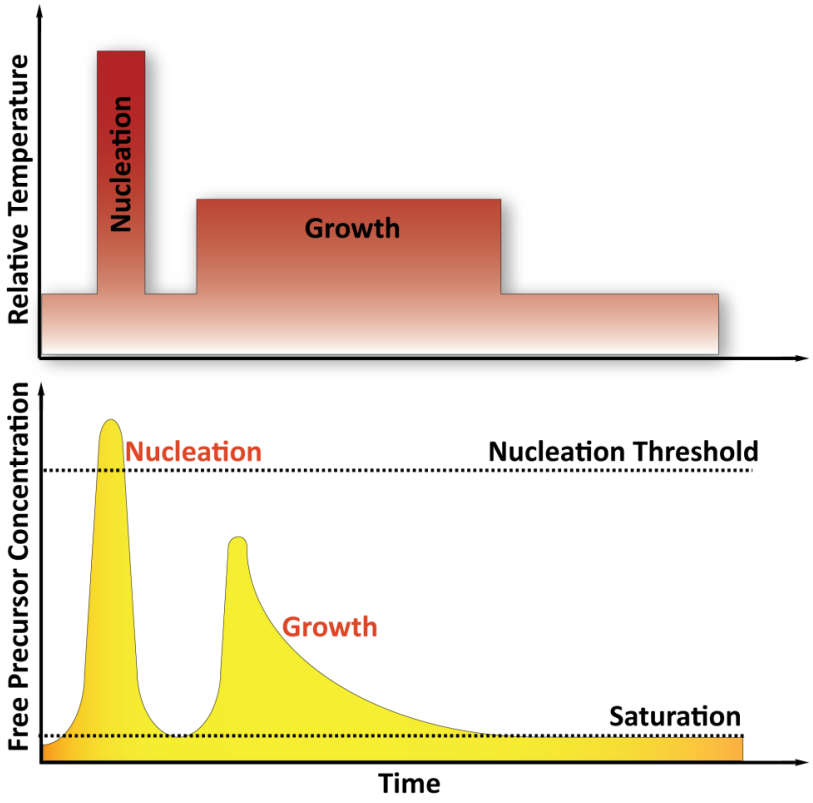

Figure 1.2: Diagram showing the ideal control method of free-precursor concentration in thermal decomposition reactions or reactions that require heat in order to synthesize monodisperse nanoparticles. After Winterton, J. [15].

The monomer formation can be monitored by controlling the reaction conditions such as pH, temperature or supply of material [14]. For example where the reaction requires heat such as in the case for thermal decomposition reactions, rapid changes in the temperature can be used to control the rate of monomer formation [14]. The concentration of monomers can be increased rapidly by increasing the temperature. At elevated temperatures, the concentration reaches the nucleation threshold and nucleation begins. After a short time, the temperature can be reduced rapidly to quench the formation of monomers and later increased to a relatively low temperature which produces monomers to be used for growth; however not enough for nucleation. The schematic that summarizes this is shown in Figure 1.2.

In the case of nanoparticle synthesis that requires hydrolysis of metal ions, monodispersity can be achieved by controlling the pH of the reaction precisely [14]. When the pH of the system is reduced rapidly, the reaction will be quenched and this can be used to control the time of nucleation stage.

1.3. Limitations of Conventional Methods

There are several different reaction types for the synthesis of nanoparticles depending on the chemistry. Some of these reactions require rapid pH changes, mixing of reagents or high temperatures. In all of these methods it is important to control the reaction conditions uniformly throughout the system such that monodisperse nanoparticles can be achieved. In conventional methods, batch type reactors are used, where large volumes of reagents are consumed. However in large scale systems, it is inevitable to get thermal gradients as well as concentration gradients. Also it is very difficult, or almost impossible, to make rapid changes required for following the LaMer diagram. There are alternative techniques, such as use of ligands, in these systems to control the size of nanoparticles. However it is not sufficient to obtain perfect size distributions as separation of nucleation and growth is not possible.

Therefore there is a need for extremely well controlled reaction systems where these limitations can be addressed. Microfluidic reactors are much smaller than most batch reactors and precise control of reaction conditions such as temperature and residence time can be achieved. It is possible to make rapid changes in reaction, thermal gradients can be avoided and reactions can be quenched by cooling the reactor rapidly. It is also possible to mix reagents quickly and uniformly in droplet-based microfluidic reactors, as discussed in the next section and in Chapter 2. In summary, microfluidic reactors provide a platform to control reaction parameters uniformly and precisely. In addition to, they also give the ability to study reaction dynamics.

1.4. Review of Microreactors for Nanoparticle Synthesis

Microfluidic reactors – or microreactors - show promise for commercial-scale synthesis of nanoparticles with well controlled size, size distribution and shape. Compared to batch-wise synthesis techniques, microfluidic technology can provide better control of the reaction conditions, which is the key to controlling the product characteristics [16-22].

Handling small volumes of liquid gives the ability to control the amount of reagents precisely and to mix them uniformly. In the case of reactions that require heating, reagents can be heated and cooled rapidly and uniformly, avoiding the large thermal gradients that are problematic in batch techniques. Nanoparticles generated by batch methods are rarely acceptable for immediate use; instead additional processing steps are needed to separate particles by size and other characteristics via centrifuging, filtration or electrophoretic methods [16]. In contrast, no additional size and shape post processing is required for high quality nanoparticles from well-controlled microreactors. The small yield of product from microreactors can be addressed by parallel processing.

Several types of microreactors have been described in the literature; good reviews on this research include [16, 18-21]. Microreactors can be classified based on their flow type. There are two types of flow in microreactors; continuous flow [23-32] and droplet-based or segmented flow [33-42].

Microreactors can also be classified based on their material they are made out of. The most common materials used to fabricate microreactors are silicon [23, 32, 42-44] and polymers [24, 26, 34-37, 39-41, 45, 46]. Glass-substrate microreactors [25, 33] and reactors made out of capillary tubes [30, 31, 38, 47, 48] have also been reported. In the next two subsections we will review microreactors in literature based on their flow and material.

1.4.1. Continuous Flow Microreactors

Continuous flow reactors use a single fluid phase inside the microchannel; reaction and precipitation occur in this phase. Unfortunately, due to the Poiseuille flow profile, the residence time of fluid elements, and hence the nanoparticles that precipitate from these fluid elements, varies according to the position within the channel, which leads to polydisperse size distribution. Flow profile in continuous flow microreactors is shown in Figure 1.3.

It is also difficult to mix reagents in continuous reactors; the small dimensions ensure a low Reynolds number, and hence laminar flow in which mixing is constrained by the diffusion length. Figure 1.4 below shows the computational model of diffusion of two aqueous solutions in a continuous flow channel. As it can be seen from the simulation, these two solutions mix at a very slow rate which is very disadvantageous for nanoparticle synthesis purposes.

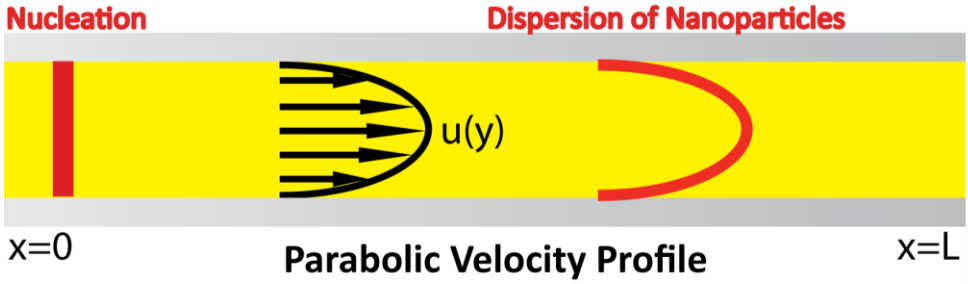

Figure 1.3: Flow profile in continuous flow microreactors. The parabolic flow profile causes changes in residence times of reagents and therefore leads to polydisperse particle formation.

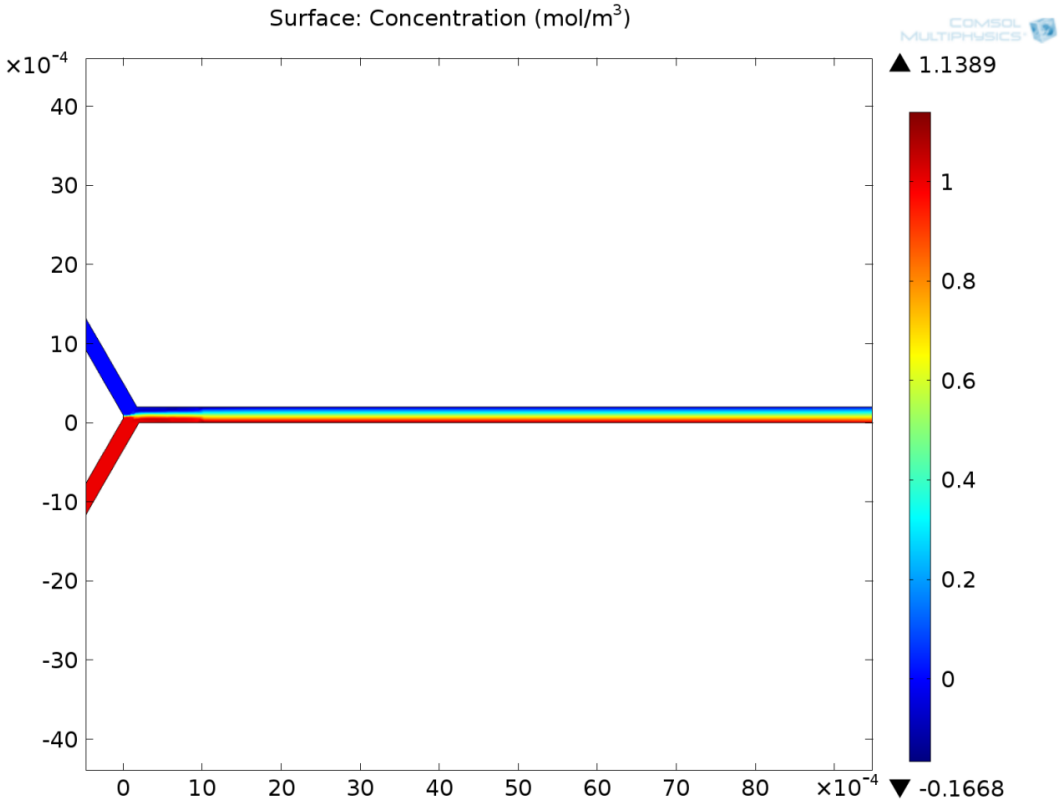

Figure 1.4: Computational model of two fluids mixing diffusively inside a microfluidic channel. As can be seen from the results, the mixing is very slow as it is diffusion limited. Both solutions (blue and red) were defined as water. Simulation was carried out by using COMSOL Multiphysics program.

The other disadvantage of continuous flow profile is that particles precipitating from the stagnant layer immediately adjacent to the channel walls may adhere to the walls, leading to disruption of flow and ultimately blockage.

One of the earliest microreactors in literature was presented by Chan *et al.* in 2003 and this microreactor was a continuous flow microreactor [25]. They used glass as their substrate material and they demonstrated the synthesis of CdSe nanoparticles at high temperatures.

1.4.2. Droplet-Based Flow Microreactors

In contrast to continuous flow microractors, reactions in droplet-based reactors occur within discrete droplets that pass through the microreactor surrounded by an immiscible carrier phase. A circulating flow profile develops within the droplets, assuring uniform reaction parameters inside the droplet and rapid mixing should this be needed [40]. Figure 1.5 shows the flow profile in this type of microreactor. Droplet-based flow provides several advantages, such as preventing nanoparticles from contacting the channel walls, providing a completely uniform residence time for all elements of the reacting fluid, and hence uniform reaction time for nanoparticles to nucleate and grow.

Figure 1.5: Flow profile in droplet-based microreactors.

Most of the microreactors in literature are based on droplet-based flows due to its advantages. One of the first examples of this type of reactor was presented by Chan *et al.* in 2005, as a follow-up work of their continuous flow reactor mentioned in the above section [33].

1.4.3. Glass Substrate Microreactors

Glass substrate microreactors are an alternative to silicon substrate microreactors for high temperature reactions. However glass has a two order of magnitude less thermal conductivity than silicon, therefore for heated reactions silicon is a more preferred material in order to get reduced time constants of heating.

1.4.4. Capillary Based Microreactors

Capillary tubes are also used in the synthesis of nanoparticles. Glass and PTFE (Teflon) tubing are most common materials in capillary based microreactors [38]. These microreactors can perform reactions that require high temperature by immersing a portion of the capillary tubing in a heated oil bath. However these microreactors have very little flexibility in their design compared to microfabricated reactors.

1.4.5. Polymer Substrate Microreactors

Polymer-substrate microreactors can be fabricated using simpler methods, such as soft lithography or hot embossing compared to other microreactors. To date, they have mostly been fabricated in polydimethlysiloxane (PDMS) or poly(methyl methacrylate) (PMMA). These reactors are attractive due to their ease of fabrication and low cost. Although

polymer-substrate microreactors are generally not suitable for high temperature reactions, they are simpler to make, cheaper than silicon and glass substrate microreactors, and they are more flexible in terms of design than capillary microreactors. A more detailed review on polymer substrate microreactors will be given in Chapter 2.

1.4.6. Silicon Substrate Microreactors

Silicon-substrate microreactors are fabricated by conventional microfabrication techniques that include deep reactive ion etching and anodic bonding to a glass surface for the encapsulation of microchannels. These reactors are particularly attractive for reactions requiring heat. They are resistant to many chemicals and the good thermal conductivity of silicon allows for good temperature control. However, silicon requires expensive and time-consuming fabrication techniques.

A more detailed review on silicon substrate microreactors and microreactors that require heating will be given in Chapter 3.

1.5. Thesis Overview

For the purpose of synthesizing nanoparticles with high control over reaction conditions two different microreactors were designed. In Chapter 2, the first microreactor that is made out of a polymer material will be discussed. This microreactor was designed for relatively low temperature reactions that do not require any heating but require mixing of two reagents. A very robust polymer material, polyurethane, is used for fabricating the reactor and the channels of the reactor are made by using a CO_2-laser printer.

In Chapter 3 the second microreactor that is designed for relatively high temperature reactions that require heating is discussed. This microreactor has thermally isolated, heated regions for the purpose of separating nucleation and growth of nanoparticles in order to achieve monodispersity and in order to provide a platform to study the parameters such as temperature and residence time that affect the nanoparticle formation.

In Chapter 4 two different techniques to separate droplets that carry nanoparticles from the carrier fluid is discussed. The first method is based on trapping and collecting droplets and the second one is based on a pillar array mechanism that separates immiscible fluids.

In Chapter 5 a printing technique of nanoparticles on a substrate for making devices with nanoparticles for future applications is discussed.

Chapter 6 is the conclusion of this thesis work and contains the future directions that can be taken.

1.6. References of Chapter 1

[1] Hosokawa, M.; Nogi, K.; Naito, M.; Yokoyama, T., Nanoparticle Technology Handbook, Amsterdam: Elsevier, 2007.

[2] White, R. J.; Luque, R.; Budarin, V. L.; Clark, J. H., "Supported metal nanoparticles on porous materials, methods and applications," *Chem. Soc. Rev.,* vol. 38, pp. 481-494, 2009.

[3] Mahmoudi, M.; Stroeve, P.; Milani, A. S.; Arbab, A. S., Superparamagnetic iron oxide nanoparticles, New York: Nova Science Publishers, 2011.

[4] Morales, M. P.; Veintemillas-Verdaguer, S.; Montero, M. I.; Serna, C. J., "Surface and internal spin chanting in gamma-Fe2O3 Nanoparticles," *Chem. Mater.,* vol. 11, pp. 3058-3064, 1999.

[5] Karaagac, O.; Kockar, H.; Beyaz, S.; Tanrisever, T., "A simple way to synthesize superparamagnetic iron oxide nanoparticles," *IEEE Trans. on Magnetics,* vol. 46, pp. 3978-3983, 2010.

[6] Murray, C. B.; Norris, D. J.; Bawendi, M. G., "Synthesis and characterization of nearly monodisperse CdE (E=S, Se, Te) semiconductor nanoparticles," *J. Am. Chem. Soc.,* vol. 115, pp. 8706-8715, 1993.

[7] Dabbousi, B. O.; Rodriguez-Viejo, J.; Mikulec, F. V.; Heine, J. R.; Mattoussi, H.; Ober, R.; Hensen, K. F.; Bawendi, M. G., "(CdSe)ZnS Core-shell quantum dots: Synthesis and characterization of a size series of highly luminescent nanocrystallites," *J. Phys. Chem. B,* vol. 101, pp. 9463-9475, 1997.

[8] Somers, R. C.; Bawendi, M. G.; Nocera, D. G., "CdSe nanocrystal based chem-/bio-sensors," *Chem. Soc. Rev.,* vol. 36, pp. 579-591, 2007.

[9] Biju, V; Itoh, T.; Anas, A.; Sujith, A., Ishikawa, M., "Semiconductor quantum dots and metal nanoparticles: syntheses, optical properties, and biological applications," *Anal. Bioanal. Chem.,* vol. 391, pp. 2469-2495, 2008.

[10] Karch, J.; Birringer, R.; Gleiter, H., "Ceramics ductile at low temperature," *Nature,* vol. 330, pp. 556-558, 1987.

[11] Siegel, R. W.; Hahn, H.; Ramasamy, S.; Zongquan, L.; Ting, L.; Gronsky, R., "Structure and properties of nanophase TiO2," *Journal de Physique,* vol. 49, pp. C5-681-686, 1988.

[12] Castro, T.; Reifenberger, R.; Choi, E.; Andres, R. P., "Size-dependent melting temperature of individual nanometer-sized metallic clusters," *Phys. Rev. B,* vol. 42, pp. 8548-8557, 1990.

[13] LaMer, V. K.; Dinegar, R. H., "Theory, production and mechanism of formation of monodispersed hydrosols," *J. Am. Chem. Soc.,* vol. 72, pp. 4847-4857, 1950.

[14] T. Sugimoto, Monodispersed Particles, Amsterdam: Elsevier, 2001.

[15] J. Winterton, Development of a novel microfluidic reactor for highly controlled synthesis of semiconductor nanocrystals, UC Berkeley, 2008.

[16] Chang, C. -H.; Paul, B. K.; Remcho, V. T.; Atre, S.; Hutchison, J. E., "Synthesis and Post-Processing of Nanomaterials Using Microreaction Technology," *J. Nanoparticle Research,* 2008.

[17] deMello, J.; deMello, A., "Microscale reactors: nanoscale products," *Lab. Chip.,* vol. 4, pp. 11N-15N, 2004.

[18] A. J. deMello, "Control and Detection of Chemical Reactions in Microfluidic Systems," *Nature,* vol. 442, pp. 394-402, 2006.

[19] Hartman, R. L.; Jensen, K. F., "Microchemical Systems for Continuous-Flow Synthesis," *Lab. Chip.,* vol. 9, pp. 2495-2507, 2009.

[20] Marre, S.; Jensen, K. F., "Synthesis of Micro and Nanostructures in Microfluidic Systems," *Chem. Soc. Rev.,* vol. 39, pp. 1183-1202, 2009.

[21] Nightingale, A. M.; deMello, J. C., "Microscale synthesis of quantum dots," *J. Mater. Chem.,* vol. 20, pp. 8454-8463, 2010.

[22] Erhfeld, W.; Hessel, V.; Lowe, H., Microreactors: new technology for modern chemistry, Weinheim: Wiley-VCH, 2000.

[23] Marre, S.; Adamo, A.; Basak, S.; Aymonier, C.; Jensen, K. F., "Design and packaging of microreactors for high pressure and high temperature applications," *Ind. Eng. Chem. Res.,* vol. 49, pp. 11310-11320, 2010.

[24] Abou-Hassan, A.; Sandre, O.; Neveu, S.; Cabuil, V., "Synthesis of goethite by separation of the nucleation and growth processes of ferrihydrite nanoparticles using microfluidics," *Angew. Chem. Int. Ed.,* vol. 48, pp. 2342-2345, 2009.

[25] Chan., E. M.; Mathies, R. A.; Alivisatos, A. P., "Size-controlled growth of CdSe nanocrystals in microfluidic reactors," *Nano Lett.,* vol. 3, pp. 199-201, 2003.

[26] Chung, C. K.; Shih, T. R.; Wu, B. H., "Design of a novel microreactor for microfluidic synthesis of silica nanoparticles," in *Transducers*, Denver, CO, 2009.

[27] Edel, J. B.; Fortt, R.; deMello, J. C.; deMello, A. J., "Microfluidic routes to the controlled production of nanoparticles," *Chem. Commun.,* vol. 10, pp. 1136-1137, 2002.

[28] Gomez-de Pedro, S.; Martinez-Cisneros, C. S.; Puyol, M.; Alonso-Chamarro, J., "Microreactor with integrated temperature control for the synthesis of CdSe nanocrystals," *Lab. Chip.,* vol. 12, pp. 1979-1986, 2012.

[29] Gutierrez, L.; Gomez, L.; Irusta, S.; Arruebo, M.; Santamaria, J., "Comparative study of the synthesis of silica nanoparticles in micromixer-microreactor and batch reactor systems," *Chem. Eng. J.,* vol. 171, pp. 674-683, 2011.

[30] Lin, X. Z.; Terepka, A. D.; Yang, H., "Synthesis of silver nanoparticles in a continuous flow tubular microreactor," *Nano Lett.,* vol. 4, pp. 2227-2232, 2004.

[31] Takagi, M.; Maki, T.; Miyahara, M.; Mae, K., "Production of titania nanoparticles by using a new microreactor assembled with same axle dual pipe," *Chem. Eng. J.,* vol. 101, pp. 269-276, 2004.

[32] Wagner, J.; Kohler, J. M., "Continuous synthesis of gold nanoparticles in a microreactor," *Nano Lett.,* vol. 5, pp. 685-691, 2005.

[33] Chan, E. M.; Alivisatos, A. P., Mathies, R. A., "High-temperature microfluidic synthesis of CdSe nanocrystals in nanoliter droplets," *J. Am. Chem. Soc.,* vol. 127, pp. 13854-13861, 2005.

[34] Frenz, L.; El Harrak, A.; Pauly, M.; Begin-Colin, S.; Griffiths, A. D.; Baret, J. -C., "Droplet-based microreactors for the synthesis of magnetic iron oxide nanoparticles," *Angew. Chem. Int. Ed.,* vol. 47, pp. 6817-6820, 2008.

[35] Günther, A.; Khan, S. A.; Thalman, M.; Trachsel, F.; Jensen, K. F., "Transport and reaction in microscale segmented gas-liquid flow," *Lab. Chip.,* vol. 4, pp. 278-286, 2004.

[36] Hung, L.-H.; Choi, K. M.; Tseng, W. -Y.; Tan, Y. -C.; Shea, K. J.; Lee, A. P., "Alternating droplet generation and controlled dynamic droplet fusion in microfluidic device for CdS nanoparticle synthesis," *Lab. Chip.,* vol. 6, pp. 174-178, 2006.

[37] Khan, S. A.; Duraiswamy, S., "Controlling bubbles using bubbles- microfluidic synthesis of ultra-small gold nanocrystals with gas-evolving reducing agents," *Lab. Chip.,* vol. 12, pp. 1807-1812, 2012.

[38] Nightingale, A. M.; Krishnadasan, S. H.; Berhanu, D.; Niu, X.; Drury, C.; McIntyre, R.; Valsami-Jones, E.; deMello, J. C., "A stable droplet reactor for high temperature nanocrystal synthesis," *Lab. Chip.,* vol. 11, pp. 1221-1227, 2011.

[39] Shestopalov, I.; Tice, J. D.; Ismagilov, R. F., "Multi-step synthesis of nanoparticles performed on milisecond time scale in a microfluidic droplet-based system," *Lab. Chip.,* vol. 4, pp. 316-321, 2004.

[40] Song, H.; Bringer, M. R.; Tice, J. D.; Gerdts, C. J.; Ismagilov, R. F., "Experimental test of scaling of mixing by chaotic advection in droplets moving through microfluidic channels," *Appl. Phys. Lett.,* vol. 83, pp. 4664-4666, 2003.

[41] Xu, S.; Nie, Z.; Seo, M.; Lewis, P.; Kumacheva, E.; Stone, H. A.; Garstecki, P.; Weibel, D. B.;

Gitlin, I.; Whitesides, G. M., "Generation of monodisperse particles by using microfluidics: control over size, shape, and composition," *Angew. Chem. Int. Ed.,* vol. 117, pp. 734-738, 2004.

[42] Yen, B. K. H.; Gunther, A.; Schmidt, M. A.; Jensen, K. F.; Bawendi, M. G., "A microfabricated gas-liquid segmented flow reactor for high-temperature synthesis: the case of CdSe quantum dots," *Angew. Chem.,* vol. 117, pp. 5583-5587, 2005.

[43] Cabeza, V. S.; Kuhn, S.; Kulkarni, A. A.; Jensen, K. F., "Size-controlled flow synthesis of gold nanoparticles using a segmented flow microfluidic platform," *Langmuir,* vol. 28, pp. 7007-7013, 2012.

[44] Lee, S. -K.; Liu, X.; Cabeza, V. S.; Jensen, K. F., "Synthesis, assembly and reaction of a nanocatalyst in microfluidic systems: a general platform," *Lab. Chip.,* vol. 12, pp. 4080-4084, 2012.

[45] Greener, J.; Li, W.; Ren, J.; Voicu, D.; Pakharenko, V.; Tang, T.; Kumacheva, E., "Rapid, cost-efficient fabrication of microfluidic reactors in thermoplastic polymers by combining photolithography and hot embossing," *Lab. Chip.,* vol. 10, pp. 522-524, 2009.

[46] Khan, S. A.; Günther, A.; Schmidt, M. A.; Jensen, K. F., "Microfluidic synthesis of colloidal silica," *Langmuir,* vol. 20, pp. 8604-8611, 2004.

[47] Abdelhady, A. L.; Afzaal, M.; Malik, M. A.; O'Brien, P., "Flow reactor synthesis of CdSe, CdS, CdSe/CdS and CdSeS nanoparticles from single molecular precursor(s)," *J. Mater. Chem.,* vol. 21, pp. 18768-18775, 2011.

[48] Nakamura, H.; Yamaguchi, Y.; Miyazaki, M.; Maeda, H.; Uehara, M.; Mulvaney, P., "Preparation of CdSe nanocrystals in a micro-flow-reactor," *Chem. Commun.,* vol. 23, pp. 2844-2845, 2002.

Chapter 2

POLYURETHANE SUBSTRATE MICROREACTOR FOR LOW TEMPERATURE REACTIONS

Polymer-substrate microreactors are attractive due to their ease of fabrication and low cost. Although polymer-substrate microreactors are generally not suitable for high temperature reactions, they are simpler to make, cheaper than silicon substrate microreactors, and they are more flexible in terms of design than capillary microreactors. They can be fabricated using simpler methods, such as soft lithography or hot embossing. To date, they have mostly been fabricated in polydimethlysiloxane (PDMS) or poly(methyl methacrylate) (PMMA). PDMS and PMMA have poor resistance to many of the chemicals used in nanoparticle synthesis; this limits the variety of reactions that can be conducted in these reactors. In the microreactor described in this chapter, polyurethane (PU) is used as the structural material. PU has good resistance to aqueous solvents, alcohols and organic materials [1] [2]. To fabricate this microreactor, CO_2-laser micromachining is used. This technique is a relatively fast, cheap and easy method for fabricating microreactors. By using this microreactor iron-oxide nanoparticle synthesis was demonstrated and these nanoparticles were characterized by transmission electron microscopy (TEM), X-ray diffraction (XRD) and super conducting quantum interference device (SQUID).

In this chapter, first a review on polymer substrate microreactors will be given, then the design of the polyurethane substrate microreactor will be explained; this section will be followed by the explanation of CO_2-laser fabrication method; and finally the iron-oxide nanoparticle synthesis and characterization results will be demonstrated.

2.1. Review of Polymer Substrate Microreactors

Methods utilizing polymer-based technologies have been the most popular way of fabricating microfluidic devices due to their simplicity, rapidity, and low cost compared to silicon- and glass-based techniques. The most widely used fabrication methods include soft lithography; hot embossing and injection molding, with polydimethlysiloxane (PDMS) and

poly (methyl methacrylate) (PMMA) being two of the most popular polymer choices. A detailed review on polymer-based microfabrication is given by Becker *et al.* [3].

There are several examples of microreactors built by using polymer fabrication techniques. One good example of this type of microreactors was introduced by Song *et al.* [4]. They used PDMS as their substrate material and fabricated their device by soft photolithography. In this work they designed their channel geometry such that it enables mixing different solutions rapidly. This is made possible by generating a droplet that is composed of the solvents to be mixed. Due to the circulating flow profile inside the droplets and the sinusoidal shaped channel, the diffusion length was reduced; therefore the mixing time of reagents was less than for continuous flow systems where mixing is limited by diffusion length. It was reported that the mixing times can be less than 2 ms with high flow rates. The schematic of mixing is shown in Figure 2.1.

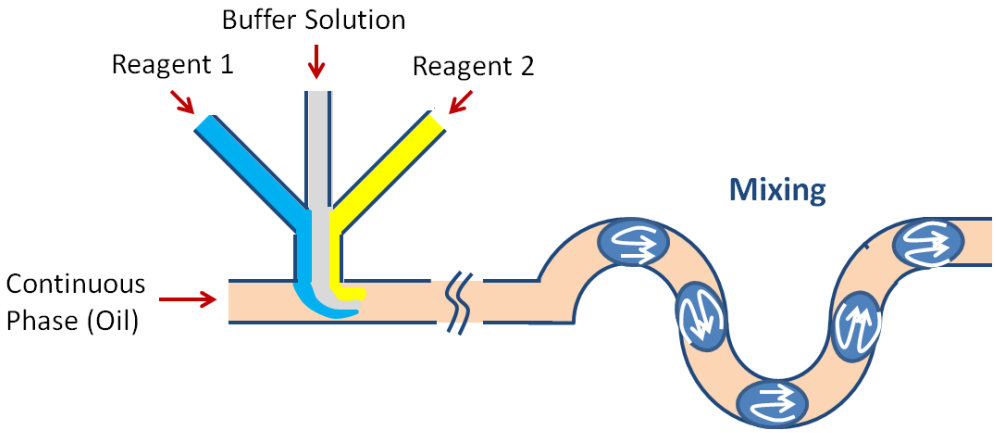

Figure 2.1: Schematic of the mixing in a sinusoidal shaped channel design. After Song *et al.* [4] This design enables rapid mixing with no dispersion.

Song *et al.* didn't demonstrate nanoparticle synthesis in this device but a follow-up paper from the same research lab used this design for the synthesis of CdS nanoparticles [5]. Their device was also fabricated in PDMS by using soft lithography. They used two inlets for delivering reagents needed for the CdS synthesis and one inlet – in the middle of these two- that delivers a buffer solution to separate these two solvents until they are inside a droplet. As a carrier phase they used oil.

Another droplet based, PDMS substrate microreactor that uses mixing in droplets was introduced by Frenz *et al.* [6]. In their method, they used a droplet coalescence method where droplets of reagents were merged by applying electrical voltage to electrodes placed in the channel. Reagents mix inside droplets as they travel down the microchannel. By using their microreactor they demonstrated the synthesis of iron oxide nanoparticles.

All of the above examples from literature were droplet based microfluidic systems where low temperature nanoparticle synthesis was performed via mixing reagents inside droplets. There are also polymer substrate microreactors where reagents are mixed inside a continuous flow system. A good example of this type of microrector is presented by Chung *et al.* [7]. Their microreactor is also fabricated in PDMS by using soft lithography.

They demonstrated the synthesis of silica nanoparticles by mixing two reagents without using droplets. Instead, they used a continuous flow micromixer composed of 'obstacles' and 'gaps'.

Even though the mixing speed can be increased by using this geometry, this design still carries the disadvantages of channel contamination and variation in residence time distributions due to continuous flow profiles. Also the mixing time with droplet-based systems is always shorter due to the circulating flow profile inside droplets.

Although PDMS and PMMA have advantages such as low cost, ease of handling and well established fabrication techniques; they are unsuitable for applications such as nanoparticle synthesis that require high chemical resistance (mainly to organic solvents and alcohols) and reusability. Thus a new polymer material is needed that is as easy to use and fabricate as PDMS and PMMA but does not have these shortcomings. Recently polyurethane (PU), a robust material that has long been used as a reusable mold material, has been introduced as a substrate material for microfluidics [2, 8-11] due to its excellent chemical resistance to aqueous solvents, alcohols and organic materials [2] and its biocompatibility, with lower levels of fouling than many other polymers including PDMS and PMMA [8].

To the best of our knowledge, all PU microfluidic devices that have been described in literature were fabricated by soft lithography [2, 8-11]. Kim *et al.* used UV-cured PU for making microfluidic immunoassay platforms [9]; Piccin *et al.* made a capillary electrophoresis system from PU and investigated the chemical resistance of the material [2]; Xu *et al.* built a flow focusing PU device for synthesizing polymeric microparticles [10, 11], and Wu *et al.* developed polyurethane-based microfluidic devices for blood contacting applications [8].

In contrast to the literature, in this chapter, a microreactor made out of a polyurethane substrate that is designed for low temperature nanoparticle synthesis reactions is introduced. Different than the fabrication methods of previously reported microfluidic reactors, this microreactor is fabricated by using an alternative and straightforward technique that utilizes a CO_2-laser.

2.2. Design of the Polyurethane Substrate Microreactor

The polyurethane microreactor is specifically designed for reactions that occur at relatively low temperatures without any need for external heating and by mixing two reagents. We can also name this as 'contact driven' reactions where contact (mixing) of reagents is required for the synthesis. Therefore it is important to mix reagents in an efficient and fast method. The best way to mix two liquids on a small scale is to use a droplet-based system in which internal flow inside the droplets is actively promoted, reducing the time required for mixing compared to mixing methods in continuous flow profiles [6]. Two different liquids containing reagents are introduced into the system and at a T-junction are broken up by shear forces into droplets inside a carrier fluid, as shown in Figure 2.2. The channel design of the PU microreactor is similar to that described by Song *et al.* [4] and Shestopalov *et al* [5] however it is different in its material, fabrication and the

nanoparticles synthesized inside.

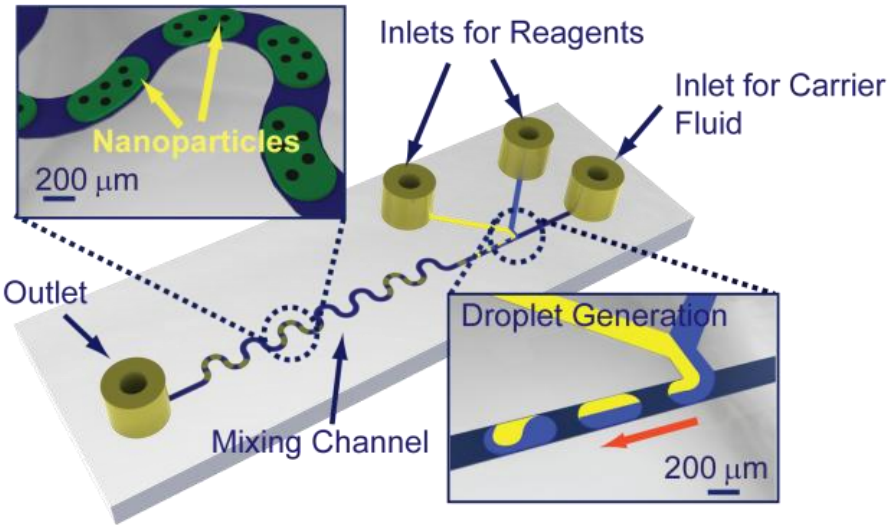

(A)

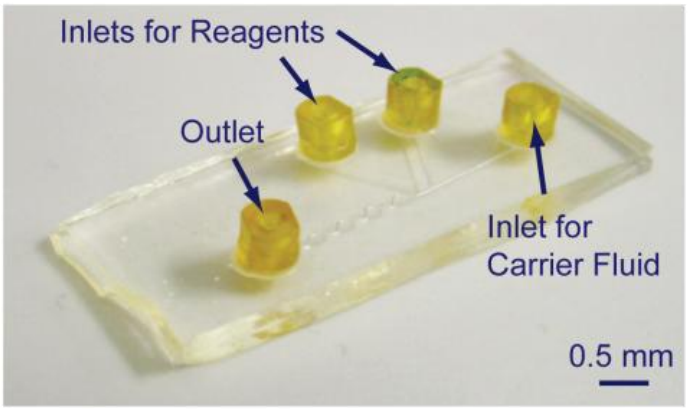

(B)

Figure 2.2: A) Schematic showing the design of the PU based microfluidic reactor. B) Actual image of the PU based microreactor.

To increase the internal flow within the droplets, and hence the mixing of reagents, the two-phase flow follows a channel with a sinusoidal shape, referred to as the mixing channel. The sinusoidal shape of this channel deforms the droplets (stretches and folds), thereby decreasing the diffusion length (or striation length) [4], which eventually decreases the time required for mixing compared to continuous flow profiles. This type of mixing is named as 'mixing by chaotic advection' and the flow characteristic inside the droplets is explained by Baker's transformation [4]. Derivation of the mixing time is done by Song et al. assuming that the mixing time, t_{mix} is the time at which the time scale for convective mixing t_{conv} is equalized with the time scale of diffusive mixing t_{diff}. Mixing time is given as,

$$t_{mix} \sim \left(\frac{aw}{U}\right) \square\square\square Pe \quad (1)$$

where a is the dimension of the droplet with respect to the channel width w and U is the flow rate and Pe is the Péclet number given as Uw/D where D diffusion length. From this result it is apparent that mixing time is dependent on the flow rate, width of channel and size of droplets.

In order to verify that mixing occurs inside droplets in a very short time, an experiment was conducted with DI water dyed with ink. The carrier fluid was mineral oil with a surfactant (Span 80, 2% wt.). Images of mixing are shown in Figure 2.3. This experiment verifies that mixing happens in a very short time within the droplets.

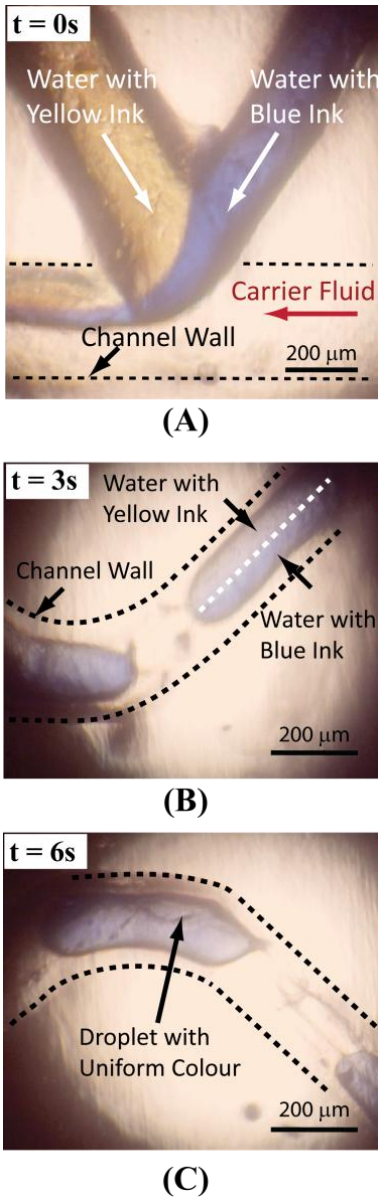

Figure 2.3: Mixing inside the PU substrate microfluidic reactor. Yellow ink and blue ink dissolved in DI water enter from two separate inlets and they break up into droplets with the carrier fluid. Mixing inside droplets is very rapid. C shows deformation of a droplet at a section where the channel direction changes; this promotes mixing.

The synthesis reaction requires specific mixing ratios of reagents, determined by the reaction stoichiometry. These can be controlled by both the concentration of the reagents in their respective solutions, and the relative flow rates of each solution. Syringe pumps were used in this work to achieve the precise control over solution flow rates to obtain the necessary mixing ratios of the reagent streams.

2.3. Fabrication with CO_2-Laser

In this section an alternative and straightforward technique for fabricating PU microfluidic devices using a CO_2-laser is explained. Laser ablation of polyurethane substrates was demonstrated earlier by using a UV laser [12-16]. These studies did not target making microfluidic channels; instead, they focused on the laser ablation process itself [12, 16] or on cutting polyurethane membranes for use in medical devices [14]. Although UV lasers can open a cavity on a substrate, earlier work showed that they create poorly defined cross sections [15]. UV lasers also require a photomask or computer-controlled sample movement set-up. In contrast, CO_2-laser printers are commercially available and simpler to use; making them a better candidate for fabrication. This contact-free fabrication methodology is fast and inexpensive; several microfluidic devices can be "printed" in a few minutes.

CO_2-laser ablation can be as simple as printing a document with a conventional printer. Specifically, there is no need for a physical mask or a microfabrication facility, which allows for rapid design modification, testing, and further modification. The polyurethane used in this work cures at room temperature without any need for UV treatment, which decreases the cost, number of tools required and fabrication steps.

CO_2-lasers have been used to ablate microchannels on polymer substrates previously [17, 20]. Laser ablation of a PMMA substrate was studied earlier, and produced channel surfaces with bumps on the order of 30 μm [17]. This method was also used on a PDMS substrate by Liu et al. [20]; however the laser-ablated channels had a very uneven surface. These surface irregularities would be unacceptable for many microfluidic reactors, because they would disrupt flow, particularly two-phase flow, and would likely cause blockages in channels that carry solids. To the best of our knowledge, CO_2 laser ablation has not been used before to make PU microchannels. However, we have obtained repeatable, very smooth channel surfaces without any residues.

2.3.1. Materials and CO_2-Laser Printer

Loctite M-11FL Hysol Medical Device Urethane Adhesive (Henkel Corporation) was used to fabricate the microfluidic reactor. This polyurethane is designed for disposable medical devices because of its biocompatibility. The adhesive is supplied as a self-reactive resin and hardener dispensed from a dual cartridge. This type of PU is simpler to utilize than the UV curable polyurethanes used in the literature for microfabrication [9, 11, 21] because it cures at room temperature without any extra processing. The substrate was formed by dispensing the resin and hardener onto a flat surface using an applicator gun and a mixing nozzle.

Laser printing was performed by using a VersaLaser 200 Printer (Universal Laser Systems), which has a maximum output power of 30 W. The lowest power setting for cutting paper was used in order to create small feature sizes. The power was varied between 0.96 W and 1.44 W by changing the laser intensity. After printing, the channels were encapsulated by using N,N-dimethylformamide (anhydrous, Sigma-Aldrich).

2.3.2. Mechanism of Ablation

The polyurethane microchannels were printed onto a cured PU substrate using the CO_2-laser printer, controlled from a CAD file, as depicted in Figure 2.4. There are three mechanisms of material removal with the CO_2-laser, which depend on the type of the polymer being used. These mechanisms are melt shearing, vaporisation and chemical degradation [22]. For example in the case of PMMA, the CO_2-laser photothermally melts and vaporises the material, creating a cavity [17, 22]. In contrast, PU, with a different chemical structure, undergoes chemical degradation, leaving a residual carbon-based layer on top of the surface while releasing some hydrogen cyanide during the process [22]. Polyurethane is a class of polymers composed of chains of isocyanate, and the precise chemical decomposition process may differ somewhat for different types of polyurethanes. In addition to chemical degradation, a layer of molten polymer is also observed. This indicates that the CO_2-laser also melts the material. Some fumes were also released during ablation; but an analysis of the gas composition was not attempted because of the acute toxicity of hydrogen cyanide. For the PU composition used here, it is postulated that the CO_2 laser forms microchannels through a combination of vaporisation and chemical degradation.

After laser ablation, the surfaces were cleaned with ethanol-soaked tex wipes to remove physical debris from the channel walls.

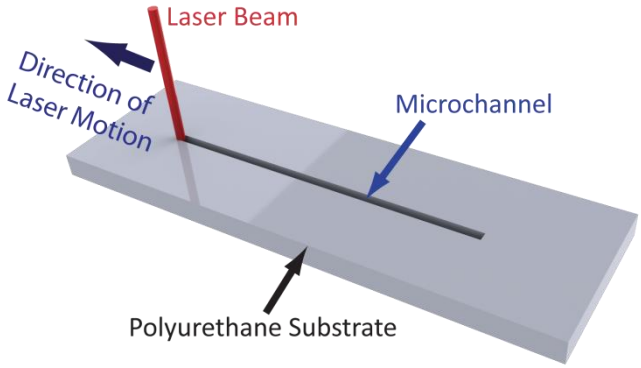

Figure 2.4: Schematic showing the procedure of laser ablation.

2.3.3. Characterization of Laser Ablated Microchannels

PU channels ablated by the CO_2 laser were characterized by profilometer and scanning electron microscopy (SEM). Printed channels have a Gaussian profile that correlates with

the Gaussian distribution of the intensity of the laser beam. Figure 2.5 shows the Gaussian fit to the measured channel profile.

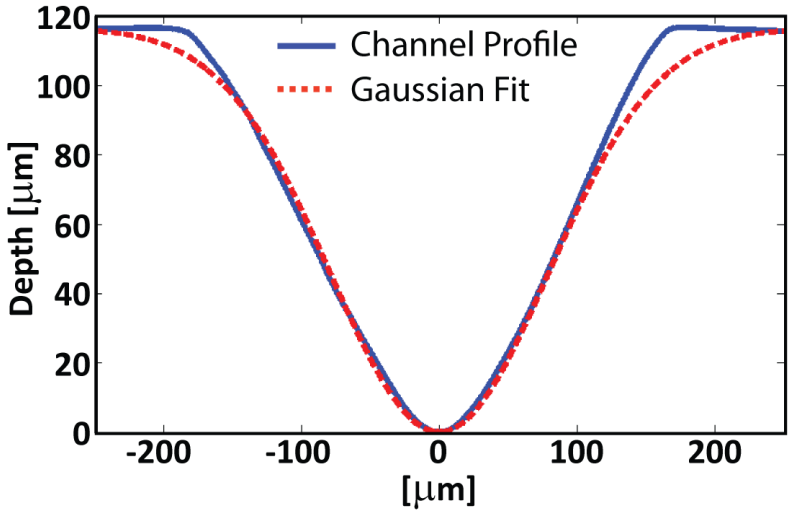

Figure 2.5: Gaussian fit to the laser ablated channel profile. Channel is printed at 1.2 W power setting with a single pass of laser beam.

Laser ablated PU channels were also imaged by using Scanning Electron Microscope (SEM). These images were taken after a gold sputtering step on PU channels for imaging. SEM images of printed microchannels are shown in Figure 2.6. The channels are generally smooth with low surface roughness. It is presumed that the few visible imperfections are due to dust particles or defects from the gold sputtering step prior to imaging. The surface roughness is estimated to be less than 1 μm.

The Gaussian profile of the laser ablated PU microchannel and an encapsulated channel after solvent treatment are shown in Figure 2.6A and Figure 2.6B respectively. An X-junction formed by the laser is shown in Figure 2.6C; it is evident that this method is suitable for forming functional microfluidic components for droplet formation. Laser engraved parallel microchannels are shown in Figure 2.6D; these channels are connected at the end; this geometry can be used to create long channels.

Microchannel width and depth depends on the laser power intensity and the number of laser passes. The channel width and depth increased with increasing laser power, as shown in Figure 2.7A. The depth of the microchannel also increases as the number of laser passes increases, as shown in Figure 2.7B. After 5 passes, the depth becomes constant as the laser is no longer focused on the base of the channel. If the focus of the laser were adjusted after each pass, the depth would increase. Multiple laser passes can be used to make 3D microfluidic structures such as tapered microchannels without additional steps. The printer can be programmed such that some portions of the design are passed multiple times.

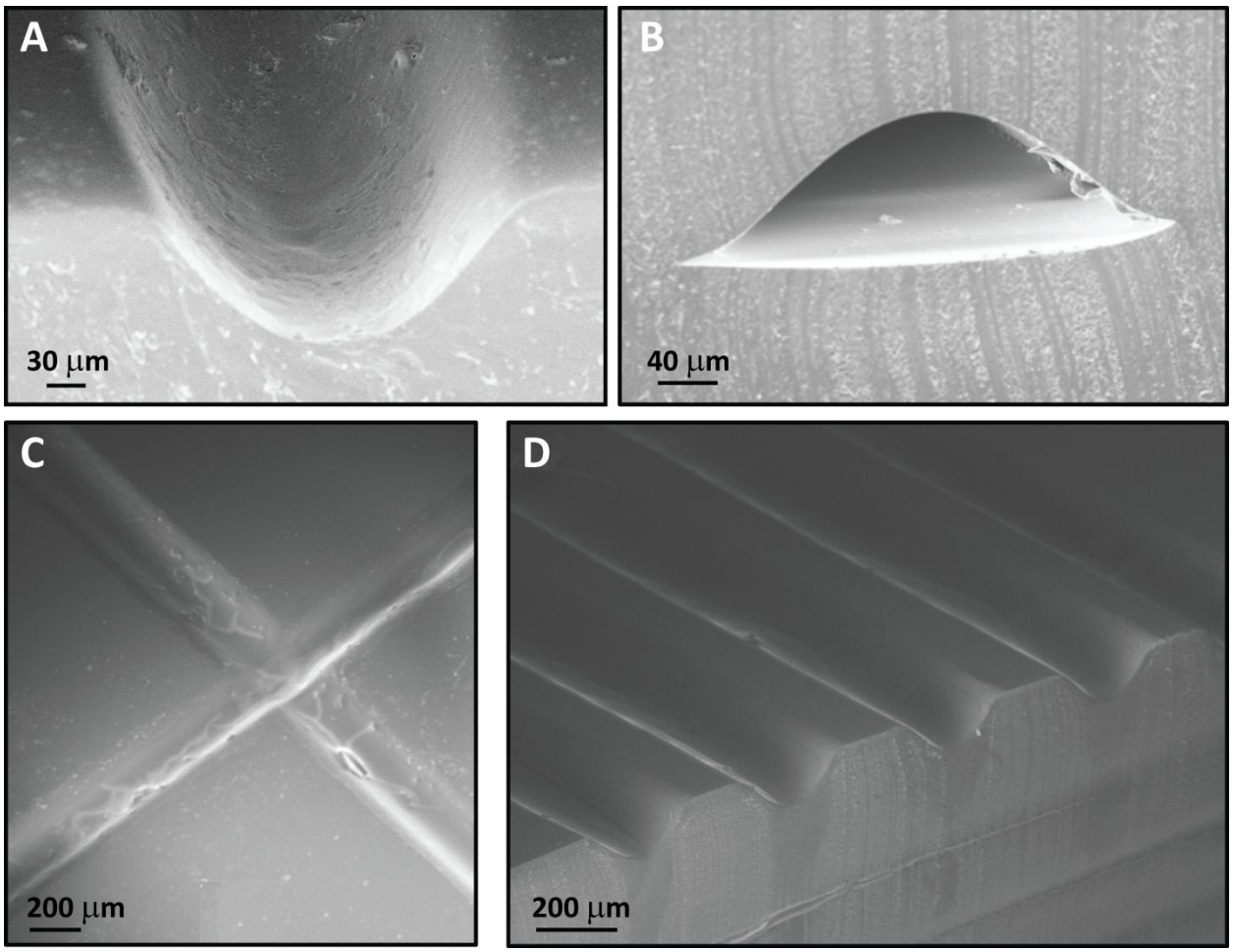

Figure 2.6: SEM images of laser engraved microchannels. A) Gaussian profile of a microchannel. B) Encapsulated microchannel. C) X-junction formed by CO_2 laser. D) Parallel microchannels. All channels were printed at 1.2 W with single laser pass.

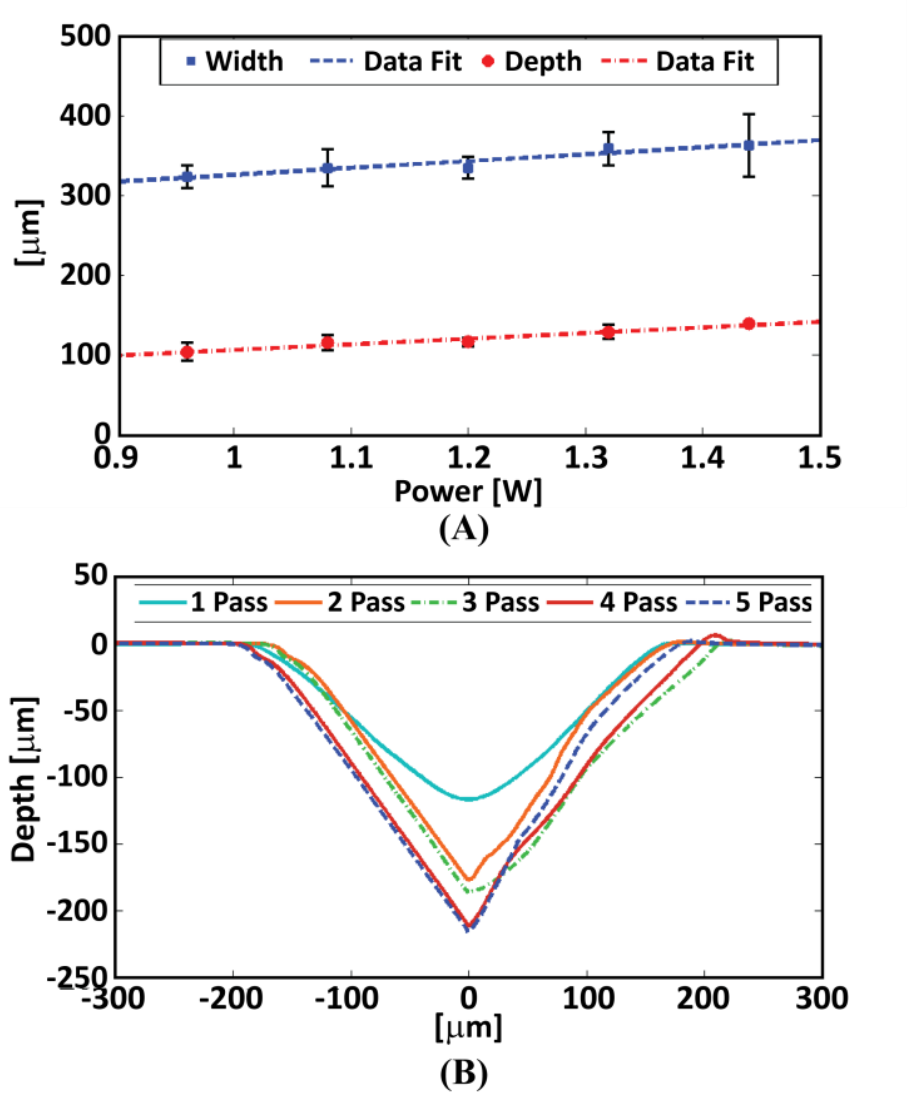

Figure 2.7: A) The depth and width of channels increase with increasing power. The data fit shows that this increase is linear. B) As the number of laser passes is increased, the depth of the channel also increases and channel profile becomes more triangular.

2.3.4. Encapsulation of Laser Ablated Microchannels

Solvent-assisted bonding was used to bond PU substrates to another PU layer to encapsulate the microchannels. This method begins by brushing dimethylformamide (DMF) onto both surfaces. The DMF dissolves a thin, nanoscale layer at the surface of the polyurethane, and when two such substrates are contacted, they create a water- and gas-tight bond that can withstand pressures up to 130 kPa.

During the synthesis of nanoparticles, clogging of the channel at the droplet formation junction was periodically observed, indicating that nanoparticules nucleate very rapidly after mixing, before the solutions have had time to move away from the droplet formation zone. Therefore an alternative way to encapsulate channels was used later, as discussed by Brackbill *et al.* [23]. The bonded substrates were clamped between two acrylic sheets as

shown in Figure 2.8. By this way the microreactor could be debonded from the PU substrate, cleaned and bonded again. The same procedure was used between experimental runs to thoroughly clean the microreactor. This allowed a microreactor to be reused several times. The clamped rearrangement can withstand larger pressures without any leakage.

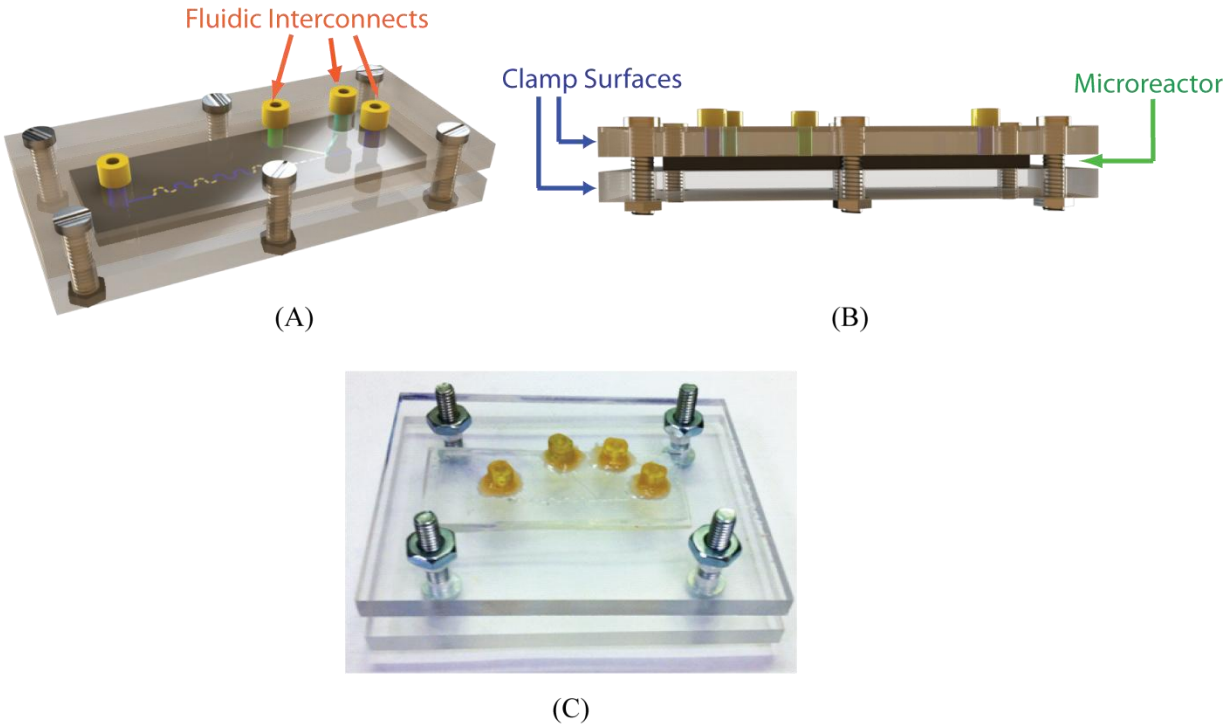

Figure 2.8: Clamp mechanism for the PU microreactor. (A) General view, (B) Side view, (C) Actual device.

The clogging problem due to rapid nucleation was addressed by Shestepalov *et al.* by adding another channel between the two reagent inlets, in order to provide a buffer in between two reagents until they form a droplet [5].

2.4. Flow in Laser Ablated Microchannels

Laser-ablated microchannels have a Gaussian profile, unlike microchannels fabricated with other microfabrication techniques where the typical profile is more nearly rectangular. In order to understand the effect of geometry on fluid flow, we compared the flow profile and friction factor of laser ablated microchannels with rectangular microchannels. The laminar flow inside a Gaussian microchannel with no slip boundary conditions, simulated with the COMSOL Multiphysics program is shown in Figure 2.9. The flow profile is similar to the Poiuseuille flow profile observed in rectangular and circular channels, with the maximum velocity at the center of the channel.

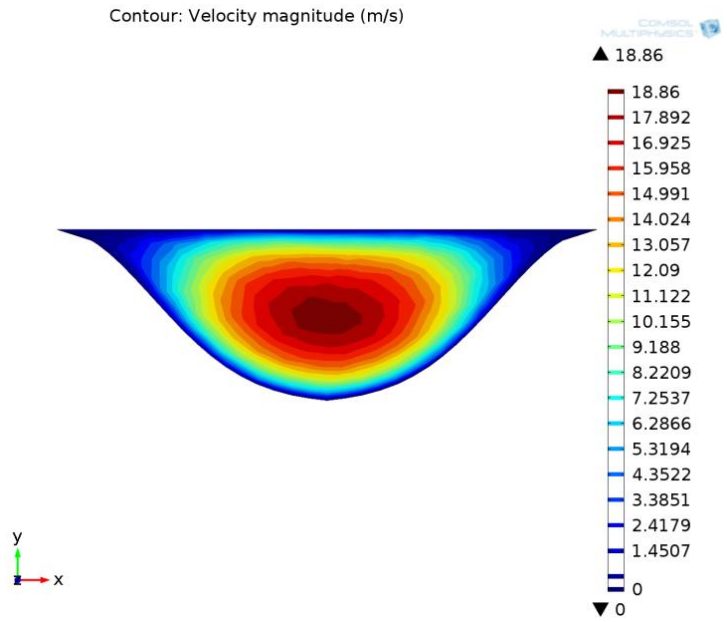

Figure 2.9: Velocity profile inside a Gaussian channel printed at 1.2 W power setting for water flow under a pressure gradient of 50 kPa/mm. Simulation is done with the COMSOL Multiphysics program.

The Fanning friction factors of Gaussian and rectangular microchannels were also compared. The Fanning friction factor relates the pressure drop, mean velocity and channel geometry as shown below [24]:

$$f = \frac{Po}{Re} = \frac{}{} \frac{dp}{dx} \frac{D_}{\rho u_m^} \quad (2)$$

where Po is the Poiseuille number, Re the Reynolds number, p the pressure, x is the distance, ρ is the density, D_h the hydraulic diameter and u_m the mean velocity. The hydraulic diameter for non circular channels is given as

$$D_ = \frac{A_c}{P_w} \quad (3)$$

where A_c is the cross sectional area and P_w the wetted perimeter. For a microchannel laser-ablated at 1.2 W settings, we calculated the hydraulic diameter as 0.1 mm. The friction factors of the Gaussian and rectangular microchannels under the pressure drop of 130 kPa with same hydraulic diameter were calculated as 16 and 826 respectively. Thus, equation (2) shows that higher pressure gradients are necessary to achieve the same flow rate in rectangular channels compared to Gaussian channels with same hydraulic diameter.

2.5. Experimental Results of Nanoparticle Synthesis

2.5.1. Materials

Iron (III) chloride hexahydrate, (97%, Sigma-Aldrich); iron (II) chloride tetrahydrate, (≥ 99% Sigma-Aldrich); hydrochloric acid, (1 N, Fisher Scientific); and ammonium

hydroxide (29% Fisher Scientific) were used to prepare the aqueous solutions. Mineral oil and Span 80 was obtained from Sigma-Aldrich.

2.5.2. Experimental Set-up

Two different synthesis methods were used for the synthesis of iron oxide. The first method synthesized them under an inert gas environment in order to prevent oxidation of Fe(II) by the O_2 in air. In order to provide such an environment a clear box was filled with Ar gas as shown in Figure 2.10. Reagents and the carrier fluid were delivered by using syringe pumps at a constant flow rate. A high-speed camera was used for imaging.

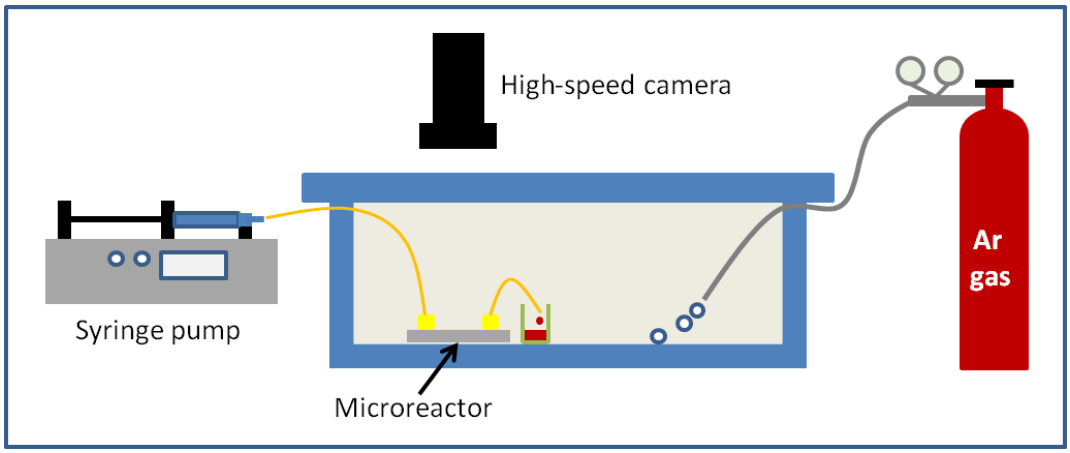

Figure 2.10: Schematic of the experimental set-up for nanoparticle synthesis under Ar gas environment. In the actual experiment three syringe pumps were used (one for each solvent); in the schematic only one is shown for demonstration purposes.

2.5.3. Synthesis Method

Iron oxide nanoparticles were synthesized using two slightly different methods that required different mixing ratios to show that we can control reagent concentrations precisely.

The first method is based on a hydrolyzing an aqueous mixture containing 0.48 M $FeCl_3{\cdot}6H_2O$, 0.24M $FeCl_2{\cdot}4H_2O$ and 0.5M HCl (reagent 1) using 2 M aqueous ammonia (reagent 2) following the method of Frenz et al. [6]. This provides iron (III) and iron (II) in the appropriate proportions for precipitating magnetite, Fe_3O_4 upon contact with ammonia:

$$2Fe^{3+} + Fe^{2+} + 8NH_4OH = Fe_3O_4 + 8NH_4^+ + 4H_2O \quad (4)$$

Both solutions were prepared with deaerated, deionized (DI) water under argon gas to minimize the oxidation of Fe^{2+} during reaction. The reaction was carried out under an argon environment. The microreactor was not degassed before use because, unlike materials such as PDMS, PU has a very low permeability to gas, and hence would not be expected to retain significant quantities of oxygen.

The two reagents enter the reactor from separate channels; briefly mix to initiate

hydrolysis, and form a droplet in a third channel containing mineral oil as a carrier fluid. Nanoparticles are generated as reaction 1 proceeds inside the droplet. The flow rate of base solution (reagent 2) was double that of the iron salt solution (reagent 1), which yielded a mixed solution initially containing 0.16 M $FeCl_3$ and 0.08 M $FeCl_2$, with a stoichiometric excess of base. When the flow rates were equal, which provided a sub-stoichiometric amount of base, some iron precipitated but the resulting particles were non-magnetic, presumably because there was insufficient base to hydrolyze all of the Iron (II), which is less readily hydrolyzed than iron (III). Without significant hydrolysis of iron (II), one would expect non-magnetic hematite, goethite, or ferrihydrite as the primary product. This means that the mixing ratio of reagents needs to be controlled precisely and it was possible to do this with the microreactor.

The second method employed to synthesize nanoparticles used 12.1 M aqueous ammonia to hydrolyze an aqueous solution containing 0.15 M $FeCl_3 \cdot 6H_2O$ and 0.1 M $FeCl_2 \cdot 4H_2O$ following the method of Karaağaç *et al.* [25]. The solutions were not degassed and the reaction was carried out under an air environment. The flow rates of the ammonia and iron chloride solutions were equal, yielding a solution initially containing 0.075 M $FeCl_3$ and 0.05 M $FeCl_2$ (assuming no oxidation of the Fe(II)). Although the initial Fe(II) to Fe(III) ratio was higher than that in the first method, and higher than the proportions in magnetite, at least some of the Fe(II) present initially would be expected to undergo oxidation by dissolved oxygen. One would only expect Fe_3O_4 to appear if some of the Fe(II) remained unoxidized. During the synthesis, as the carrier fluid, mineral oil with Span 80 (2% wt) is used.

During the synthesis, mineral oil with Span 80 (2% wt) is used as the carrier fluid.

After collecting synthesized nanoparticles from the microreactor, particles were centrifuged in acetone and ethanol mixture three times. Particles were later suspended in acetone and sonicated for 5 minutes in order to reduce agglomeration.

2.5.4. Results and Discussion

Real time images of nanoparticle synthesis inside the microreactor are shown in Figure 2.11. Two reagents mix inside the droplets and form nanoparticles. The ratio of reagents is very important to control concentration of reagents and it is maintained by the control of flow rates via syringe pumps.

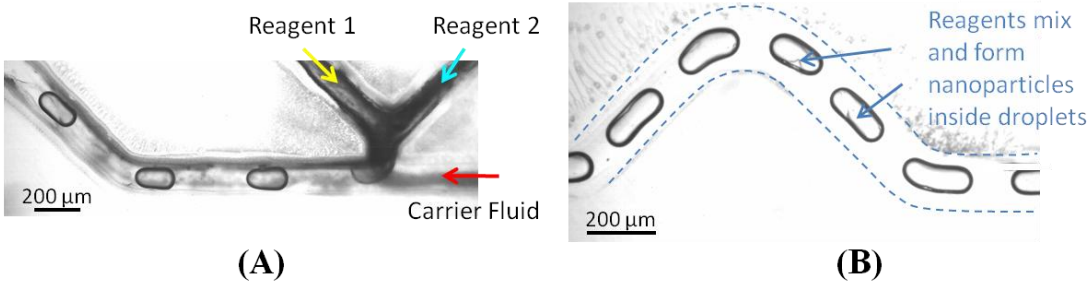

Figure 2.11: High-speed camera images of the synthesis of nanoparticles inside the microreactor. A) Reagents form a droplet at the T-junction by shear induced break-up. Flow rate of carrier fluid

(mineral oil) is 600 µL/hr whereas flow rate of reagent 1 and 2 are 200 µL/hr and 400 µL/hr respectively. B) Reagents are mixed inside droplets while carried by the carrier fluid.

Characterization of particles was done by using TEM (JEOL JEM 2011) and x-ray diffractometry (Siemens D5000 X-Ray Diffractometer). Figure 2.12 shows TEM images of nanoparticles synthesized in the microreactor by hydrolyzing the deaerated aqueous chloride solution with a 1:2 Fe(II):Fe(III) ratio. Size of nanoparticles were 5 ± 0.5 nm in diameter, representing a 10% standard deviation in size which is a narrower size distribution than obtained by Fang *et al.* using a similar aqueous chemistry in a batch process [26].

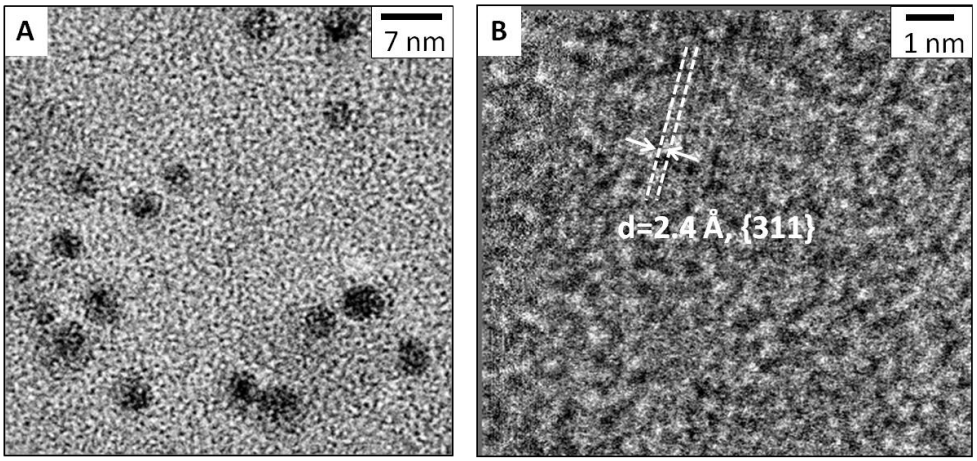

Figure 2.12: A) TEM image of nanoparticles synthesized by hydrolysis of deaerated solution initially containing 0.16 M $FeCl_3$ and 0.08 M $FeCl_2$. B) Zoomed image of a magnetite nanoparticle showing the spacing of {311} planes. Size of nanoparticles were 5 ± 0.5 nm.

The TEM image in Figure 2.12A shows individual nanoparticles on the TEM carbon grid. However when the other parts of the TEM grid was observed, it was seen that there were also agglomerated particles as shown in Figure 2.13. In order to avoid agglomeration of particles, ligands or surfactants can be used.

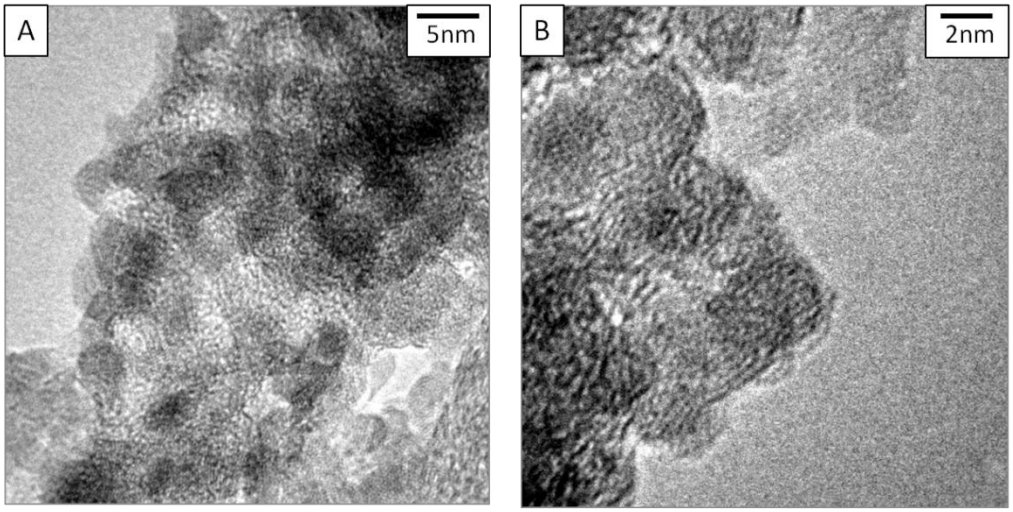

Figure 2.13: TEM images of nanoparticles synthesized by hydrolysis of aerated solution.

XRD analysis was also performed to understand the composition of the material as shown in Figure 2.14. The peaks in the XRD pattern were identified using the reference tables in Cornell *et al.* [27]. Two of the major peaks appeared to correspond to magnetite, Fe_3O_4. However, two additional peaks, at 22˚ and 48˚ did not correspond with major magnetite peaks. The former appears to correspond to goethite, αFeOOH, and the latter to the silicon substrate on which the particles were mounted.

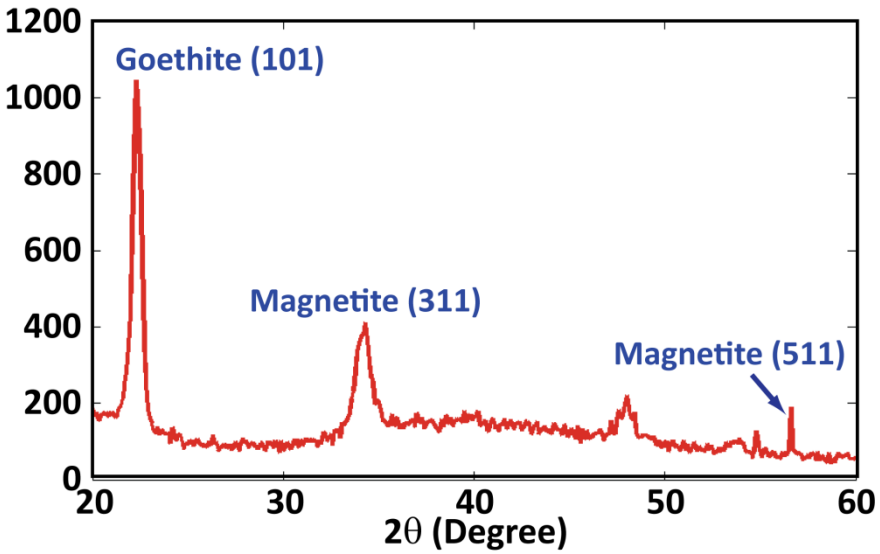

Figure 2.14: X-ray diffraction pattern of nanoparticles synthesized by hydrolysis of deaerated solution initially containing 0.16 M $FeCl_3$ and 0.08 M $FeCl_2$.

Experiments with different iron chloride concentration were also conducted by using the same methodology. The concentration of the iron chloride reagent was doubled, 0.32 M $FeCl_3$ and 0.16 M $FeCl_2$, and the concentration of base solution was kept the same. With this new concentration, slightly larger particles were obtained as shown in Figure 2.15. This

result shows that by changing the initial concentration of reagents, the size of particles can also be modified.

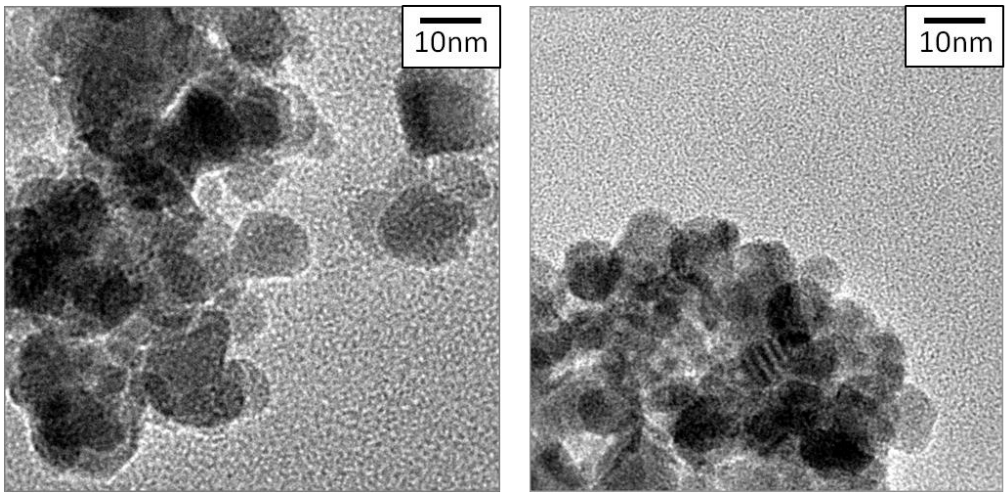

Figure 2.15: TEM images of iron oxide nanoparticles synthesized with double concentration of iron chloride solution. Size of nanoparticles is 7.5nm ± 0.5 nm.

In the second method of synthesizing iron oxide nanoparticles, more dilute, aerated chloride solution is used. The TEM images of the nanoparticles synthesized in the microfluidic reactor using this method are shown in Figure 2.16. These particles were 4.6 ± 0.7 nm in diameter, representing a 15% standard deviation in size, narrower than the size distribution reported by Karaağaç *et al.* [25] for nanoparticles synthesized in batch hydrolysis of similar solutions. There were parts of the TEM grid where agglomeration was observed, however it was as much as in the case of the previous method. Figure 2.17 shows an X-ray diffraction pattern distinctly different from that in Figure 2.14, indicating that either the lower concentration of iron, or the presence of dissolved oxygen capable of oxidizing Fe(II) did, indeed, affect the nature of the product. Three of the major peaks in Figure 2.17 appeared to correspond to maghemite, γFe_2O_3. This would suggest that all of the Fe(II) had been oxidized to Fe(III) before precipitation. As in Figure 2.14, two additional peaks were seen at 22˚ and 48˚, probably corresponding to goethite, αFeOOH, and the silicon substrate on which the particles were mounted.

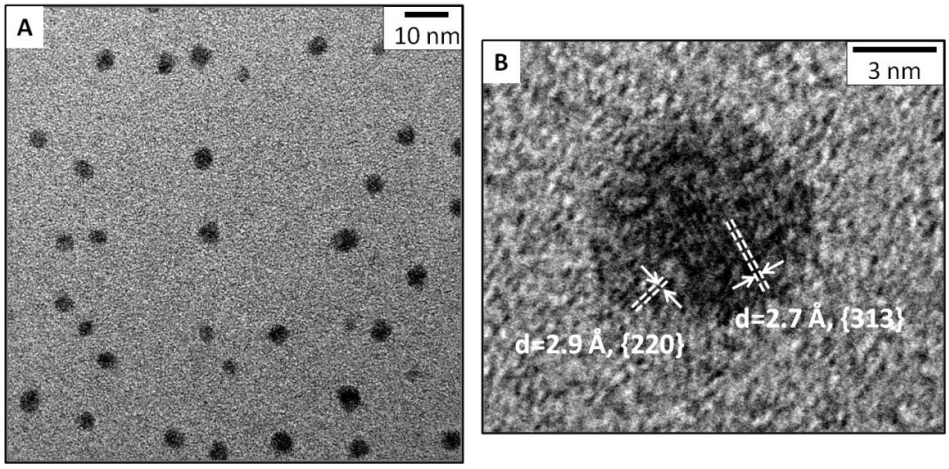

Figure 2.16: A) TEM Image of nanoparticles synthesized by hydrolysis of aerated solution initially containing 0.075 M $FeCl_3$ and 0.05 M $FeCl_2$. B) Zoomed image of a maghemite nanoparticle showing the spacing of the {220} and {313} crystal planes. Diameter of nanoparticles was 4.6 ± 0.7 nm.

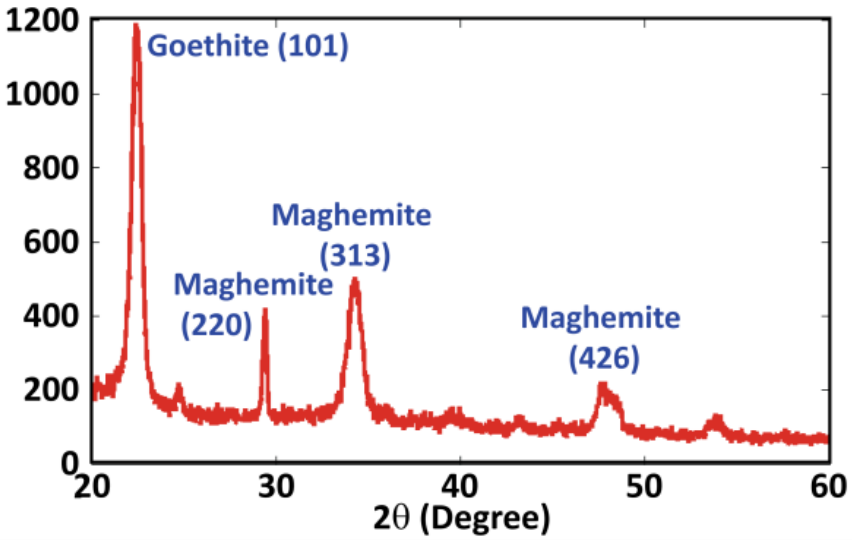

Figure 2.17: X-ray diffraction pattern of nanoparticles synthesized by hydrolysis of aerated solution initially containing 0.075 M $FeCl_3$ and 0.05 M $FeCl_2$. Three peaks correspond to maghemite, γFe_2O_3.

Precipitates of both methods were magnetic. Figure 2.18 shows the interaction of the precipitate, dispersed in acetone with a magnet; it is evident that nanoparticles were magnetic.

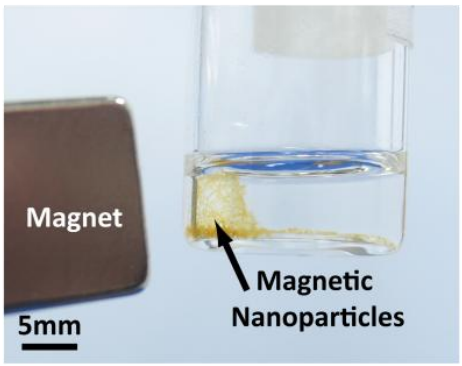

Figure 2.18: Interaction of nanoparticles dispersed in acetone with a magnet.

The magnetic behavior of the synthesized particles was analyzed using a super conducting quantum interference device (SQUID). Figure 2.19 shows the magnetization curve of the maghemite nanoparticles synthesized in the microreactor by hydrolysis of aerated solution initially containing 0.075 M $FeCl_3$ and 0.05 M $FeCl_2$. The magnetization of the particles increases linearly with the applied magnetic field with no hysteresis, characteristic of a paramagnetic material. Bulk maghemite is ferromagnetic; however, in the nanoparticulate form each nanoparticle acts as a single magnetic domain whose internal field aligns with the applied magnetic field; consequently a collection of maghemite nanoparticles displays paramagnetic characteristics. We analyzed the magnetic behavior of the nanoparticles synthesized by hydrolysis of deaerated solution initially containing 0.16 M $FeCl_3$ and 0.08 M $FeCl_2$. However the signal from the sample was very low, which might be due to the agglomeration of nanoparticles and existence of goethite in the sample, therefore these measurements were inconclusive.

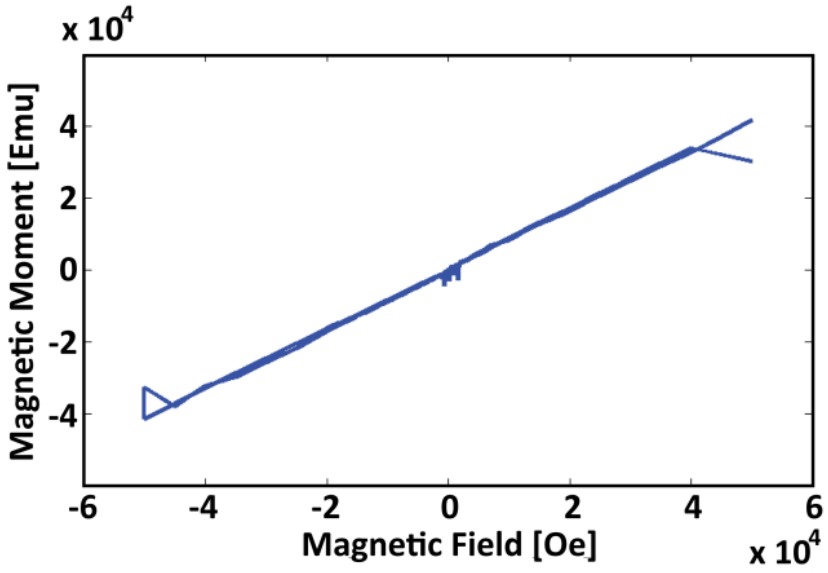

Figure 2.19: Magnetization curve of maghemite nanoparticles synthesized in a microreactor by hydrolysis of aerated solution initially containing 0.075 M $FeCl_3$ and 0.05 M $FeCl_2$. Particles show paramagnetic behavior.

2.6. Conclusion

In this chapter a droplet-based polyurethane microfluidic reactor that is fabricated by direct-writing with a CO_2-laser on a cured polyurethane substrate is demonstrated. Very smooth channel surfaces were obtained. This fabrication method is simple, cheap and less time consuming compared to methods such as soft lithography, hot embossing or silicon microfabrication. It is also shown that such a microreactor can be used to synthesize magnetic iron oxide nanoparticles with narrower size distributions than nanoparticles synthesized from similar solutions in batch reactors. The microreactor could be used to synthesize other types of nanoparticles by using appropriate reagents and controlling the flow rates of reagent streams to obtain the necessary residence times. The polyurethane substrate material has good resistance to acidic conditions, making it suitable for synthesizing nanoparticles of a wide range of oxide nanoparticles.

In conclusion, advantages of this microreactor include the easy fabrication methodology and good resistance to chemicals as well as biocompatibility. This microreactor is useful for the synthesis of nanoparticles at room temperature. For reactions that require high temperatures or longer residence times, materials such as glass and silicon would be suitable for fabrication. A microreactor that is designed for high temperature reactions aiming for high monodispersity and controllability of reaction conditions is introduced in Chapter 3.

2.7. References of Chapter 2

[1] Engel, J. M.; Chen, J.; Bullen, D.; Liu, C., "Polyurethane rubber as a MEMS material: characterization and demonstration of an all-polymer two-axis artificial hair cell flow sensor," in *IEEE MEMS*, Miami, FL.

[2] Piccin, E.; Coltro, W. K. T.; da Silva, J. A. F.; Neto, S. C.; Mazo, L. H.; Carrilho, E., "Polyurethane from biosource as a new material for fabrication of microfluidic devices by rapid prototyping," *J. Chromatogr. A,* vol. 1173, pp. 151-158, 2007.

[3] Becker, H.; Gartner, C., "Polymer microfabrication technologies for microfluidic systems," *Anal. Bioanal. Chem.,* vol. 390, pp. 89-111, 2008.

[4] Song, H.; Tice, J. D.; Ismagilov, R. F., "A microfluidic system for controlling reaction networks in time," *Angew. Chem. Int. Ed.,* vol. 42, pp. 768-772, 2003.

[5] Shestopalov, I.; Tice, J. D.; Ismagilov, R. F., "Multi-step synthesis of nanoparticles performed on millisecond time scale in a microfluidic droplet-based system," *Lab. Chip.,* vol. 4, pp. 316-321, 2004.

[6] Frenz, L.; El Harrak, A.; Pauly, M.; Begin-Colin, S.; Griffiths, A. D.; Baret, J. -C., "Droplet-based microreactors for the synthesis of magnetic iron oxide nanoparticles," *Angew. Chem. Int. Ed.,* vol. 47, pp. 6817-6820, 2008.

[7] Chung, C. K.; Shih, T. R.; Wu, B. H., "Design of a novel microreactor for microfluidic synthesis of silica nanoparticles," in *Transducers*, Denver, CO, 2009.

[8] Wu, W. I.; Sask, K. N.; Brash, J. L.; Selvaganapathy, P. R., "Polyurethane-based microfluidic devices for blood contacting applications," *Lab. Chip.,* vol. 12, pp. 960-970, 2012.

[9] Kim, S. H.; Yang, Y.; Kim, M.; Nam, S. -W.; Lee, K. -M.; Lee, N. Y.; Kim, Y. S.; Park, S., "Simple route to hydrophilic microfluidic chip fabrication using an ultraviolet (UV)-cured polymer," *Adv. Funct. Mater.,* vol. 17, pp. 3493-3498, 2007.

[10] Xu, S.; Nie, Z.; Seo, M.; Lewis, P.; Kumacheva, E.; Stone, H. A.; Garstecki, P.; Weibel, D. B.; Gitlin, I.; Whitesides, G. M., "Generation of monodisperse particles by using microfluidics: control over size, shape, and composition," *Angew. Chem. Int. Ed.,* vol. 117, pp. 734-738, 2004.

[11] Xu, Q.; Mayers, B. T.; Lahav, M.; Vezenov, D. V.; Whitesides, G. M., "Approaching zero: using fractured crystals in metrology for replica molding," *J. Am. Chem.Soc.,* vol. 127, pp. 854-855, 2005.

[12] Martele, Y.; Naessens, K.; Daele, P. V.; Baets, R.; Callewaert, K.; Schacht, E., "Micropatterning polyurethane surfaces with lasers," *Polym. Int.,* vol. 52, pp. 1641-1646, 2003.

[13] Nakayama, Y.; Matsuda, T., "Surface microarchitectural design in biomedical applications: preparation of microporous polymer surfaces by an excimer laser ablation technique," *J. Bimed. Mater. Res.,* vol. 29, pp. 1295-1301, 1995.

[14] Nakayama, Y.; Nishi, S., Ishibashi-Ueda, H.; Matsuda, T., "Surface microarchitectural design in biomedical applications: in vivo analysis of tissue ingrowth in excimer laser-directed micropored scaffold for cardiovascular tissue engineering," *J. Bimed. Mater. Res.,* vol. 51, pp. 520-528, 2000.

[15] R. Srinivasan, "Pulsed ultraviolet laser interactions with organic polymers—dependence of mechanism upon laser power," *Polym. Degrad. Stab.,* vol. 43, pp. 101-107, 1994.

[16] Suzuki, K.; Matsuda, M.; Hayashi, N., "Polymer resist materials for excimer ablation lithography," *App. Surf. Sci.,* Vols. 127-129, pp. 905-910, 1998.

[17] Klank, H.; Kutter, J. P.; Geschke, O., "CO2-laser micromachining and back-end processing for rapid production of PMMA-based microfluidic systems," *Lab. Chip.,* vol. 2, pp. 242-246, 2002.

[18] Jensen, M. F.; Noerholm, M.; Christensen, L. H.; Geschke, O., "Microstructure fabrication with a CO2 laser system: characterization and fabrication of cavities produced by

raster scanning of the laser beam," *Lab. Chip.,* vol. 3, pp. 302-307, 2003.

[19] Snakenborg, D.; Klank, H.; Kutter, J. P., "Microstructure fabrication with a CO2 laser system," *J. Micromech. Microeng.,* vol. 14, pp. 182-189, 2004.

[20] Liu, H. -B.; Gong, H. -Q., "Templateless prototyping of polydimethylsiloxane microfluidic structures using a pulsed CO2 laser," *J. Micromech. Microeng.,* vol. 19, pp. 037002-037009, 2009.

[21] Xia, Y.; Kim, E.; Whitesides, G. M., "Micromolding of polymers in capillaries: applications in microfabrication," *Chem. Mater.,* vol. 8, pp. 1558-1567, 1996.

[22] J. Powell, CO2 laser cutting, Berlin: Springer-Verlag, 1993.

[23] T. Brackbill, "Polymer microfluidic device for high-throughput single-cell encapsulation, lysis, and biological assay," University of California, Berkeley, 2012.

[24] Kandlikar, S. G.; Garimella, S.; Li, D.; Colin, S.; King, M. R., Heat transfer and fluid flow in minichannels and microchannels, Oxford: Elsevier Ltd., 2006.

[25] Karaağaç, Ö. Koçkar; Beyaz, S.; Tanrısever, T., "A simple way to synthesize superparamagnetic iron oxide nanoparticles in air atmosphere: iron ion concentration effect," *IEEE Trans. Magnetics,* vol. 46, pp. 3978-3983, 2010.

[26] Fang, M.; Strom, V.; Olsson, R. T.; Belova, L.; Rao, K. V., "Particle size and magnetic properties dependence on growth temperature for rapid mixed co-precipitated magnetite nanoparticles," *Nanotechnol.,* vol. 23, pp. 145601(1-9), 2012.

[27] Cornell, R. M.; Schwertmann, U., The iron oxides: structure, properties, reactions, occurences and uses, Weinheim: John Wiley & Sons, 2006.

Chapter 3

SILICON SUBSTRATE MICROREACTOR FOR HIGH TEMPERATURE REACTIONS

Temperature is one of the most important reaction parameters in the production of nanoparticles. Many nanoparticle synthesis reactions are thermally activated, for example hydrolysis of salts to generate oxides, or decomposition of organometallic precursors to generate semiconductors [1]. In order to obtain monodisperse or near-monodisperse size distributions, the nucleation and growth stages must be separated as explained in Chapter 1.2. In batch techniques with relatively large solution volumes, it is very difficult to achieve uniform temperatures throughout the reaction mixture for a specified amount of time, or to suddenly change the temperature. Thus it is difficult to separate nucleation and growth precisely, leading to broad size distributions. But in microfluidic systems solution temperatures can be controlled precisely and changed rapidly by controlling the temperature of different zones of the reactor through which the reaction mixture flows. A microreactor with multiple heated areas would also provide a platform for studying the effects of processing conditions temperature on the nanoparticle synthesis, thereby improving understanding of the underlying mechanisms.

In this chapter, a new microreactor that has thermally isolated heated and cooled zones is introduced. TiO_2 nanoparticles were selected as a model system to demonstrate the functionality of the microreactor, and study the effects of multiple nucleation and growth temperatures zones on the nanoparticle characteristics. First a review on high temperature microreactors in literature will be given; then the design of the silicon substrate microreactor will be explained followed by the description of the fabrication method. Finally the temperature control in this microreactor will be described and TiO_2 nanoparticle synthesis and characterization results will be discussed.

3.1. Review of High Temperature Microreactors

Several high temperature microreactors have been described in literature for the purpose of nanoparticle synthesis [2-13]. One of the fist examples of a high temperature

microreactor was introduced by Chan *et al*. [3]. This was a continuous flow; glass microreactor that was used for the synthesis of CdSe nanoparticles at elevated temperatures of 180-210˚C. They have studied the effects of change of temperature and residence time on the size and wavelength of nanoparticles. They obtained average nanoparticle sizes of 2.44, 2.54, 2.64, and 2.69 (±0.06 nm) as temperature increased from 180 to 210˚C in increments of 10˚C.

The next generation of their high temperature microreactor was a droplet-based, glass microreactor as introduced by Chan *et al.* [4] to synthesize CdSe nanoparticles. In this microreactor they used a droplet-based flow in order to prevent cross-contamination from channel walls. This study was one of the first microreactors in literature that explained the importance of droplet-based flow in nanoparticle synthesis for preventing the clogging of channels as well as avoiding residence time distributions in continuous flow profiles. These designs in [3] and [4] did not have a thermally isolated area; therefore every part of the reactor had to be heated and was at the same temperature.

Another type of high temperature reactors is capillary based systems which consist of capillary tubes [2, 6, 9, 11, 13, 14]. In these types of reactors capillary tubes are immersed in a heated oil bath. One of the good examples of this type of microreactors was introduced by Nightingale et al [6] as they were using droplet based flow unlike the other capillary reactors [2, 9, 11, 13, 14]. They synthesized CdSe, TiO_2 and Ag nanoparticles. They utilized droplet-based flow in the synthesis of CdSe and TiO_2 nanoparticles whereas they used continuous flow profile in Ag nanoparticle synthesis. They showed that continuous flow causes fouling in their channels. Their size distributions for CdSe nanoparticles were narrow, and were comparable to results of Chan et al. [4]; however they did not report the size distribution of their TiO_2 nanoparticles. The TEM image of their TiO_2 nanoparticles showed that particles were agglomerated and it was difficult to distinguish individual nanoparticles. Their synthesis of Ag nanoparticles resulted in polydisperse sizes of 12±4 nm and this might be mainly caused by the continuous flow profile used in this particular reaction.

Due to its high thermal conductivity, silicon substrate microreactors were also used in literature [5, 7, 8, 12]. Compared to capillary microreactors, microfabricated reactors have more flexibility in terms of their microchannel design. Also much smaller channels can be obtained in this type of reactors without being restricted by commercially available capillary tube sizes. Some of the high temperature microreactors utilize single-phase (or continuous flow profile) [2, 3, 5, 9-11, 13, 14] In single-phase microreactors, the Poiseuille flow profile resulting from the low Reynolds number dictates that, the residence time of fluid elements varies according to the radial position within the channel, which leads to a polydisperse size distribution. Particles precipitating from the stagnant layer immediately adjacent to the channel walls may adhere to the walls, leading to disruption of flow and ultimately blockage. In contrast, reactions in two-phase droplet-based microreactors occur within discrete droplets that pass through the microreactor with ideal plug flow, surrounded by an immiscible carrier phase [4, 6-8, 12, 15]. This provides several advantages, such as preventing nanoparticles from contacting the channel walls, providing a completely uniform residence time for all elements of the reacting fluid, and hence

uniform reaction time for nanoparticles to nucleate and grow.

Yen *et al.* designed a droplet-based, silicon substrate microreactor for high temperature synthesis of CdSe nanoparticles [7]. This was also one of the first high temperature microreactors reported for nanoparticle synthesis along with [3] and [4]. In this reactor there is one heated zone and one cooled zone that are thermally isolated from each other. This microreactor utilizes two-phase flow with gas and liquid phases. The gas phase is used to obtain segments of the reagent solution (liquid phase) and therefore prevent residence time distribution by avoiding the Poseuille flow profile. However the reagent solvent makes contact with the channel walls, which might eventually lead to cross contamination.

Almost all of the microreactors reported in literature have a single heated zone where nucleation and growth of particles happen concurrently at the same temperature. Yang et al. introduced a capillary based microreactor for the purpose of having a high temperature zone followed by a low temperature zone [13]. However due to the lack of thermal isolation between these two zones, there was a thermal gradient in between these two zones. Thermal gradients might cause some further chemical activity occurring between the two regions, disabling the possibility to separate nucleation and growth.

Winterton *et al.* introduced the concept of a microfluidic reactor fabricated in silicon with thermally isolated zones in which nucleation and growth could occur [15]. These authors also investigated the ability to maintain sharply different temperatures on a single wafer. This microreactor also utilized a droplet based flow. The fabrication process was designed and performed by Fung *et al.* [16]. However this microreactor was not demonstrated for nanoparticle synthesis, it was only tested for uniform droplet generation.

The microreactor introduced in this chapter builds on Winterton's earlier work to fabricate a functioning multi-temperature zone microreactor on a silicon substrate. It has thermally isolated heated and cooled zones. TiO_2 nanoparticles were selected as a model system to demonstrate the functionality of the microreactor, and study the effects of nucleation and growth temperatures on the nanoparticle characteristics. TiO_2 micro and nanoparticles are used in paints, cosmetics and the food industry [18] as well as in solar cell and sensor technology [19].

3.2. Design of the Multi-Temperature Zone Microreactor

The microreactor utilizes two-phase flow with thermally isolated heated and cooled regions, and passive generation of droplets. The schematic of the microreactor is shown in Figure 3.1. The microreactor is fabricated on a silicon substrate and sealed by a Pyrex wafer on top. The microchannels are 200 μm in width and depth. In this section the design details of this microreactor will be explained.

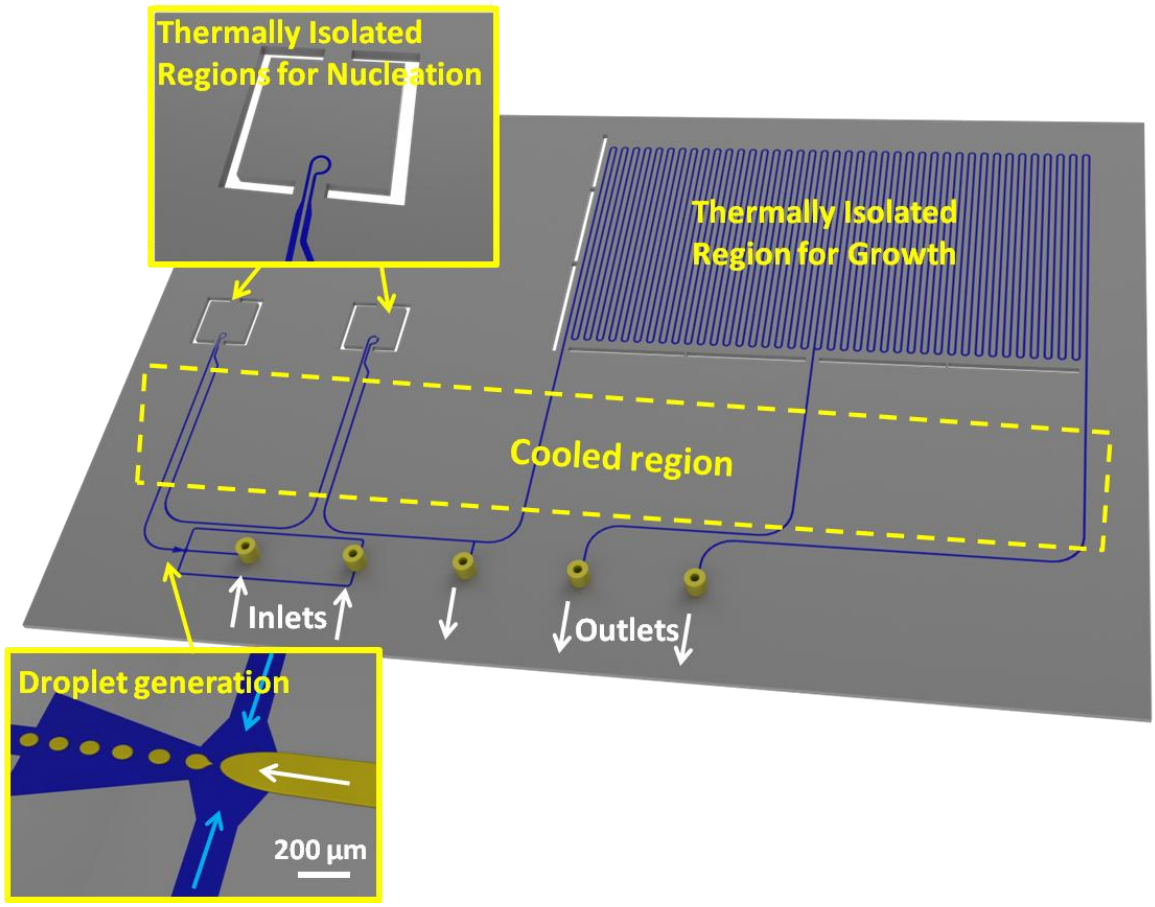

Figure 3.1: Schematic of the microreactor designed for high temperature nanoparticle synthesis reactions. The microreactor has thermally isolated heated and cooled zones and it utilizes a droplet-based flow profile.

3.2.1. Droplet Generation

As discussed above, two-phase flow provides uniform residence times for given fluid elements throughout their passage through the reactor, and prevents deposition of nanoparticles on the channel walls, with attendant disruption of flow. Also the circulating velocity profile inside droplets maintains continuous mixing of reaction liquid therefore maintains uniform residence times as well as temperatures for all nanoparticles. For stable, continuous operation, droplet generation should be stable and the droplet size uniform.

In order to ensure uniform reaction conditions throughout the system, every generated droplet should be of the same size. Droplets form by the shear force applied by the carrier fluid. The shear rate in a channel is given as

$$= \frac{V_c}{w} = \frac{Q_c}{w^2 d} \quad (1)$$

where G is the shear rate, V_c is the flow velocity, w is the channel width, Q_c is the volumetric flow rate and d is the channel depth. As it is seen from the equation above, the shear rate is dependent on the channel width and it increases with the decreased width.

Droplets within an immiscible carrier fluid are generated by using a tapered channel to form uniform and stable droplets following the method in [20]. The schematic of the droplet generation design is shown in Figure 3.2. Droplets form as a result of the carrier phase impinging on the continuous stream of dispersed phase, applying shear stress to pinch the stream. With this design the flow velocity changes as the width of the channel changes and it is maximum at the narrowest location. This designed gradient ensures that there is only one maximum point of velocity, and therefore stress within the generation unit where the break-up of droplets can occur. The numerical analysis of this phenomenon is shown in Figure 3.3; which shows the velocity field of fluids inside the droplet generation unit. Droplets always break up at the location of maximum shear stress. If the channel after the meeting point of the carrier and discrete phases was a straight channel, velocity would be uniform and droplet formation would not be guaranteed to occur at the same location at each time. Having a point of maximum velocity ensures uniform and stable droplet generation.

Figure 3.4 shows the real time images of the formation of droplets and droplets in the growth zone respectively. Carrier fluid and the droplet phase are delivered to the microreactor by using syringe pumps. The flow rate of the carrier phase (hexadecane) was 800 µL/hr and the droplet phase (deionized (DI) water) was 100 µL/hr.

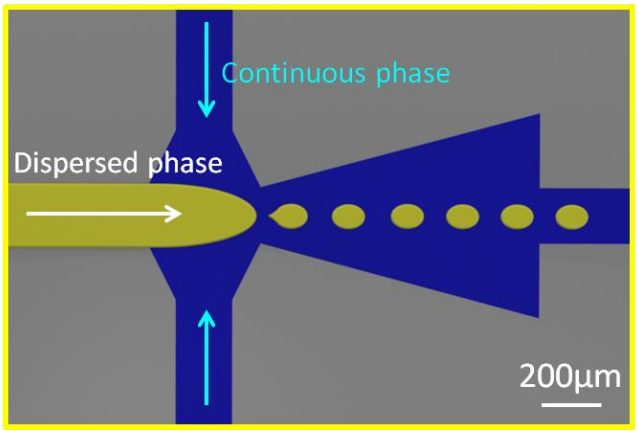

Figure 3.2: Schematic of the microreactor droplet generation unit.

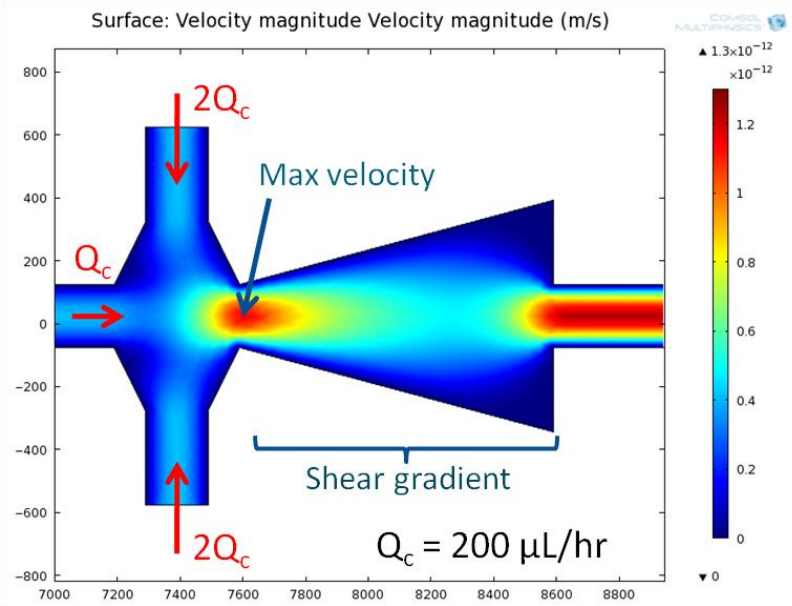

Figure 3.3: Velocity distribution in a tapered microchannel. As seen from the image, there is one maximum velocity point at the junction. This is the location where droplet breaks-up. Simulation is performed in COMSOL Multiphysics program.

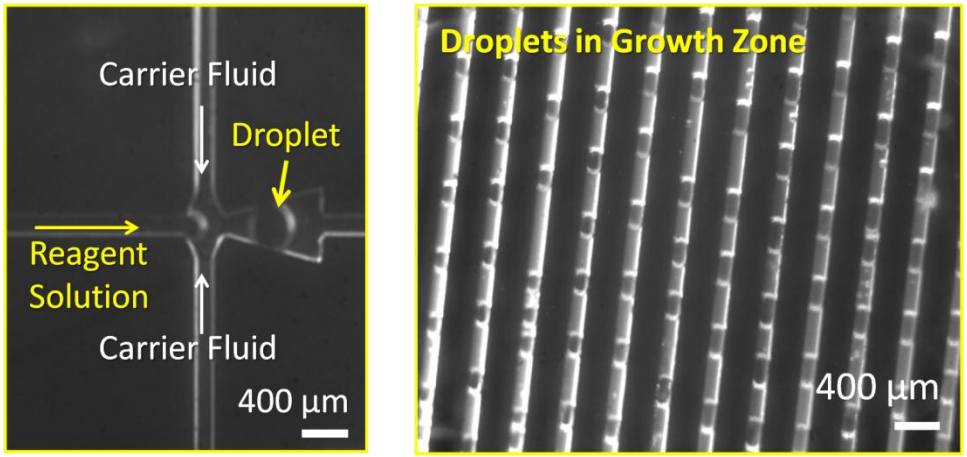

Figure 3.4: Real time images of the droplet generation and droplets in the growth zone.

3.2.2. Thermally Isolated Heated Regions

The microreactor has multiple temperature zones in order to separate nucleation and growth of particles as well as to provide a platform to study the effects of temperature and residence time on the product characteristics. There are three reaction zones that can be heated independently and the rest of the microreactor is cooled by using a cooling channel to quench reactions when solvents exit the reaction zones. These heated and cooled zones are thermally isolated from each other by through etched silicon substrate with an

isolation gap of 0.5 mm around the zones. Figure 3.5 shows the detailed view of heated zones.

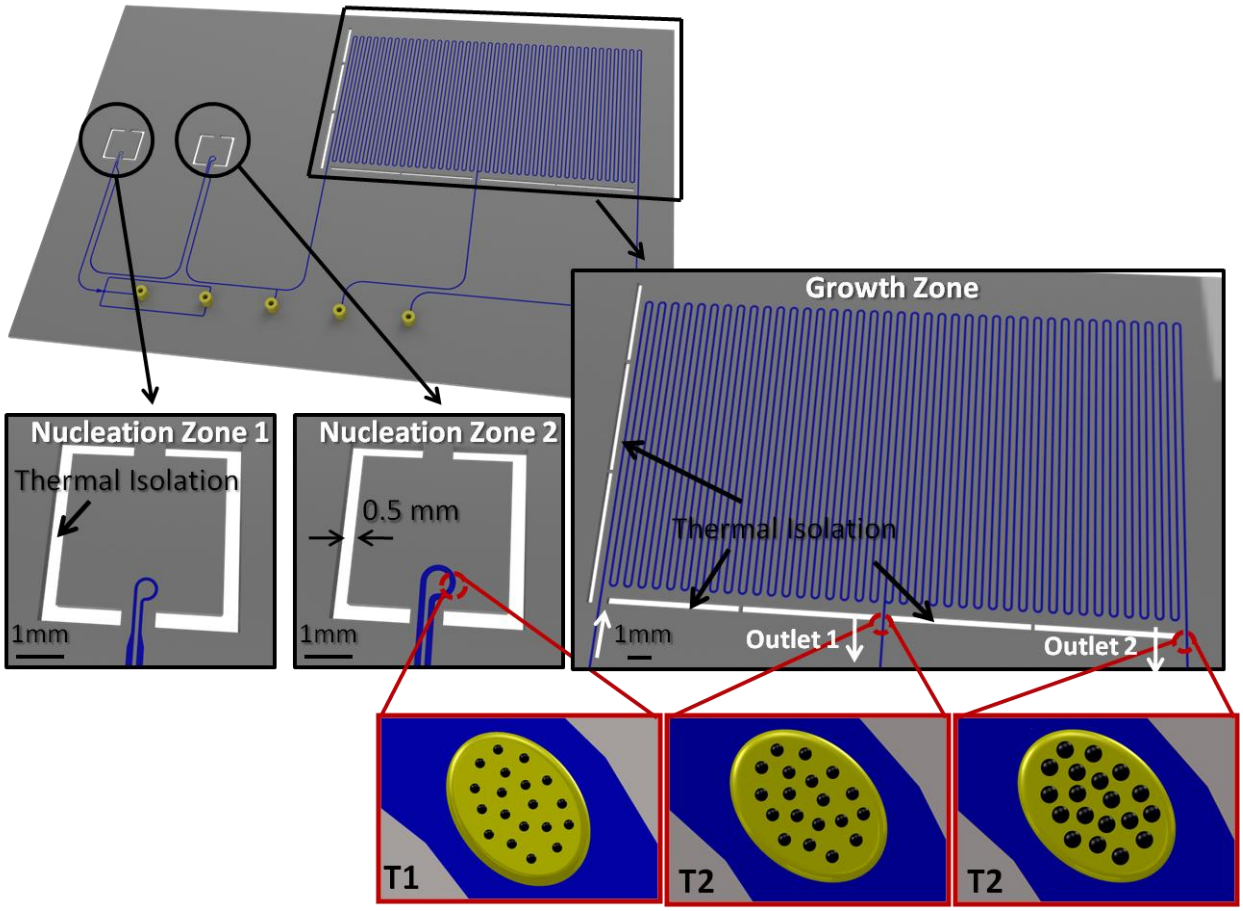

Figure 3.5: Schematic showing the details of the nucleation and growth zones of microreactor. There are two nucleation zones with same length of microchannel but different width. The channel width in the first and second nucleation zones is 100 μm and 200 μm respectively. The growth zone composed of a much longer channel (4 m) with a width of 200 μm. The bottom schematic shows the formation of nanoparticles in droplets inside these zones. 'T' refers to the temperatures at the reaction zones. Nucleation zones can be kept at different temperatures than the growth zone.

Two of the reaction zones are short. These were designed as the nucleation zones for high temperature reactions. These two zones have different channel widths to offer two different residence time options for a given flow rate. In general, only one nucleation zone would be active at a given time. After nucleation, droplets travel to the next reaction zone after passing through the cooled region (not shown in the schematic) to quench the nucleation.

The third zone is longer than the nucleation zones and can be used for slower processes, such as growth of nuclei. This growth zone was designed with two different outlets, to allow discharge of product from either the middle or the end of the zone, thereby offering two different possible growth times.

These regions are heated by using ceramic heaters attached at the bottom surface of the microreactor. The heating and cooling elements are discussed in Chapter 3.4.

Outlets in the microreactor could also be used to inject additional reagents, such as ligands or stabilizers, or even additional reactants for forming hybrid nanocomposite particles. In this work, however, they were used to discharge the reaction mixture at different stages for characterization.

3.3. Fabrication

Microreactor was fabricated on a silicon substrate in the Marvell Nanofabrication Facility at UC Berkeley. Two different chrome masks were used in the fabrication. The first mask defines the microchannels; the second mask defines the thermal isolation trenches. In order to ensure thermal isolation, through etching of silicon around the heated zones is required. Thermal isolation and microchannels were formed by deep reactive ion etching of silicon. At the end of the fabrication process, Pyrex wafer is anodically bonded to the silicon substrate to encapsulate microchannels. Figure 3.6 shows the fabrication steps.

The fabrication steps can be listed as follows:

1. After cleaning the wafers, the first step is low temperature oxide (LTO) deposition at 350˚C inside furnace. This forms an oxide layer of 2 μm on silicon surface.

2. The back side oxide layer is removed by wet etching in buffered HF (BHF) solution. This is done with the help of a plastic bucket filled with BHF. The top of the silicon wafer is coated with photoresist (PR) to protect the top oxide layer. Bottom surface of the wafer is floated on the surface of the BHF. Within one minute, the backside oxide is etched. After the oxide removal step, the PR on the photoresist is removed, the wafer is cleaned and a new layer of G-line PR is coated on the wafer.

3. Photoresist is patterned with the first mask by using the photolithography method. This mask defines the microchannels.

4. The oxide layer is etched by using dry etching with CF_4 and CHF_3.

5. The photoresist is removed with O_2 plasma.

6. Five layers of PR layer are coated. After the coating wafer is hard baked at 120˚C for 12 hours.

7. Second mask is used for patterning the PR that will determine the thermal isolation trenches.

8. The silicon is etched with deep reactive ion etching until a 200 μm of substrate is left. This 200 μm is the defined depth of channels.

9. Photoresist is removed with PRS 3000 solution. At this stage removing by O_2 plasma is not possible as PR is hard baked in step 6.

10. The wafer is attached to a handle wafer by using a thermorelease tape. This tape is detachable from the surface when it is heated.

11. The silicon is etched with deep reactive ion etching and at the end of this step, both microchannels and trenches are formed.

12. Handle wafer is removed by baking on a hot plate at 120˚C for less than one minute.

13. Oxide layer on top of the silicon substrate is removed with BHF.

14. Wafer is cleaned with piranha solution.

15. A Pyrex wafer is anodically bonded to the silicon wafer. Pyrex allows observation of the reaction channels and also has low thermal conductivity compared to silicon so it prevents large thermal conduction on the top surface.

16. As a final step, the bonded wafer is cut around the microreactor for removing extraneous parts of the wafer that do not belong to the microreactor system.

The image of the microreactor right before step 13 is shown in Figure 3.7. The parallel lines that appear near the inlets and between the nucleation zones were added to equalize the etch rate throughout the wafer. In deep reactive ion etching, the etch rate is higher in larger surfaces exposed to the plasma. Since the growth region has a larger surface area than other parts of the microreactor, the parallel lines were added in relatively less dense parts of the design.

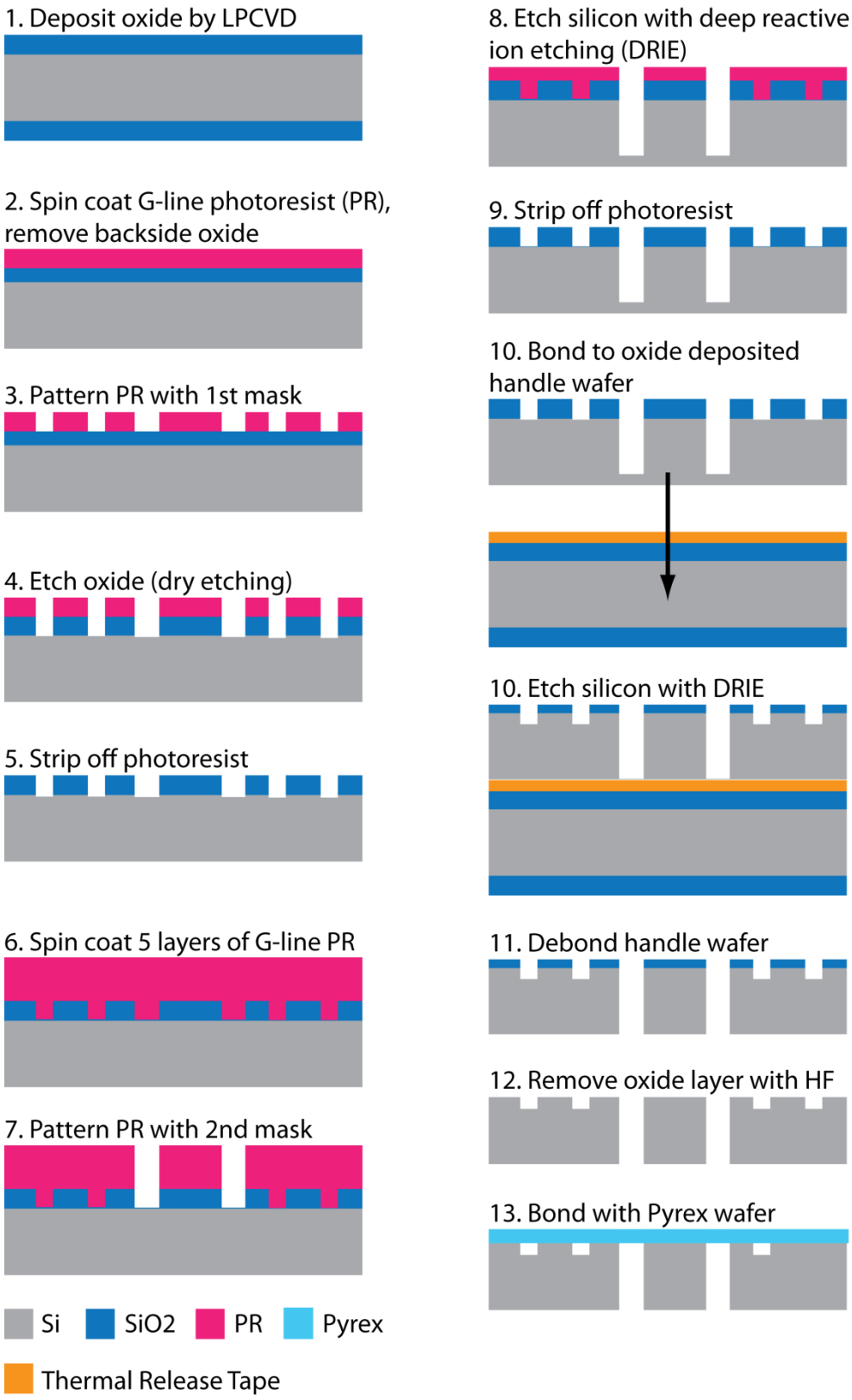

Figure 3.6: Schematic of the fabrication steps of the silicon substrate microreactor.

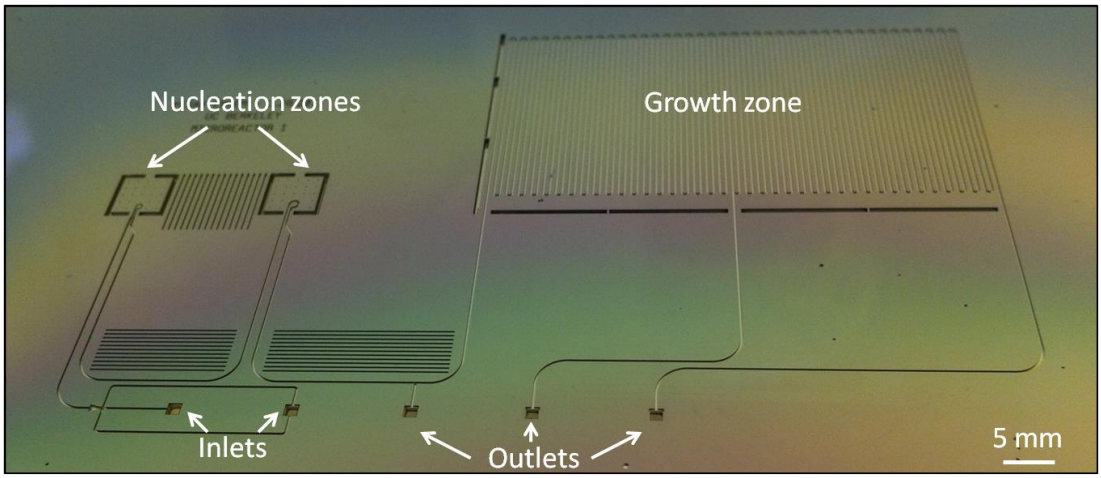

Figure 3.7: Fabricated microreactor after step 13.

3.4. Thermal Control

Temperature control of the microreactor is essential for maintaining uniform reaction conditions for all nanoparticles. The microreactor has both heating and cooling units that are thermally isolated from each other.

3.4.1. Heating

Reaction zones were heated by using external ceramic heaters (Sakaguchi E. H. Voc Corp.) attached on the silicon surface (back side) of the microreactor as demonstrated in Figure 3.8. For heating the nucleation zone we used a ceramic heater that is exactly the same size as the reaction zone (5 mm × 5 mm). For heating the growth zone, two 2.54 cm × 2.54 cm ceramic heaters were used. Heaters are attached by using a thermo paste to prevent any air gap between surfaces and clamped on the substrate by using C-clamps. Thermocouples are attached to the microreactor to monitor the temperatures.

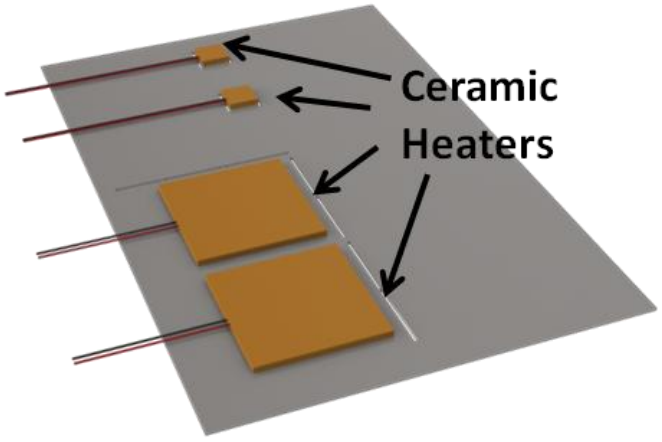

Figure 3.8: Schematic of ceramic heaters and their attachment to the microreactor.

3.4.2. Cooling

The microreactor was cooled with an aluminum block with an engraved fluid channel through which cooled water is passed. This block is shown in Figure 3.9. The Al block makes contact with the silicon surface of the microreactor close to the heated regions, such that it quenched fluid emerging from the heated zones, to suppress nucleation or growth outside of the heated zones, assuring well defined residence times at a given temperature, as well as increasing thermal gradients.

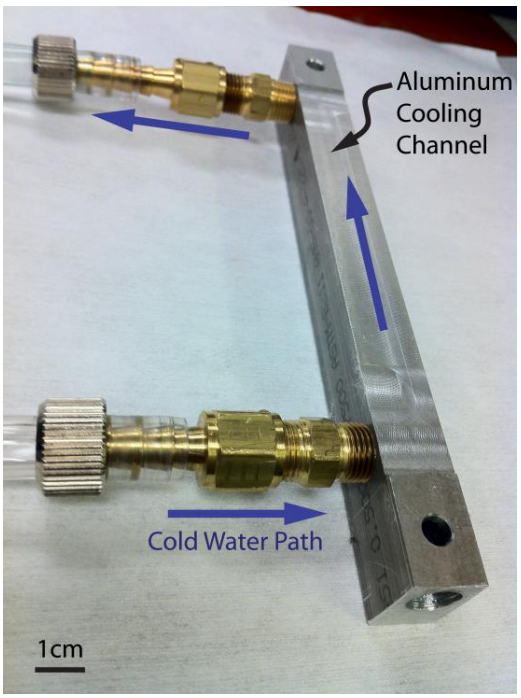

Figure 3.9: Cooling channel made out of Al block to cool the microreactor. It is attached to a coolant system that pumps water through the channel.

The cooling channel is attached such that it makes contact with the bottom surface of the microreactor as demonstrated in Figure 3.10. The schematic of the cooling channel is not exactly the same as the actual channel shown in Figure 3.9; it is just for demonstration of the attachment.

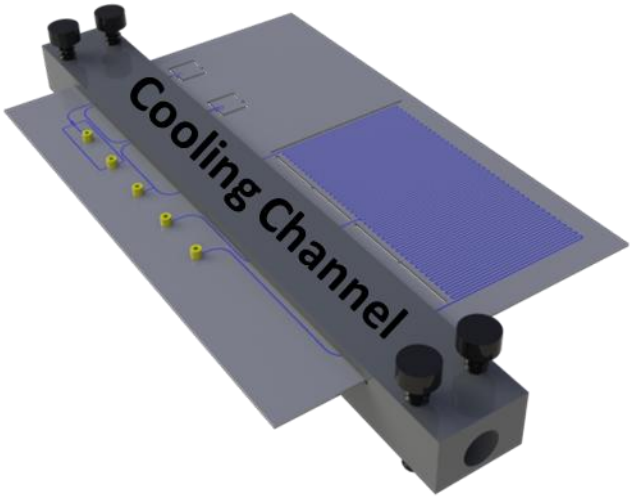

Figure 3.10: Cooling channel attachment to the microreactor.

3.4.3. IR Camera Measurements

In order to show that thermal isolation is maintained we have imaged the heated and cooled zones of the microreactor by using an IR camera (FLIR Systems, A325sc). Figure 3.11 shows the IR camera image of the reactor in operation. This method was useful to observe thermal isolation between the heated zones and the cooled zone.

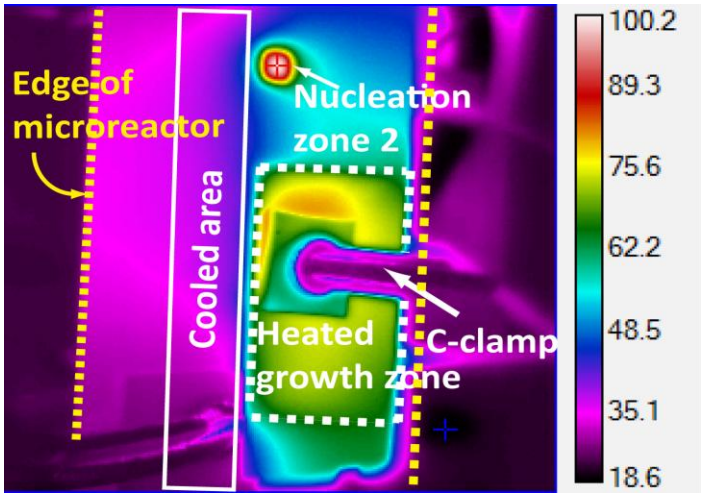

Figure 3.11: IR image of the heated microreactor in operation. The image shows the top view (Pyrex side) of the microreactor; heaters were attached to the bottom of the Si wafer.

Figure 3.11 shows that there is a very steep thermal gradient in the vicinity of the nucleation zone. The thermal isolation is clearly effective with the result that fluid flowing into this zone would heat up rapidly, and then cool rapidly upon leaving the nucleation zone. The cooling channel maintains the unheated regions of the microreactor at about 35˚C. Although the temperature between the two heated zones is somewhat higher, there is no microchannel in this area therefore cooling is not necessary.

Even though the thermal conductivity of Pyrex is much lower than Silicon, there is still heat being conducted through Pyrex according to the IR camera results. Therefore a better thermal control could be achieved with having through etched zones in the top Pyrex layer as well. However this would bring additional fabrication steps. It is also evident that the clamp used to hold the large ceramic heaters to the growth zone served as a local heat sink. Future versions of the microreactor will use a different method.

3.5. Experimental Results of Nanoparticle Synthesis

3.5.1. Materials

Titanium (III) chloride solution (~10wt. % in 20-30 wt. % hydrochloric acid, Sigma-Aldrich) and sodium hydroxide (1 N, Fisher Scientific) were used to prepare the aqueous solution (dispersed phase). Sodium oleate, octadecane and Span 80 were obtained from Sigma-Aldrich.

3.5.2. Experimental Set-up

Experimental set-up of the microreactor system consists of the microreactor, ceramic heaters for heating, the cooling channel, water cooling system to deliver cold water to the cooling channel, a high-speed camera for observation and imaging, two syringe pumps to deliver reagents, two power supplies for ceramic heaters, thermocouples for temperature measurements, a thermocouple reader and a frame that holds the microreactor such that it only contacts the heating and cooling units. The schematic of this experimental set-up is shown in Figure 3.12. The frame is not shown in the schematic for simplicity.

The inlet and outlet fluidic interconnects were purchased from LabSmith and bonded onto the microreactor with an epoxy. Silica capillary tubing (purchased from LabSmith) was used to deliver reagents from glass syringes to the microreactor.

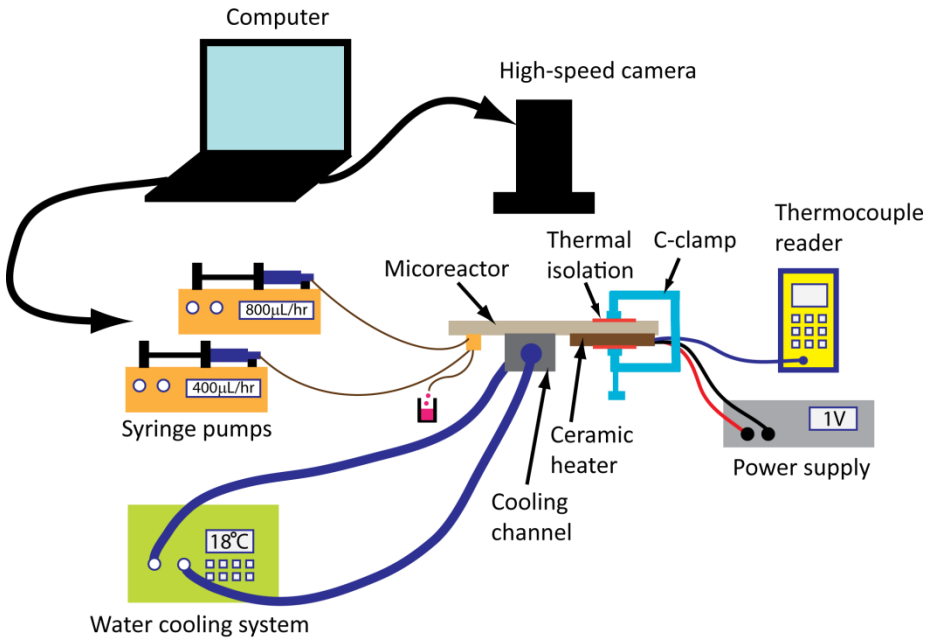

Figure 3.12: Schematic of the experimental set-up for nanoparticle synthesis.

3.5.3. Synthesis Method

TiO_2 nanoparticles were synthesized inside the microreactor via hydrolysis and oxidation of $TiCl_3$ by following the method of Cassaignon et al. [21]. The hydrolysis reactions that create TiO_2 nanoparticles are very sensitive to temperature, pH and solution concentration. In this study the solution chemistry was kept constant, and the impact of temperature and residence time on the resulting nanoparticles was studied. The aqueous reagent was prepared by partially neutralizing 0.15M $TiCl_3$ solution (in 20-30 wt. % hydrochloric acid) using 0.25 M NaOH to a pH of 0.5 [21]. A 2 wt% solution of Span 80 in octadecane was used as the carrier phase.

The reaction product was collected at the outlets of the microreactor in a small beaker. After the synthesis, the collected sample was centrifuged with a 2:1 mixture of acetone and ethanol to remove the octadecane with surfactant and to disperse the nanoparticles in acetone. The centrifuge was done by using acetone and ethanol with a mixing ratio of 2:1 multiple times at 4000 rpm for 15 min. Nanoparticles were eventually dispersed in acetone.

3.5.4. Results and Discussion

TiO_2 nanoparticles were synthesized in the microreactor under several different temperature and residence time conditions to investigate the effects of these parameters. In this section the results from these various reaction conditions will be presented.

The hydrolysis reactions responsible for the formation of TiO_2 proceed via the formation of hydroxo-bridged oligomers that grow, dehydrate, and gradually increase in crystallinity. Unless there is a significant driving force, such as high pH, hydrolysis reactions are slow at

ambient temperature. The microreactor affords the opportunity to observe the impact of temperature and time on particle characteristics.

Several different temperature and residence time combinations were probed. In all these experiments the unheated parts of the microreactor were kept at room temperature by using the cooling set-up.

As a first step, only the nucleation zone was used. Three different nucleation temperatures were applied and their effects were studied. In all of these experiments, the second nucleation zone (with channel width 200 μm) was used while keeping the rest of the microreactor at room temperature. The flow rate was controlled to provide a 6s residence time in the nucleation zone. The nucleation zone was heated to 35˚C, 70˚C and 100˚C. The TEM images of the material extracted immediately after nucleation at 35˚C, 70˚C and 100˚C are shown in Figure 3.13, Figure 3.14 and Figure 3.15 respectively. The TiO_2 particles appear sheet-like, not yet in a discrete form, and agglomerated. As the temperature of the nucleation zone was increased, relatively more organized structures were formed. It can also be observed that small particles are formed and accumulated in spherical clusters. This accumulation is to reduce the surface area and therefore the surface energy. The average sizes of these clusters were similar at different nucleation temperatures. Figure 3.14D shows this type of a cluster formed with nucleated particles. This is similar to an oligomerization process which produces films as a result of a given kinetic energy to the system. Kinetic energy moves atoms and bonds and a metastable structure is formed. In this case, a sheet of titanium hydroxide oligomers was formed. When enough kinetic energy is given, more organized structures – individual nanoparticles- can be obtained.

TiO_2 nanoparticle synthesis is different than quantum dot synthesis where free precursors are formed with applied heat and when they reach the concentration saturation limit nucleus of particles are formed. This is named as 'nucleation'. The formation of TiO_2 sheet-like structures can also be referred as nucleation as there is still an 'embryo' formation even though we cannot distinguish individual nuclei. Therefore the same terminology of 'nucleation' and 'growth' will be used for TiO_2 nanoparticle synthesis.

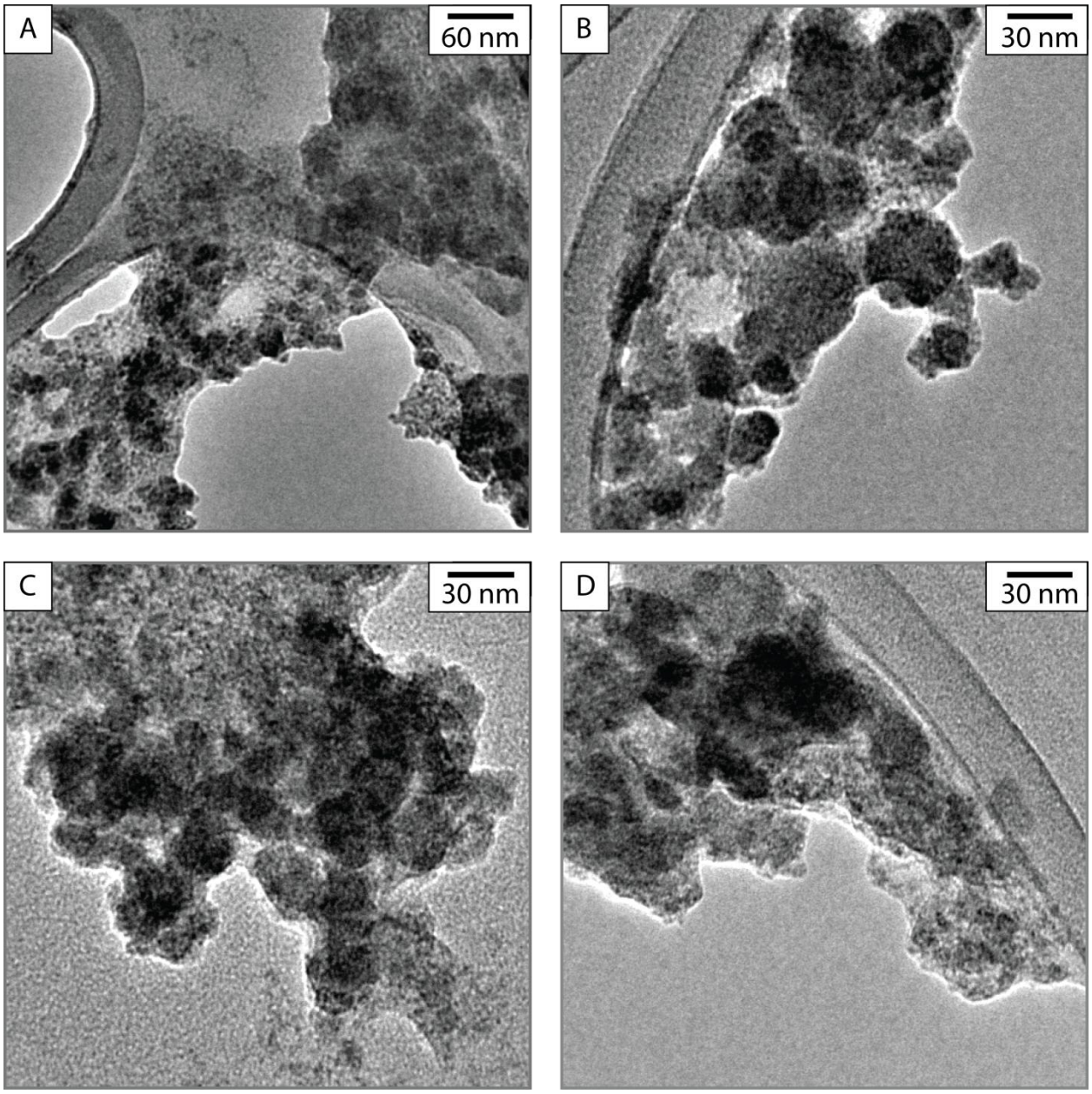

Figure 3.13: TEM images of TiO_2 nanoparticles nucleated at 35˚C for 6s without any further growth.

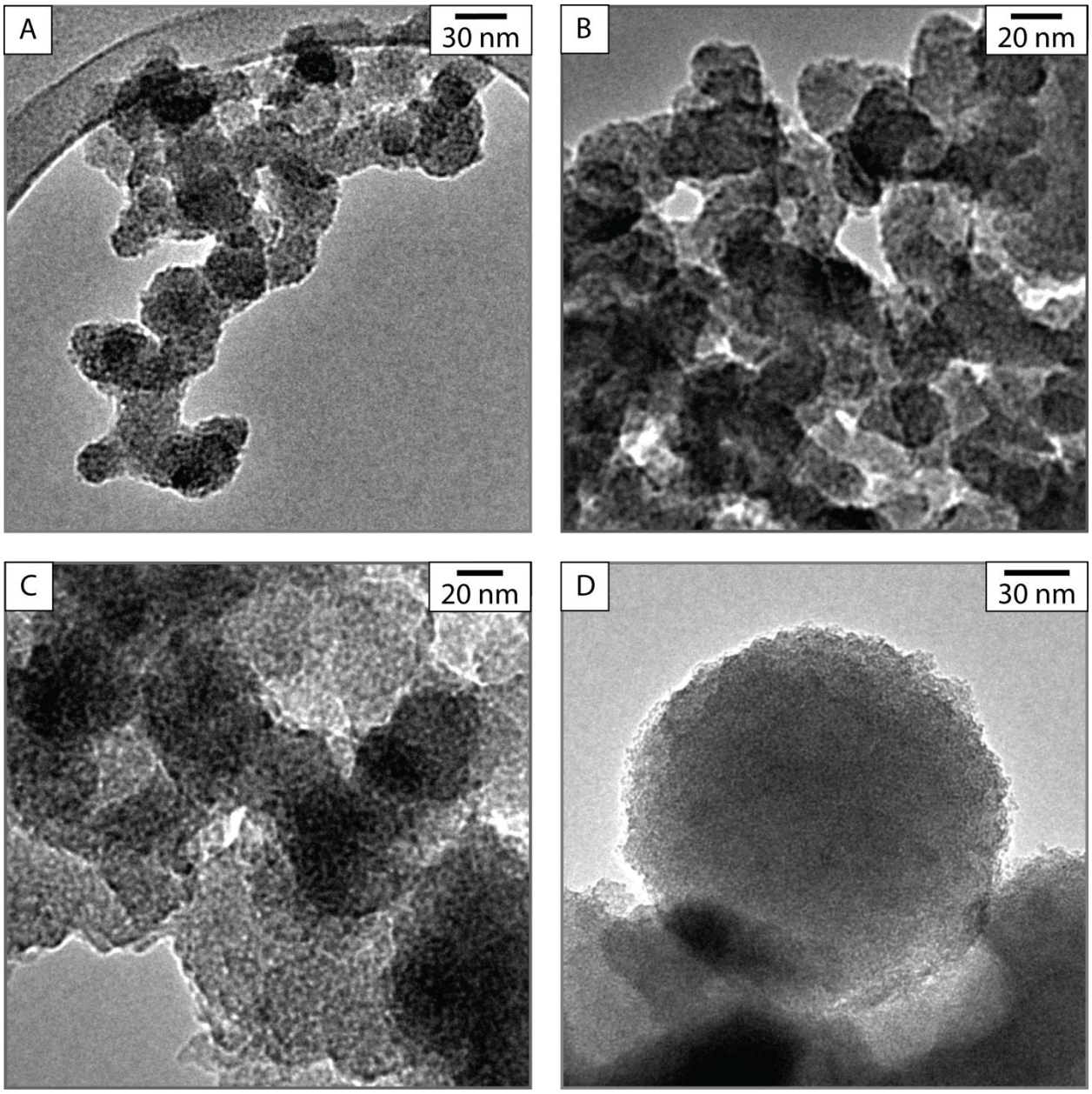

Figure 3.14: TEM images of TiO_2 nanoparticles nucleated at 70˚C for 6s without any further growth.

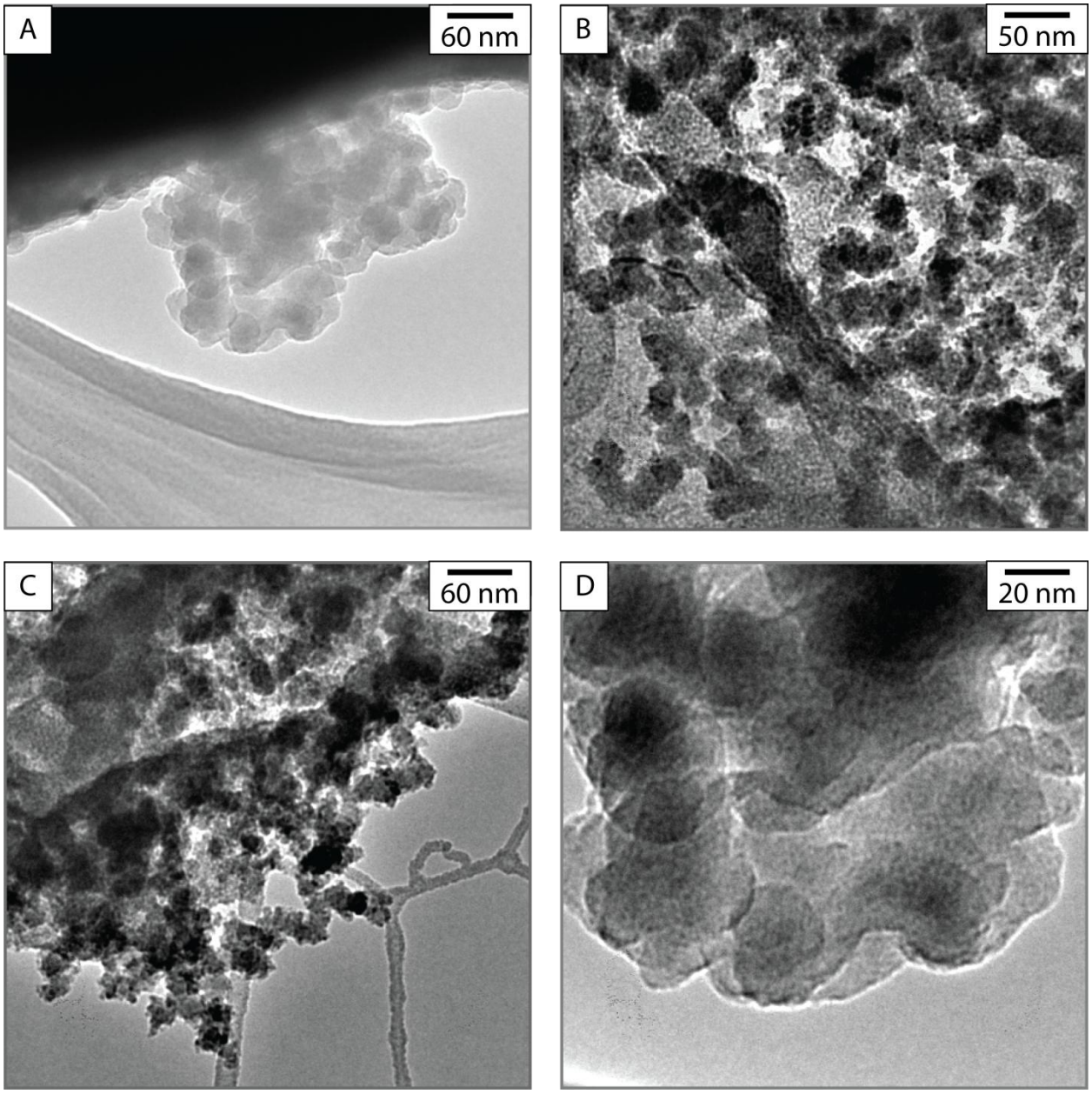

Figure 3.15: TEM images of TiO_2 nanoparticles nucleated at 100˚C for 6s without any further growth.

Next, the effect of growth zone on nanoparticle formation was studied. The nucleation zone was again held at 35˚C but the fluids passed through the first half of the growth zone held at 70˚C, before discharge. The residence time was 6s in the nucleation zone and 120s in the growth zone. Figure 3.16 shows the product. It is apparent that holding for 120s at 70˚C did, indeed allow the particles to grow, and form organized, separated structures of spherical particles. The size distribution of particles was not very uniform; the average size of their diameter was 189.2 ∓ 28.7 nm.

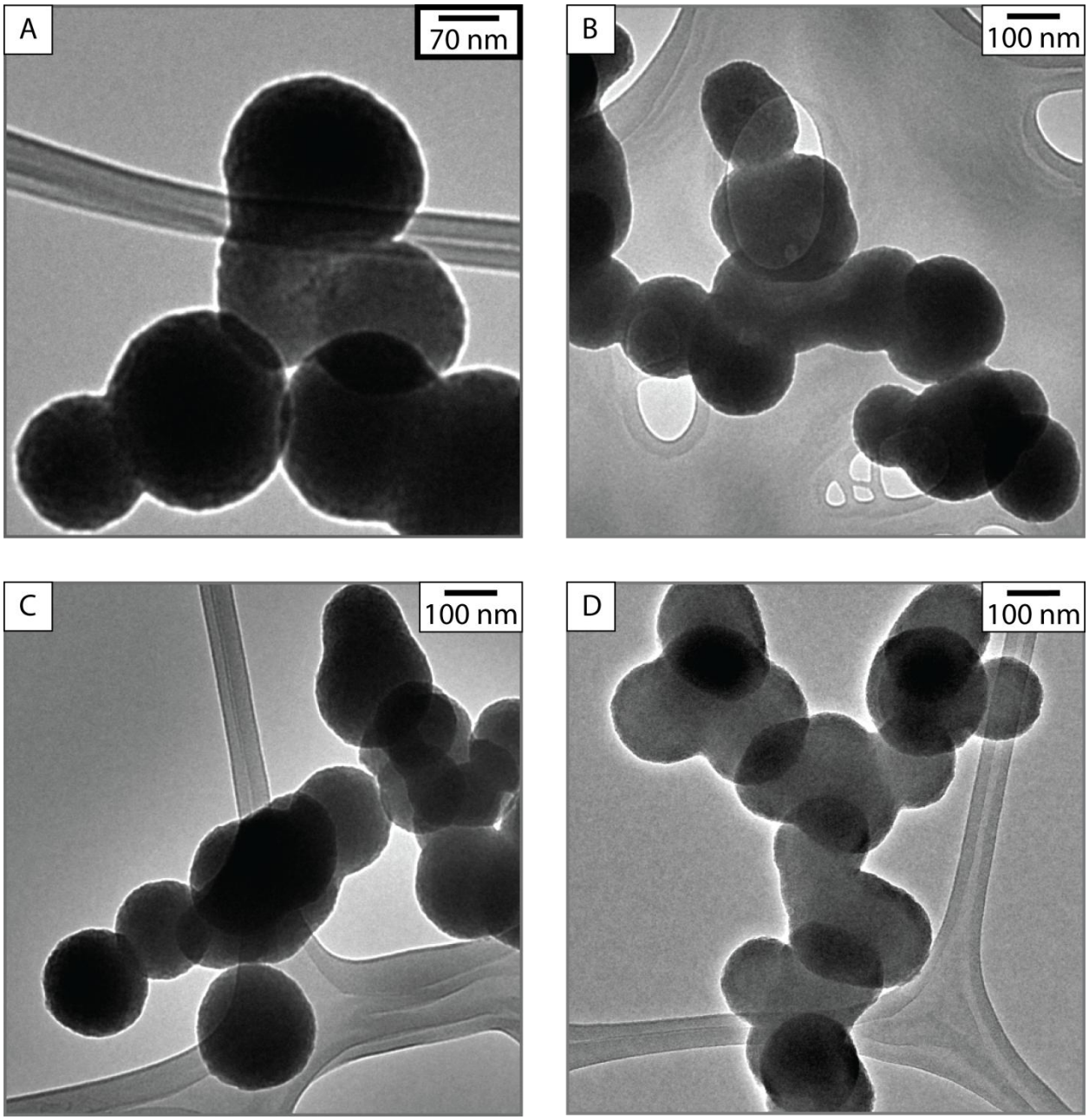

Figure 3.16: TEM images of TiO_2 nanoparticles nucleated at 35˚C for 6 s and grown at 70˚C for 120 s. The average size of nanoparticles was 189.2∓ 28.7 nm.

Nanoparticles that were nucleated at 70˚C for 6 s (Figure 3.14) were also grown at 70˚C for 114 s (120s for a total time of nucleation and growth). TEM images of the product are shown in Figure 3.17. These particles were much smaller than the ones that were nucleated at 35˚C. The average size of these particles was 5.2∓0.3 nm. Crystal planes of these nanoparticles are noticeable from the TEM images. This shows that with the increase of nucleation temperature, size of particles decreased and also they became crystalline. Their size distribution was also better.

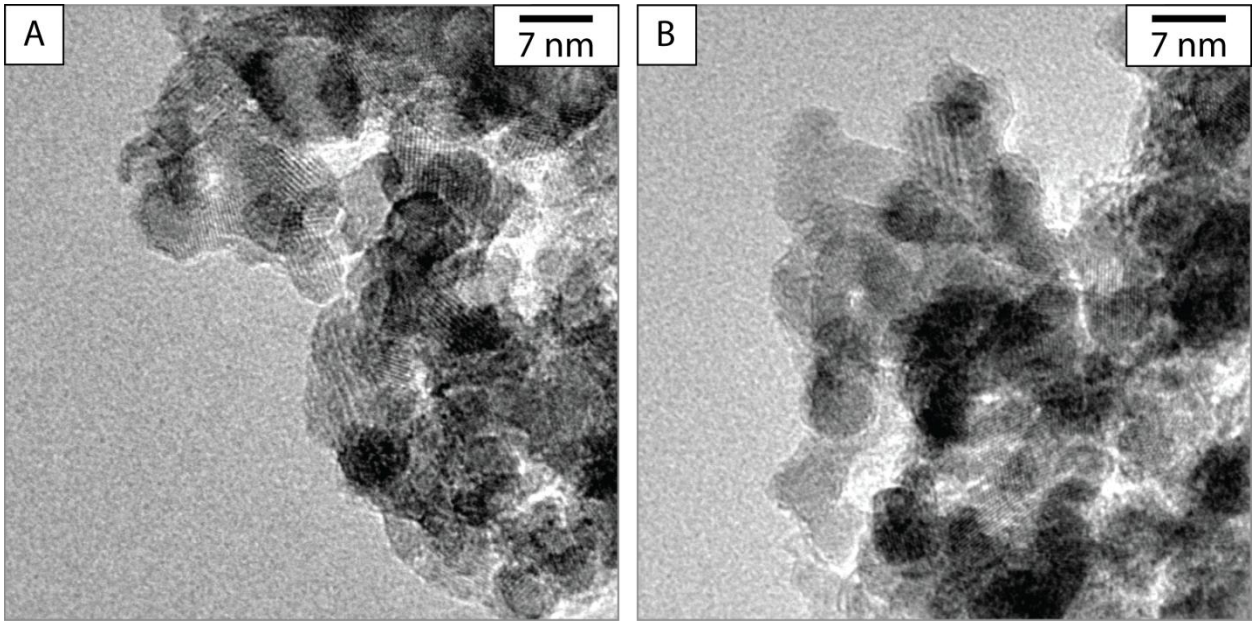

Figure 3.17: TEM images of TiO_2 nanoparticles nucleated at 70˚C for 6s and grown at 70˚C for 120s. The average size of these particles was 5.2∓0.3nm.

Nanoparticles that were nucleated at 100˚C were also grown at 70˚C for 120 s. The TEM images of these particles are shown in Figure 3.18. From these TEM images, it appears that a finer grade is obtained with high temperature nucleation and a secondary rearrangement might have happened. However it was not possible to obtain a reliable size distribution from the TEM images.

The effect of growth temperature can be understood by having the same nucleation temperature and varying the temperature of the growth zone. This time, the nucleation temperature and time was kept at 100˚C and 6s respectively and the temperature of the growth zone was increased to 80˚C with a residence time of 120 s. The TEM images of the resulting nanoparticles were shown in Figure 3.19. The average size of nanoparticles in Figure 3.19 was approximately 42.6nm∓8.12 nm. When the images in Figure 3.15, Figure 3.18 and Figure 3.19 are compared, it is seen that with growth and with higher temperatures more organized structures were formed. This can be attributed to the fact that crystalline regions grow further and form discrete particles when enough energy is supplied to the system.

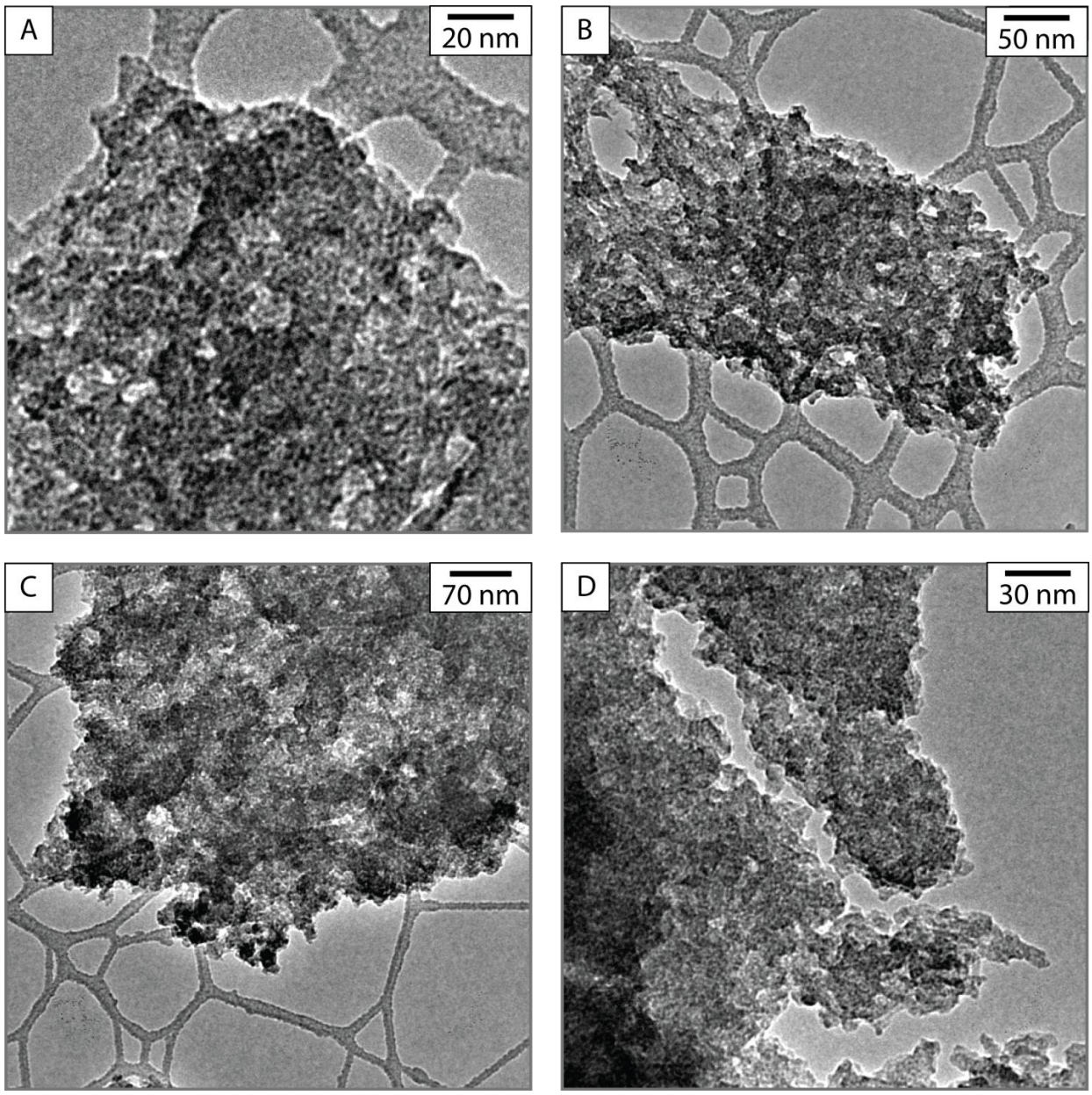

Figure 3.18: TEM images of TiO_2 nanoparticles nucleated at 100°C for 6 s and grown at 70°C for 120 s.

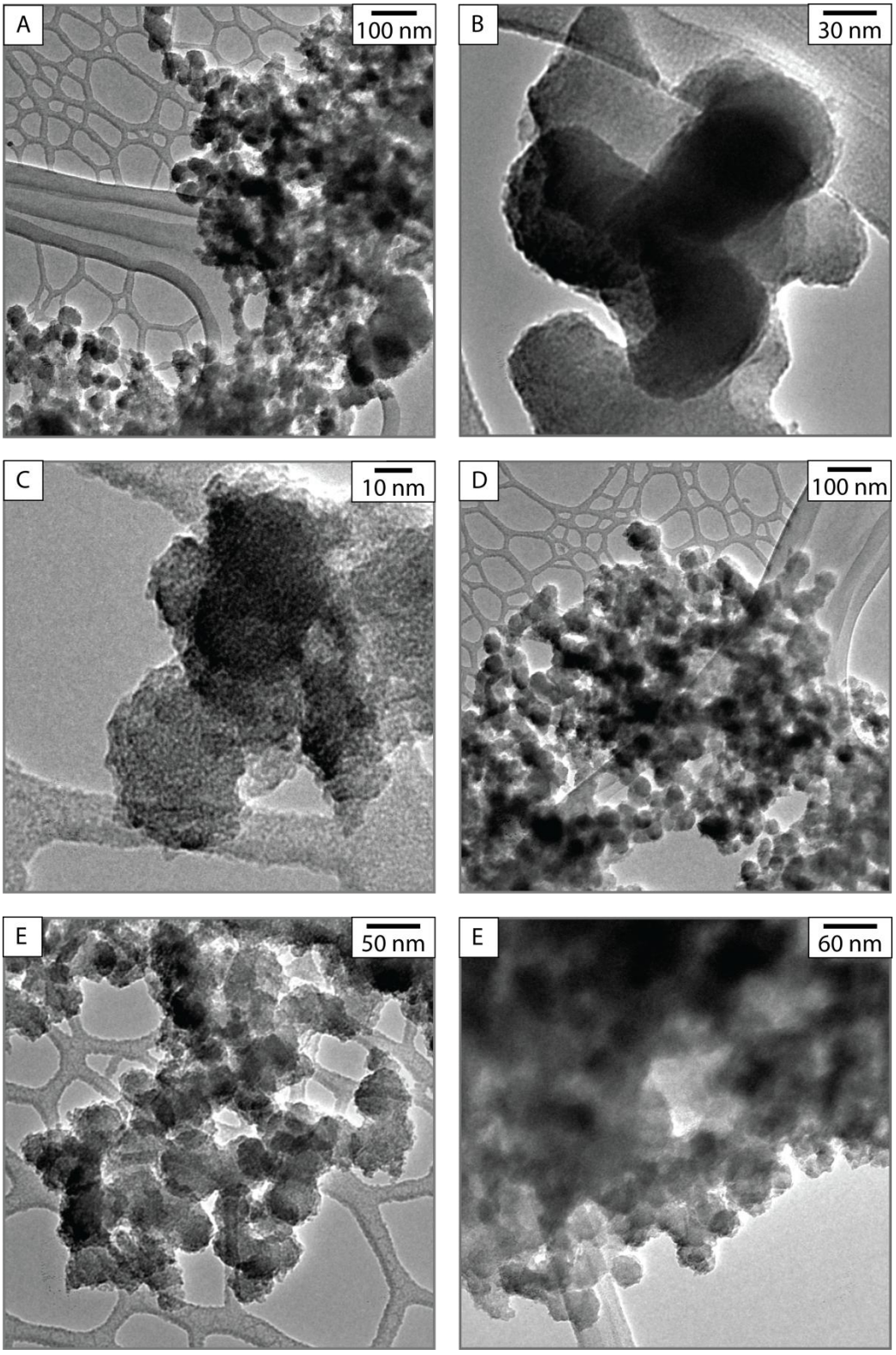

Figure 3.19: TEM images of TiO_2 nanoparticles nucleated at 100˚C for 6 s and grown at 80˚C for 120 s. The size of nanoparticles were 42.6∓8.12 nm.

As a next step, both the nucleation and growth zones were held at 100˚C, and the solutions passed through them had a total residence time of 240 s. This yielded the particles shown in Figure 3.20. These are more uniform than those in Figure 3.19.

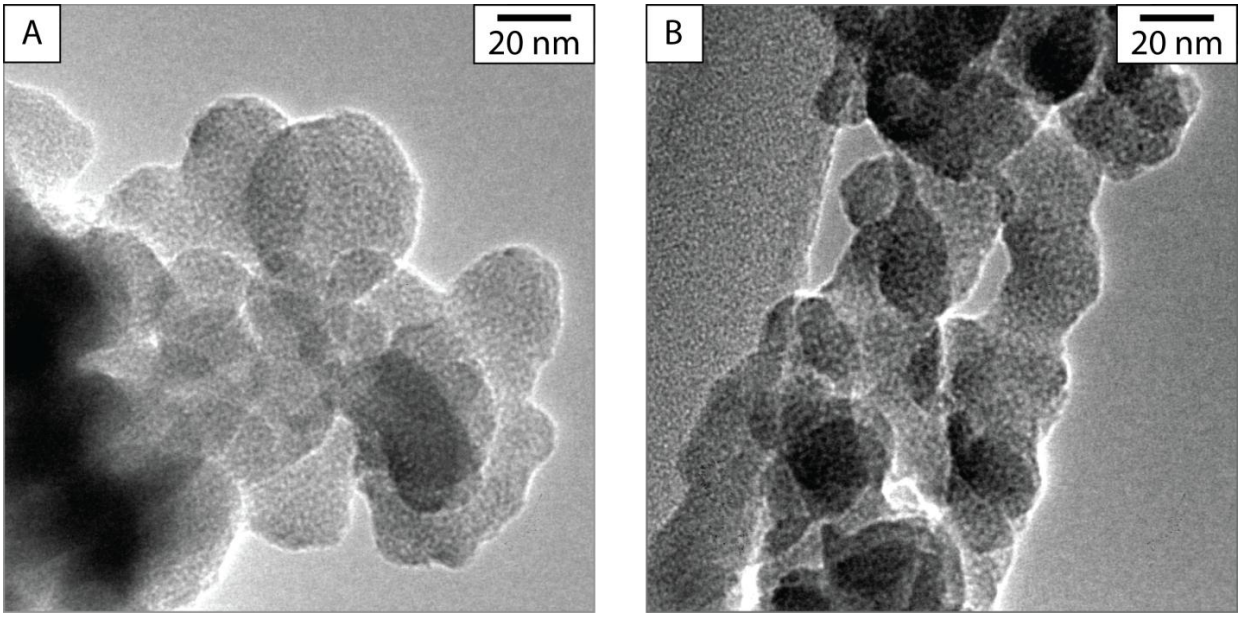

Figure 3.20: TEM images of TiO_2 nanoparticles nucleated and grown at 100˚C for a total time of 240 s.

The samples from the experiment shown in Figure 3.20 were also coated with sodium oleate in order to see if this would reduce the agglomeration of nanoparticles. After nanoparticles were centrifuged in acetone and ethanol mixture; they were dispersed in DI water that contained Na-oleate. The nanoparticles coated with Na-oleate are shown in Figure 3.21. With the addition of Na-oleate, it was possible to distinguish nanoparticles from each other and a size distribution study was possible, unlike the case in Figure 3.20. The average particle diameter is 26.5nm$\mp$1.6 nm with high yield. The Na-oleate absorbed on nanoparticles was approximately 3nm thick. It is presumed that the Na-oleate was absorbed on nanoparticle surfaces by electrostatic attraction, eventually reducing the zeta potential [22]; however a detailed analysis of this process was not performed. It was expected that Na-oleate would reduce agglomeration via repulsive electrostatic forces. However particles were still agglomerated. This might be due to nonpolar, hydrophobic chains on nanoparticles extending to the aqueous solution and promoting particles to agglomerate to reduce the surface area interacting with the water molecules [22]. The Na-oleate coating can be clearly seen in Figure 3.21E. Since the Na-oleate was added after the synthesis, it didn't have an effect on the size distribution as well as agglomeration. However it facilitated the imaging of nanoparticles in TEM.

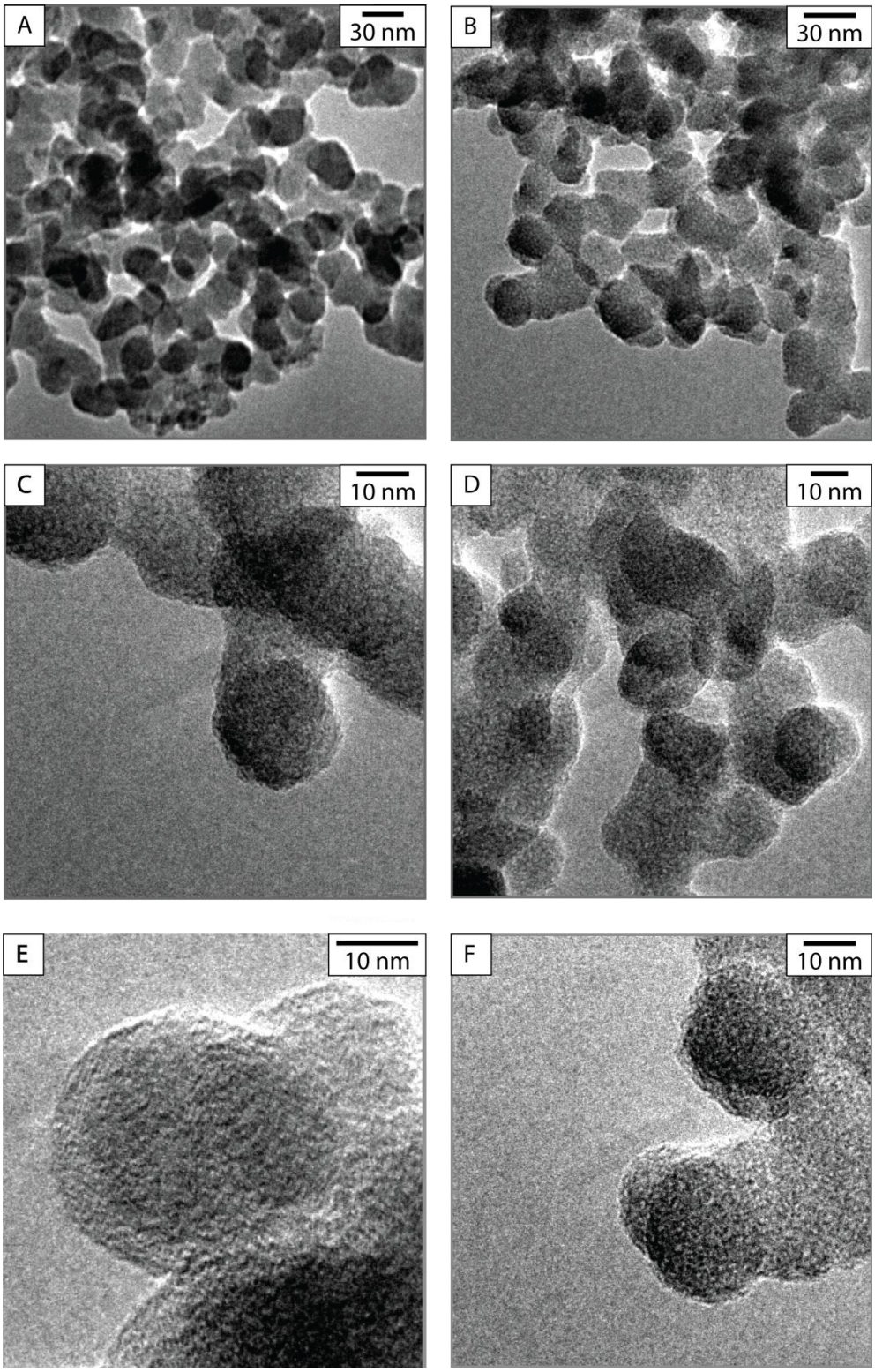

Figure 3.21: TEM images of nanoparticles coated with Na-oleate. These particles were nucleated and grown at 100°C for 240 s. This is the only sample where Na-oleate coating was used. The average size of nanoparticles was 26.5∓1.6 nm.

Nanoparticles nucleated at 70˚C for 6 s were also grown at a higher temperature (90˚C) for a longer time (240 s) to see the effect of both growth temperature and residence time. Figure 3.22 shows the TEM image of these nanoparticles. Compared to the particles nucleated and grown at 70˚C for a total time of 126 s shown in Figure 3.17; these nanoparticles had a similar average size of 5.2 ∓ 0.7 nm. However due to a lot of agglomeration and the low quality of these images, these numbers are approximate. This result means that higher growth temperature and longer residence time did not affect the size and size distribution of nanoparticles after being nucleated at 70˚C. The fact that increasing the residence time and growth did not affect the size might be due to reaching a stable state and not having any reagent left for further growth.

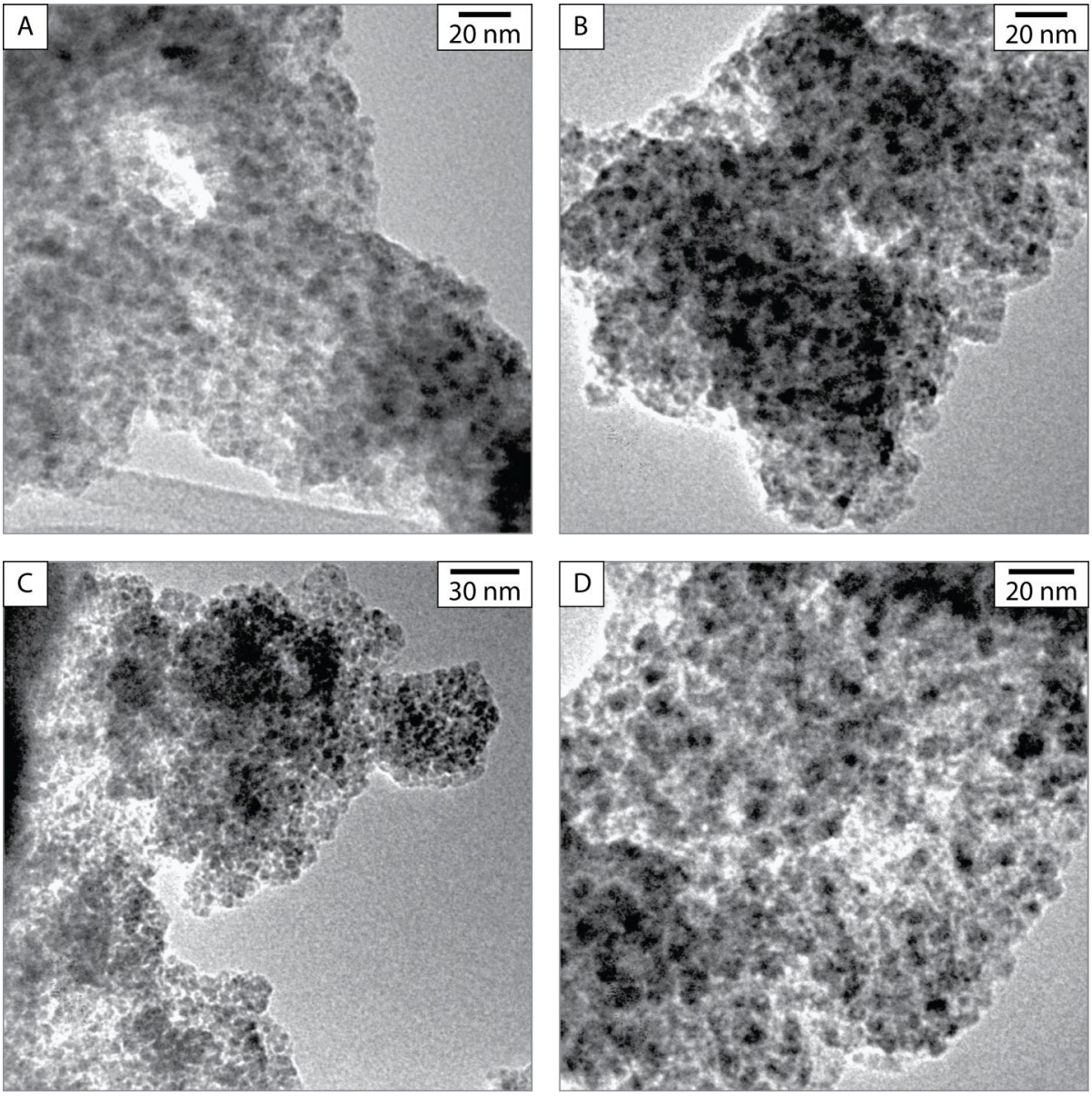

Figure 3.22: TEM images of TiO_2 nanoparticles nucleated at 70˚C for 6 s and grown at 90˚C for 240 s.

Finally, the nucleation temperature was increased to 200˚C and the growth temperature was kept at 80˚C to see the effect of high nucleation temperature. The nucleation was for 6s and growth was for 240 s. The resulting nanoparticles are shown in Figure 3.23. The average size of nanoparticles was 14.9∓3.1 nm. Compared to the nanoparticles nucleated at 100˚C for 6s and grown at 80˚C for 120s (Figure 3.19); particles that were nucleated at 200˚C are much smaller in size. The standard deviation of particle size in percentage did not change much (19% and 20%). The other important observation is that the particles that were nucleated at 200˚C have better defined shapes compared to the ones nucleated at 100˚C. The fact that their size is smaller is that most of the reagents were used for nucleation at 200˚C and fewer reagents were left for growth. That means the process was dominated by nucleation and there was actually very little growth. The growth could also be named as 'growth transformation process' as it is not a classical growth mechanism. It was also observed that the size distribution of nanoparticles nucleated at 200˚C was the highest standard deviation among other results (20.8%). One reason of this could be the renucleation of particles, that is to say nucleation and growth could have happened at the same time.

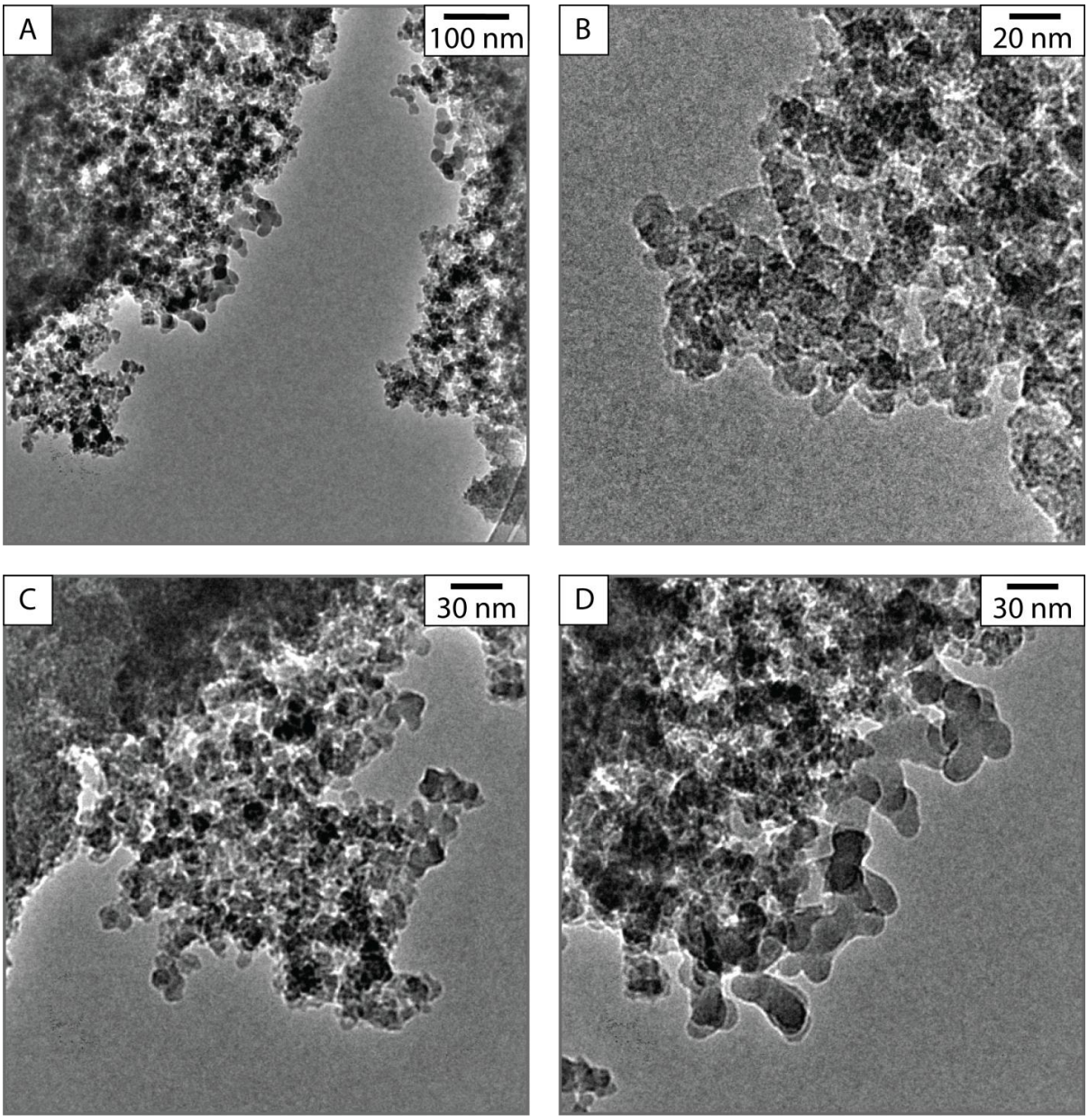

Figure 3.23: TEM images of TiO_2 nanoparticles nucleated at 200˚C for 6 s and grown at 80˚C for 240 s.

The summary of all results discussed above is shown in Table 3.1. It is observed that size of nanoparticles is highly dependent on the temperature of both nucleation and growth zones. For different nucleation temperatures, growth temperatures had different effects; this is summarized in the graph shown in Figure 3.24. For nucleation at 70˚C, the increase of the growth temperature did not have any effect and the average size was 5.2 nm for both cases with small standard deviation. In the case of nucleation at 100˚C, the resulting nanoparticles have larger sizes and the standard deviation increased for growth at 80˚C. The first values in the graph represent the particles that were only nucleated but not grown at a temperature higher than room temperature. That's why the temperature value is 25˚C.

The size for this case is just the size of nanoparticle clusters. It is very hard to distinguish the individual diameters of nuclei from the TEM images; therefore the initial cluster size is given. This cluster sizes were almost the same for all nucleation temperatures. This may not mean that the size of particles right after nucleation zone were the same but this may mean that the clusters they form to reduce their surface energy were similar size.

Table 3.1: Summary of experimental results.

Nucleation Temperature	Growth Temperature	Growth Time	Average Size (nm)	Notes
35˚C	-	-	25.4±4.4	Not individual nanoparticles, size is given for aggregates
70˚C	-	-	24.5±2.8	Not individual nanoparticles, size is given for aggregates
100˚C	-	-	24.5±2.6	Not individual nanoparticles, size is given for aggregates
35˚C	70˚C	120 s	189.2±28.7	Large, individual nanoparticles
70˚C	70˚C	114 s	5.2±0.3	Crystalline structures
70˚C	90˚C	120 s	5.2±0.7	Aggregated, spherical structures
100˚C	70˚C	120 s	20.91±1.73	Difficult to distinguish individual nanoparticles, this size is approximate
100˚C	80˚C	120 s	42.6±8.1	Individual nanoparticles were observed
100˚C	100˚C	234 s	26.5±1.6	These were sodium oleate coated nanoparticles
200˚C	80˚C	240 s	14.9∓3.1	Highest temperature for nucleation

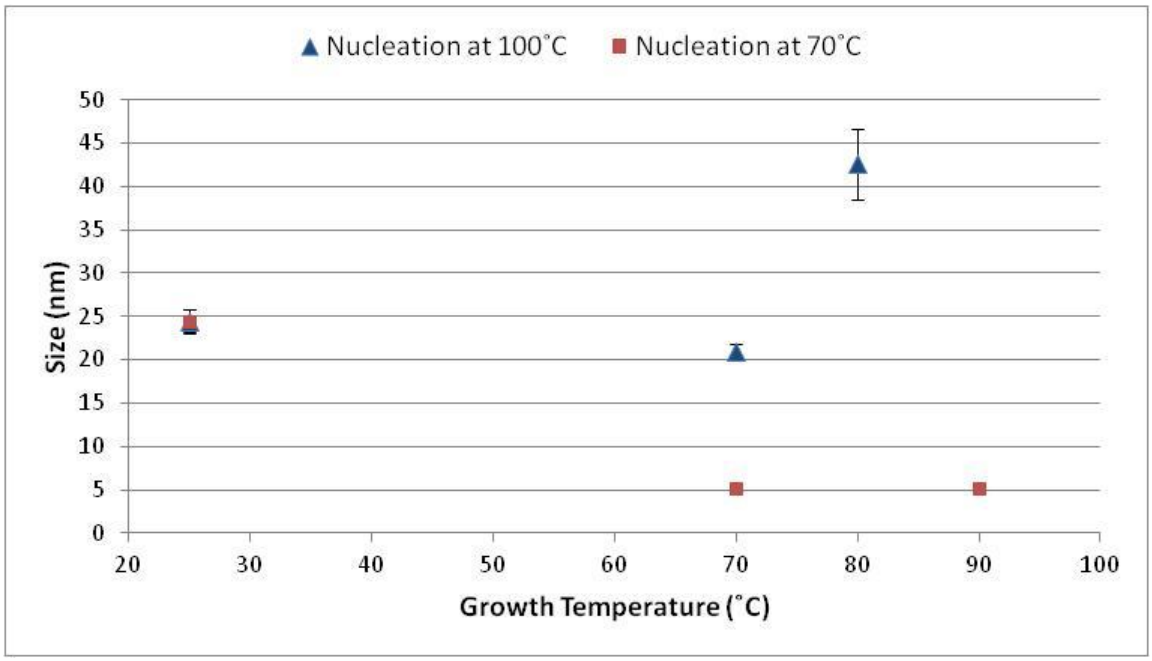

Figure 3.24: Effect of growth temperature for different nucleation temperatures. Residence times for each growth were 120 s. The growth at 25˚C represents particles that were only nucleated in the microreactor and later kept at room temperature. The size of these particles was the size of the clusters.

The comparison of results for the same growth temperature at 70˚C for varying nucleation temperatures is shown in Figure 3.25. It is observed that at the low temperature nucleation, the size of particles were much larger, however the size distribution was also very large. The best size distribution was obtained at nucleation at 70˚C.

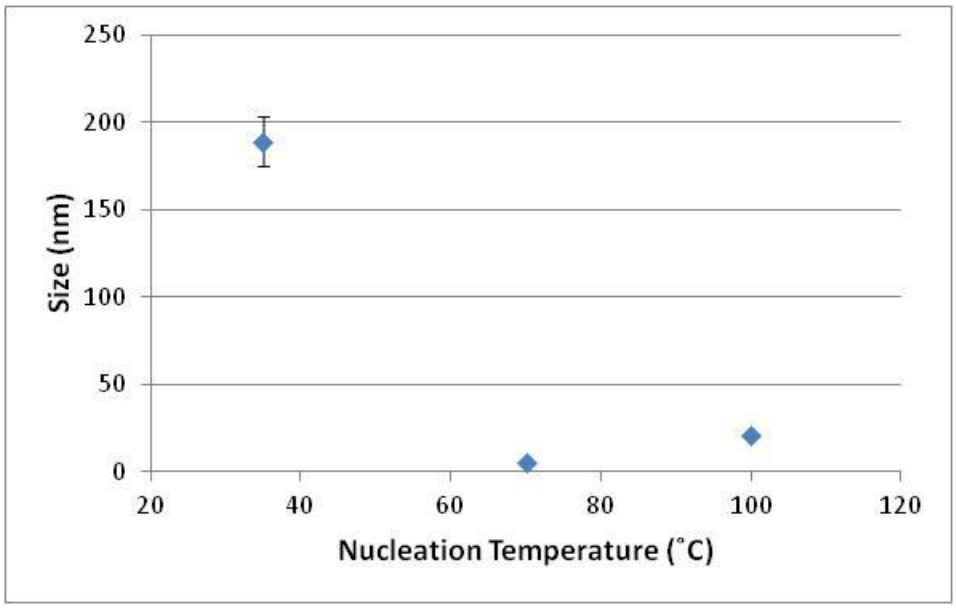

Figure 3.25: Nanoparticles nucleated at different temperatures but grown at 70˚C.

3.6. Conclusion

In this chapter a droplet-based, silicon substrate microfluidic reactor with multiple thermally isolated zones for the synthesis of nanoparticles is described. This study exemplifies the utility of the microfluidic device for studying the evolution of nanoparticles. In addition, the device shows significant promise for generating nanoparticles. A study on TiO_2 nanoparticle synthesis by using this microreactor is demonstrated and the intermediate steps of the formation of nanoparticles from a sheet-like structure to more organized particles are shown. It was shown that the temperature of the nucleation and growth steps plays a key factor in the formation of nanoparticles. The controlled temperature and residence times yielded particles with a size distribution less than 10%, this result is better than that achieved in previous methods [21].

As a future work, various other types of nanoparticle synthesis can also be performed in this reactor. More specifically it would be interesting to look at reactions that require higher temperatures such as quantum dots or other metal nanoparticles such as gold and silver. It would also be interesting to look at the use of ligands in the synthesis to prevent the nanoparticle agglomeration.

In this work the microreactor was used as a 'closed' environment, where additional reagents were not added during the synthesis. Therefore, in some cases it was observed that increasing the growth time did not make changes in the particle size as there were no reagents left. As a future work, the microreactor can be used as an 'open' system, where extra reagents were delivered right before the growth region.

3.7. References of Chapter 3

[1] Hosokawa, M.; Nogi, K.; Naito, M.; Yokoyama, T., Nanoparticle technology handbook, Amsterdam: Elsevier, 2007.

[2] Abdelhady, A. L.; Afzaal, M.; Malik, M. A.; O'Brien, P., "Flow reactor synthesis of CdSe, CdS, CdSe/CdS and CdSeS nanoparticles from single molecular precursor(s)," *J. Mater. Chem.,* vol. 21, pp. 18768-18775, 2011.

[3] Chan, E. M.; Mathies, R. A.; Alivisatos, A. P., "Size-controlled growth of CdSe nanocrystals in microfluidic reactors," *Nano Lett.,* vol. 3, pp. 199-201, 2003.

[4] Chan, E. M.; Alivisatos, A. P.; Mathies, R. A., "High-temperature microfluidic synthesis of CdSe nanocrystals in nanoliter droplets," *J. Am. Chem. Soc.,* vol. 127, pp. 13854-13861, 2005.

[5] Marre, S.; Adamo, A.; Basak, S.; Aymonier, C.; Jensen, K. F., "Design and packaging of microreactors for high pressure and high temperature applications," *Ind. Eng. Chem. Res.,* vol. 49, pp. 11310-11320, 2010.

[6] Nightingale, A. M.; Krishnadasan, S. H.; Berhanu, D.; Niu, X.; Drury, C.; McIntyre, R.; Valsami-Jones, E.; deMello, J. C., "A stable droplet reactor for high temperature nanocrystal synthesis," *Lab. Chip.,* vol. 11, pp. 1221-1227, 2011.

[7] Yen, B. K. H.; Gunther, A.; Schmidt, M. A.; Jensen, K. F.; Bawendi, M. G., "A microfabricated gas-liquid segmented flow reactor for high-temperature synthesis: the case of CdSe quantum dots," *Angew. Chem.,* vol. 117, pp. 5583-5587, 2005.

[8] Lee, A. -K.; Liu, X.; Sebastian Cabeza, V.; Jensen, K. F., "Synthesis, assembly and reaction of a nanocatalyst in microfluidic systems: a general platform," *Lab. Chip.,* vol. 12, pp. 4080-4084, 2012.

[9] Lin, X. Z.; Terepka, A. D.; Yang, H., "Synthesis of silver nanoparticles in a continuous flow tubular microreactor," *Nano Lett.,* vol. 4, pp. 2227-2232, 2004.

[10] Gomez-de Pedro, S.; Martinez-Cisneros, C. S.; Puyol, M.; Alonso-Chamarro, J., "Microreactor with integrated temperature control for the synthesis of CdSe nanocrystals," *Lab Chip,* vol. 12, pp. 1979-1986, 2012.

[11] Nakamura, H.; Yamaguchi, Y.; Miyazaki, M.; Maeda, H.; Uehara, M., "Preparation of CdSe nanocrystals in a micro-flow-reactor," *Chem. Commun.,* vol. 23, pp. 2844-2845, 2002.

[12] Sebastian Cabeza, V.; Kuhn, S.; Kulkarni, A. A.; Jensen, K. F., "Size-controlled flow synthesis of gold nanoparticles using a segmented flow microfluidic platform," *Langmuir,* vol. 28, pp. 7007-7013, 2012.

[13] Yang, H.; Luan, W.; Tu, S.; Wang, Z. M., "Synthesis of nanocrystals via microreaction with temperature gradient: towards separation of nucleation and growth," *Lab. Chip.,* vol. 8, pp. 451-455, 2008.

[14] Abou-Hassan, A.; Sandre, O.; Neveu, S.; Cabuil, V., "Synthesis of goethite by separation of the nucleation and growth processes of ferrihydrite nanoparticles using microfluidics," *Angew. Chem. Int. Ed.,* vol. 48, pp. 2342-2345, 2009.

[15] Winterton, J. D.; Myers, D. R.; Lippmann, J. M.; Pisano, A. P.; Doyle, F. M., "A novel continuous microfluidic reactor design for the controlled production of high-quality semiconductor nanocrystals," *J. Nanopart. Res.,* vol. 10, pp. 893-905, 2008.

[16] N. M. Fung, "MEMS continuous microreactor for droplet-based monodispersed nanocrystal synthesis," University of California, Berkeley, 2008.

[17] J. D. Winterton, "Development of a novel microfluidic reactor for highly controlled synthesis of semiconductor nanocrystals," University of California, Berkeley, 2008.

[18] Weir, A.; Westerhoff, P.; Fabricius, L.; Hristovski, K.; von Goetz, N., "Titanium dioxide nanoparticles in food and personal care products," *Environ. Sci. Tech.,* vol. 46, pp.

2242-2250, 2012.

[19] Cottam, B. F.; Krishnadasan, S.; deMello, A. J.; deMello, J. C.; Shaffer, M. S. P., "Accelerated synthesis of titanium oxide nanostructures using microfluidic chips," *Lab. Chip.,* vol. 7, pp. 167-169, 2007.

[20] Tan, Y. -C.; Cristini, V.; Lee, A. P., "Monodispersed microfluidic droplet generation by shear focusing microfluidic device," *Sens. Act. B,* vol. 114, pp. 350-356, 2006.

[21] Cassaignon, S.; Koelsch, M.; Jolivet, J. -P., "From TiCl3 to TiO2 nanoparticles (anatase, brookite and rutile): thermohydrolysis and oxidation in aqueous medium," *J. Phys. Chem. Solids,* vol. 68, pp. 695-700, 2007.

[22] Xu, X.; Yu, Z.; Zhu, Y.; Wang, B., "Effect of sodium oleate adsorption on the colloidal stability and zeta potential of detonation synthesized diamond particles in aqueous solutions," *Diamond & Related Materials,* vol. 14, pp. 206-212, 2005.

Chapter 4

APPROACHES FOR COLLECTING NANOPARTICLES FROM MICROREACTORS

Both of the microreactors described Chapter 2 and 3 are droplet based microfluidic systems. In both cases, the carrier fluid was oil (mineral oil or octadecane) whereas droplets were aqueous solvent. Therefore the sample collected at the outlet was a mixture of these two immiscible solvents. In order to separate nanoparticles from the sample, centrifuging was necessary. Multiple centrifuging steps were required to remove the oil phase completely and in some cases this was not very successful as observed during the TEM imaging. When the oil phase was not removed completely, it coated the nanoparticles on the TEM grid and prevented obtaining a clear image. The centrifuging step also caused some loss of material and it took a long time to finish the cleaning. Also it was not always possible to clean the product, even after extensive treatment.

In this chapter, two approaches for "on-chip" separation of droplets with nanoparticles from the oil phase are discussed to address the drawbacks of centrifuging. The first approach is based on trapping droplets in the microfluidic chip and later washing the channel to collect them. The second approach is based on using a micropillar array for guiding droplets inside the microchannel and to eventually separate them from the oil phase.

4.1. First Approach: Trapping of Droplets

There are several methods for droplet trapping and collection based on various kinds of actuation principles. One popular approach is to pattern trapping structures in the channel where the hydrodynamic force exerted from inlet flow pushes droplets against them [1] [2]. Trapped droplets are collected at the inlet by supplying reverse flow from outlet. However, this system requires the carrier fluid to be supplied continuously in order to maintain droplets trapped. Also small fluctuations of flow or vibrations from external environment make droplets escape from the trapping structures. Drop-in wells beside a

microchannel [3, 4] have also been proposed for trapping droplets without continuous supply of inlet flow. But it is hard to collect the trapped droplets unless big droplets are injected to replace and push them out of wells. Stopping and resuming of droplet generation require bypass channels and pneumatic valve operations. Other methods utilizing optical [5], dielectrophoretic [6], and acoustic [7] actuations also require external power and control, and thus increase the cost and complexity. In some of these methods, only a few droplets can be manipulated concurrently and individual control of droplets reduces the throughput of the analysis system.

The approach described in this section is based on trapping and collecting droplets inside the microchannel after the synthesis of nanoparticles by using microwells inside the channel. This method is size-dependent; therefore sessile droplets or droplets formed with unstable inlet flows can be eliminated. Trapped droplets can be collected at the outlet with increased inlet flow rates or with the supply of an aqueous fluid (same fluid type as droplets). In this study iron oxide nanoparticles were synthesized by using the same microreactor design described in Chapter 2 and droplets with particles were trapped inside the channel after the synthesis step. Trapping is a passive method that does not require external control.

4.1.1. Basic Principles and Design

The surface energy of a droplet is given by its area multiplied by the surface tension. In general, droplets would be spherical, as this minimizes the surface area, and hence the surface energy, for a given droplet volume. However, if the droplet volume exceeds $(\pi d\text{^}3)/6$, where d is the diameter of the microchannel, the droplet must adopt an ellipsoidal shape. This basic idea is used for trapping droplets with nanoparticles inside a microfluidic channel. After the synthesis of nanoparticles, droplets that carry particles enter a wider channel where there is a well array for trapping. The schematic of this design is shown in Figure 4.1. When a droplet enters a well inside the microchannel with d large enough to restore its spherical shape, it is trapped at the well as its surface energy is minimized due to minimized surface area. If the droplet diameter is smaller than the depth of the microchannel, it maintains its spherical shape and it doesn't get trapped because it already has a stable status. Also droplets with diameters larger than the depth of the well cannot be trapped inside the well as their surface outside of the well gets dragged by the viscous force and removes itself from the well. Therefore, only droplets compressed in the microchannel and having similar diameter to the width of the wells are trapped and remained. The droplet inside the well can be collected by the substitution of other incoming droplets or viscous forces caused by high flow rate of the carrier fluid.

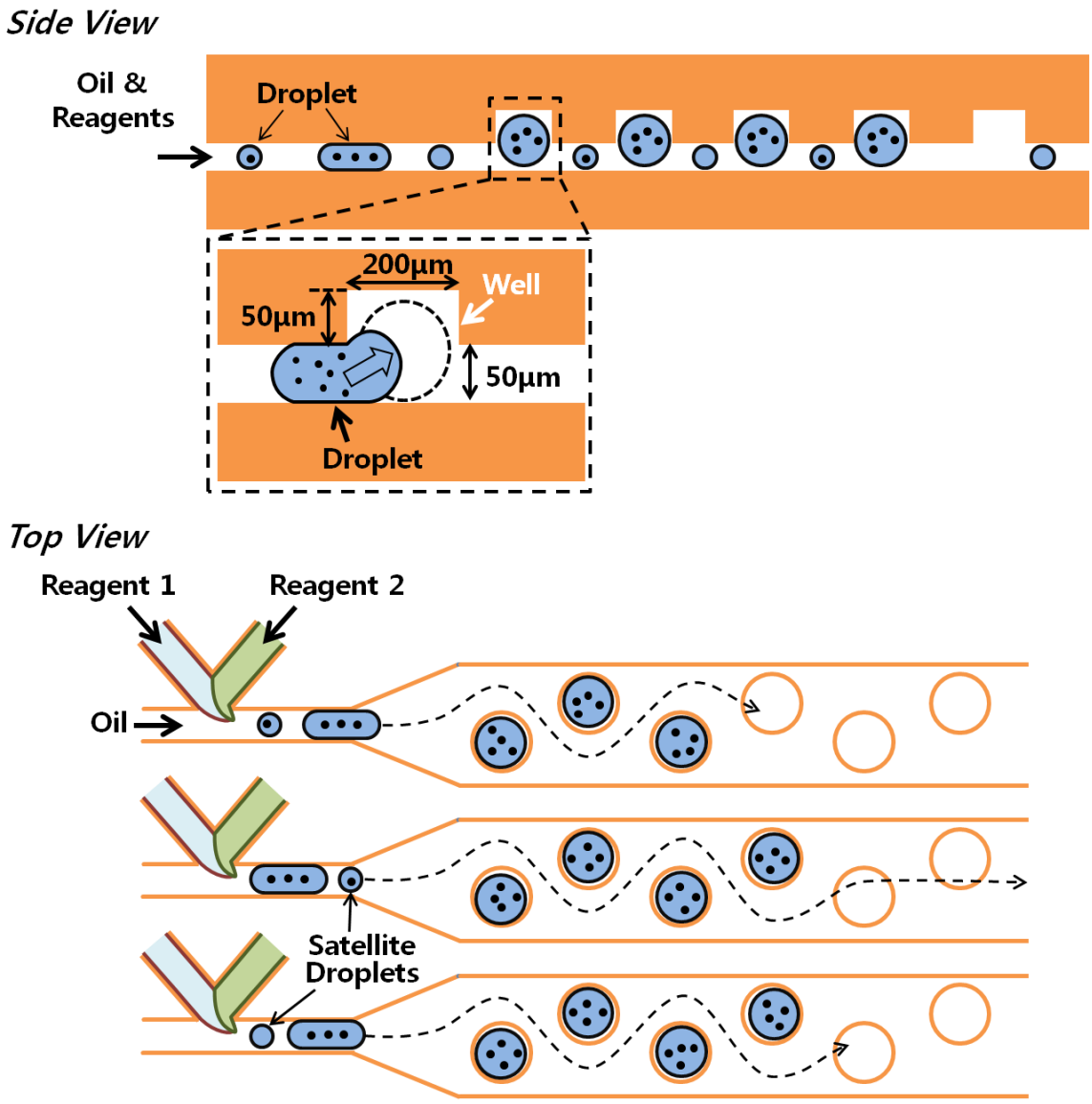

Figure 4.1: Schematic of the selective droplet trapping mechanism. Droplets smaller or larger than the desired size are not trapped and dragged by viscous forces.

The height of the microchannel and wells are 50 μm and 100 μm, respectively. Wells are designed to have a cylindrical geometry having the same diameter as target droplets, 200 μm. The width of the microchannel is 600 μm and wells are 90 μm in diameter. The distance of wells from the side walls are 100 μm. There are 512 wells in a chip, and size of the chip is 28 mm×23 mm. Design details are shown in Figure 4.2.

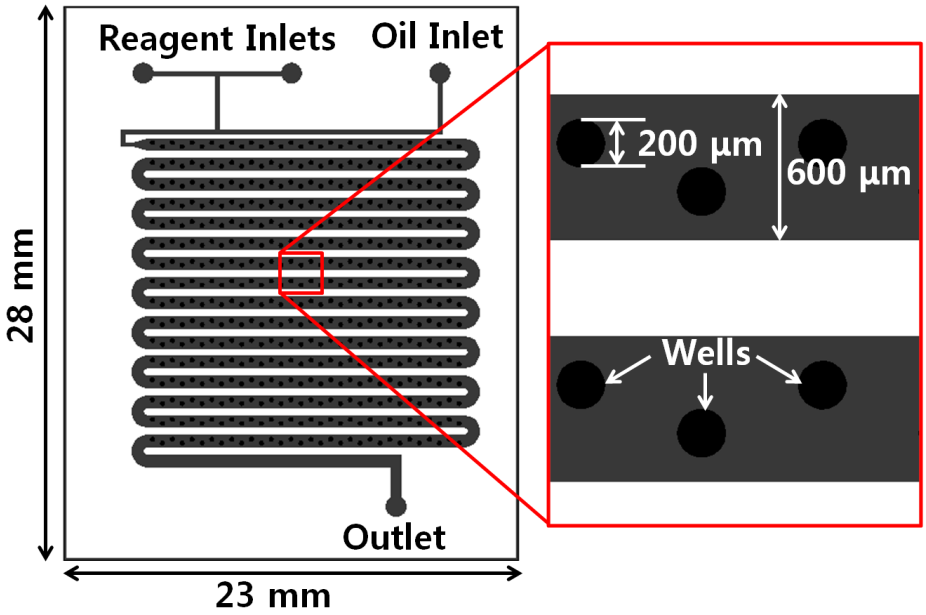

Figure 4.2: Design details of the microfluidic chip for nanoparticle synthesis and droplet trapping.

A numerical estimation using COMSOL Multiphysics was conducted to study the droplet behavior near a well. Droplet phase was defined as water while carrier fluid was defined as hexadecane. The interfacial tension between water and hexadecane was taken as 53.3 mN/m [8]. Figure 4.3 shows the simulation results. Once the droplet touches the well, it rapidly moves inside within 1ms. This is a sufficient time for a droplet flowing in the microchannel to be trapped in the well. If the time required for droplet trapping is longer than the time for droplet passing on a well, droplet will not be trapped. In the simulation, the droplet was estimated to bounce in the direction of movement at 1.2 ms, but this was not strong enough to pass through the well and therefore it returned back to the well. After trapping, droplet took a spherical shape in a few milliseconds.

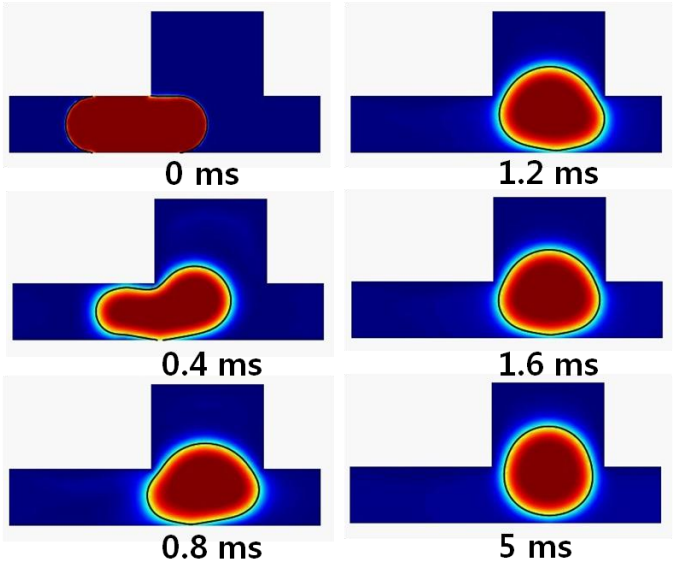

Figure 4.3: Numerical estimation of a droplet being trapped in a well. Model is created with COMSOL Multiphysics.

Devices were fabricated in polydimethylsiloxane (PDMS) by using soft lithography technique. The master mold was made out of SU8, a negative photoresist, and was patterned by using photolithography. Before development of the unexposed SU8 layer, another layer of SU8 was coated on top of it. After patterning the well array on top of the microchannel, both SU8 layers were developed together. PDMS mixture of base and cross linker (10:1, wt.) was poured on the SU8 mold and cured. After peeling off the PDMS layer from the mold, the inlet and outlet holes on PDMS layer were punched and bonded to a glass slide after oxygen plasma treatment.

4.1.2. Materials

Iron (III) chloride hexahydrate, (97%, Sigma-Aldrich); iron (II) chloride tetrahydrate, (≥ 99% Sigma-Aldrich) and ammonium hydroxide (29% Fisher Scientific) were used to prepare the aqueous reagent solutions. Hexadecane and Span 80 were obtained from Sigma-Aldrich.

For the fabrication of the device, SU8-3050 and PDMS (Sylgard 184 Silicone Elastomer Kit) was obtained from MicroChem and Dow Corning respectively.

4.1.3. Experimental Results

In the microfluidic system, iron oxide nanoparticles were synthesized by using the second method explained in Chapter 2 where reaction was carried under air environment. Reagents were ammonium hydroxide and iron chloride aqueous solutions. As the carrier fluid, hexadecane with 2% (wt.) Span 80 was used due to hexadecane's low viscosity (3.04 mPa·s) and low density (0.88 g/cm^3) at room temperature [9]. The viscosity of the carrier fluid affects the drag forces when droplets are moving into the wells, therefore low viscosity is useful to facilitate the trapping mechanism. In addition to drag forces, it also

reduces the inlet pressure which prevents leakages at bonding interfaces and inlet-outlet ports. Low density is also advantageous as the droplets can easily sink to the bottom of the microchannel.

In order to test the droplet trapping, first experiments without nanoparticle synthesis were carried out. Reagents were replaced with DI water and hexadecane was used as carrier fluid. Fluids were delivered to the device by using syringe pumps. The flow rates of the carrier fluid and DI water were 1000 and 200 μL/hr respectively. Initially air bubbles were trapped in the wells, however they were removed as the hexadecane filled the microchannels. Figure 4.4 shows the device under operation.

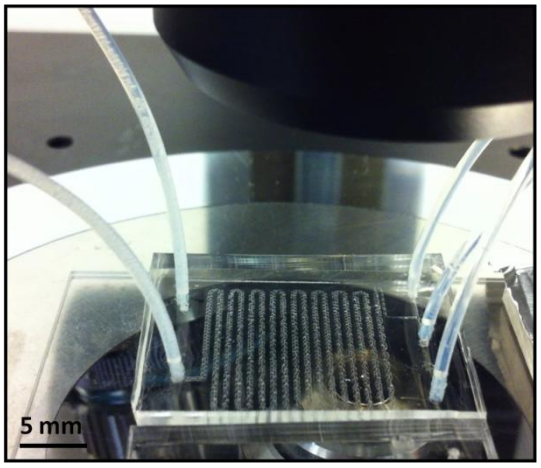

Figure 4.4: Fabricated microfluidic device.

Droplets with sizes similar to that of the wells were trapped as they encountered an empty well. Droplets that are much smaller or larger than the wells passed the well array without being trapped. As new droplets were introduced, they replaced the droplets in the pre-occupied wells. This is a useful mechanism since flow rates at the beginning are not stable; and therefore droplets formed at the beginning may not contain the desired ratio of reagent mixture and can be inadequate for analysis. Once flow rates were stabilized and initial droplets were replaced with new ones, droplet generation and trapping was stopped by stopping the flow of aqueous reagents. Figure 4.5 shows successful trapping and Figure 4.6 shows substitution of pre-occupied wells with a new incoming droplet.

Among the 512 wells in the chip, 508 wells were filled with a single droplet which means 99.2% of wells were filled. Trapped droplets were collected at the outlet with increasing the flow rate of hexadecane to 4000 μL/hr. The size of droplets trapped in wells was observed to be uniform.

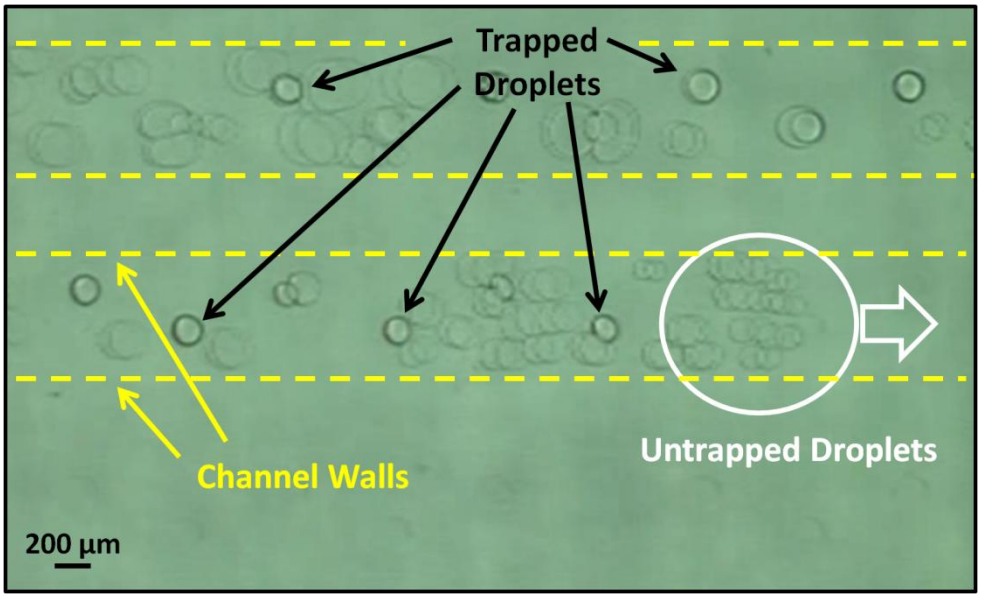

Figure 4.5: Real time image of droplet trapping with the well array.

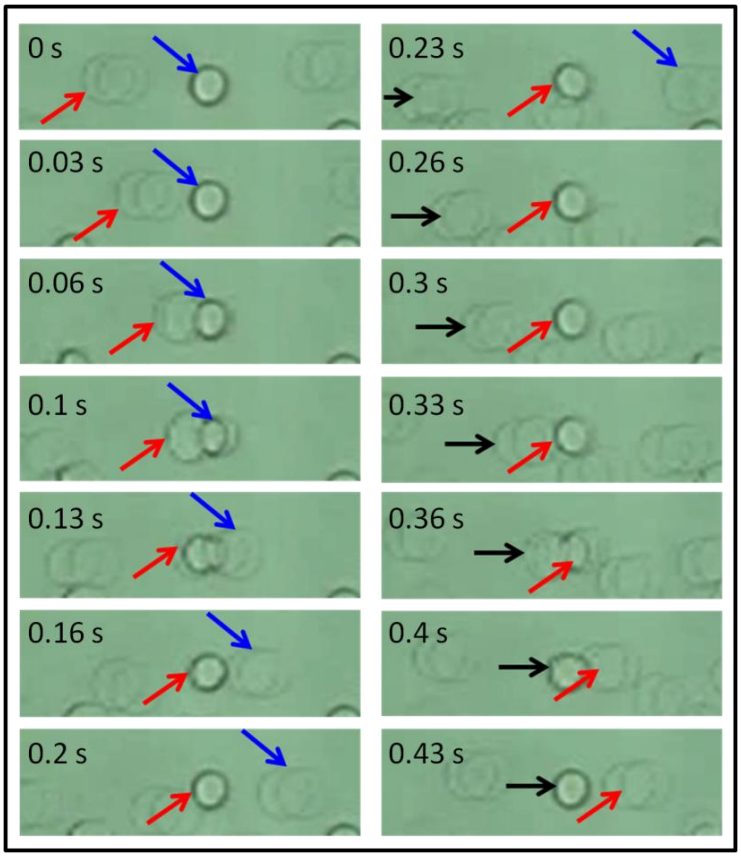

Figure 4.6: Real time images of droplet trapping and substitution in a well.

After the device was successfully tested with DI water, iron oxide nanoparticle synthesis was performed and the trapping of these droplets was demonstrated as shown in Figure 4.7. Reagents enter the device from separate channels, and form a droplet in the third

channel. Nanoparticles are generated as reagents mix inside the droplet. The concentration of nanoparticles in initial droplets was higher due to the unstabilized flow of aqueous solutions, but it decreased as the flow stabilized. Also these initial droplets with high concentration were replaced with the new ones. TEM image of synthesized nanoparticles in this microfluidic system is shown in Figure 4.8.

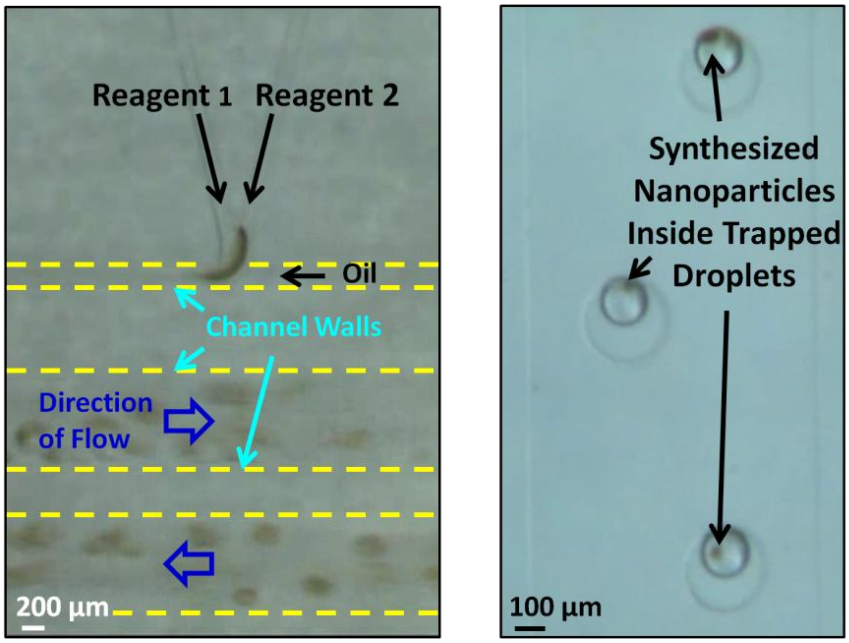

Figure 4.7: Nanoparticle synthesis in droplets.

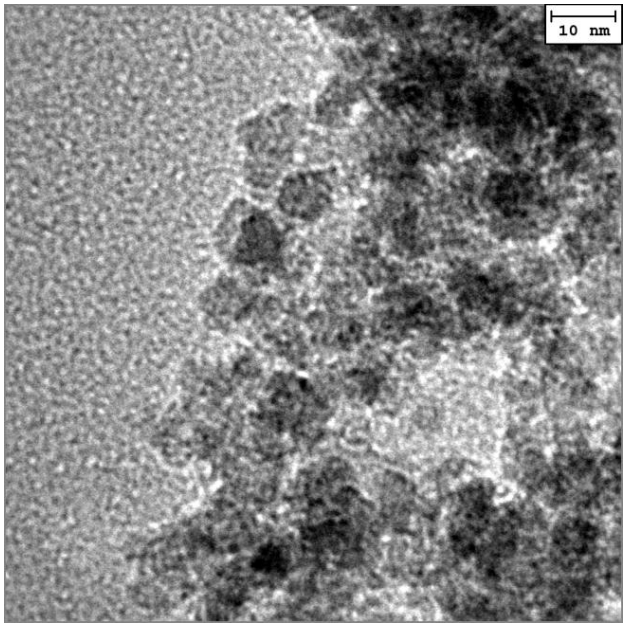

Figure 4.8: TEM images of nanoparticles synthesized in the droplet trapping microfluidic device.

4.1.4. Conclusion

In this chapter a microfluidic device that has the capability of synthesizing nanoparticles inside droplets and trapping them in the microchannel is described. This work is mainly interesting for immobilizing particles in droplets inside the channel. This design could also be used for reactions that require long residence times at high temperatures.

Most importantly, it can be used for separating the droplet phase from the carrier phase. In this work, droplets were collected with the increased flow rate of the carrier fluid, which was oil. However, after the trapping of droplets, if the carrier fluid is replaced with an aqueous solution, the droplets could be merged to this phase and at the outlet they would not be inside oil anymore. This would reduce the time spent with centrifuging and cleaning of oil after the synthesis.

4.2. Second Approach: Droplet Lysis

In droplet-based systems, it is difficult to retrieve the contents of droplets due to the surfactant on the surface preventing droplets from coalescing. In this section, a new methodology is presented to retrieve the contents of droplets into the aqueous phase by coalescing them. A similar microchannel design is used as in Chapter 2 and in [10] to synthesize iron-oxide nanoparticles. After the synthesis, droplets are guided by using a micropost array railing technique into an oil-phase wash solution to remove the surfactant and later directed into a channel with water flow to "lyse" (or coalesce) them for retrieving the nanoparticles. Synthesis and retrieval of magnetic iron-oxide nanoparticles were demonstrated successfully with this technique.

In prior works, researchers have developed micropost array railing methodologies to passively guide suspended microparticles (e.g., microbeads, cells and microdroplets) into discrete, adjacent solutions under continuous flow conditions [11-15]. Recently a droplet-based technique was introduced that utilizes a micropost array to continuously remove surfactants from the surface of the droplets in order to "lyse" them and retrieve their contents (e.g., microbeads) [16, 17]. Here, this methodology is expanded to develop a single, continuous flow microfluidic system that is capable of synthesizing iron-oxide nanoparticles inside droplets, and then retrieving these nanoparticles via a centrifuge free "on-chip" droplet "lysis" process.

4.2.1. Basic Principles and Design

In this work, initially droplets were formed in the channel with hexadecane that contained the surfactant Span 80. Span 80 is a non-ionic surfactant that has a hydrocarbon chain that makes it soluble in oil and a polar group that gives its affinity to water. The addition of surfactant decreases the interfacial tension between the oil and water phases, thereby facilitating the formation of water droplets (emulsification) as there is only a relatively small increase in the free surface energy associated with emulsion formation (free surface energy is the energy necessary to form new surface) [18]. The interfacial tension is given as

$$\gamma = \gamma_o - \pi \quad (1)$$

where γ is the interfacial tension energy after addition of the surfactant, γ_o is the initial surface tension and π is the surface pressure of the absorbed layer of surfactant and when γ is reduced enough stable droplet formation can occur [18]. The thermodynamic stability of the droplets can be explained by the Gibbs adsorption equation,

$$\Gamma = -\frac{c}{RT}\frac{d\gamma}{dc} \quad (2)$$

where Γ is the surface excess concentration, c is the concentration in the solvent, R is the ideal gas constant, T is the temperature and γ is the interfacial tension. Equation (2) enables the estimation of absorption of surfactant at the interface based on its concentration and its surface tension as a function of concentration. The concentration of the surfactant above which the interfacial tension is constant is named as critical micelle concentration (c.m.c.) [18]. The surface tension decreases until the concentration reaches the c.m.c. and then it stays constant above this value. (Based on equation (2) above the c.m.c $d\gamma/dc$ becomes zero and this suggests that the surface excess concentration is also zero; however this is not the case. The correct expression should involve the activity of the surfactant. The activity, a, becomes constant above the c.m.c., so $d\gamma/da$ is non zero. [18]). The c.m.c. of Span 80 in various oils such as hexane, pentane, decane, etc. is in the range of $(1.7 - 1.9) \times 10^{-5}$ M. The c.m.c. of Span 80 in hexadecane was not given in [19]; however it can be assumed to be in the range of 10^{-5} M due to its similar chemistry to other oils used in the experiments in [19]. The concentration of Span 80 in the initial hexadecane was 2% by weight which corresponds to a molarity of 36 mM; which is much higher than the c.m.c. In other words, droplets formed in the hexadecane with 2%Span 80 are stable and it is not possible to coalesce them easily. Therefore for the purpose of this work, a way to disrupt this stability is required. In the method presented here, droplets were washed in pure oil (hexadecane without Span 80) to reduce the concentration of surfactants below the c.m.c. and eventually increase the surface tension between oil and water phase such that the emulsion is no longer stable. After flowing droplets in pure hexadecane, it was observed that they started to merge and later release their content in water flow.

The design of the microfluidic system for nanoparticle synthesis and droplet lysis is shown in Figure 4.9. First nanoparticles are synthesized in droplets by mixing two reagents. Different than the design in Chapter 2, a third channel is used to deliver a buffer solution to separate reagents until they are inside the droplet. This helps to prevent clogging due to rapid reaction as soon as reagents make contact even before they form a droplet [10]. After the synthesis, a previously demonstrated micropost array railing technique [12-14] is then used to passively guide the nanoparticle-containing droplets between three distinct flow streams under continuous flow conditions. First, the microdroplets are transported from the oil flow with surfactant (purple) to the oil flow without surfactant (gray), which serves to remove the surfactant from the droplet surface. At the second junction, the hydrodynamic forces of the deionized (DI) water flow (blue) result in the destabilization of the microdroplets, thereby releasing the iron-oxide nanoparticles into the water flow. Thereafter, the water solution containing the nanoparticles is collected at the outlet, while the remaining oil flow is directed to the waste ports.

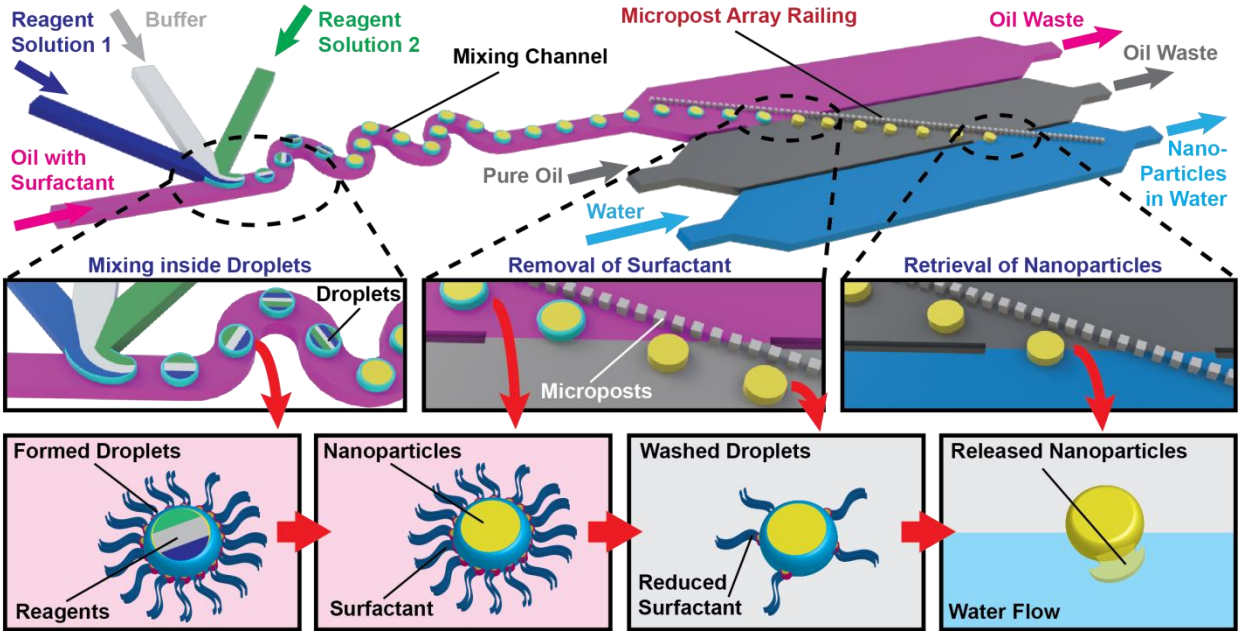

Figure 4.9: Schematic of the microfluidic system for nanoparticle synthesis and retrieval of nanoparticles. Nanoparticles are synthesized by mixing reagents in droplets. A buffer solution is used to separate reagents until they are inside the droplet to avoid clogging. Micropost arrays guide droplets into first pure oil to reduce surfactant on droplet surfaces and later into pure water to collect nanoparticles.

The width of microchannels for delivering the reagents and the oil phase as well as the winding channel for mixing is 50 μm. Micropost are 15 μm×15 μm, with 5 μm gaps, and are arrayed at a 1˚ angle with respect to the direction of flow. The three channels for oil waste, pure oil and water are 200 μm in width.

The microfluidic system was fabricated in PDMS by using the soft lithography process [20]. The fabricated device is bonded to a glass substrate with oxygen plasma treatment. Figure 4.10 shows the microfabricated device. The depth of the fabricated microchannels was 17.2 μm.

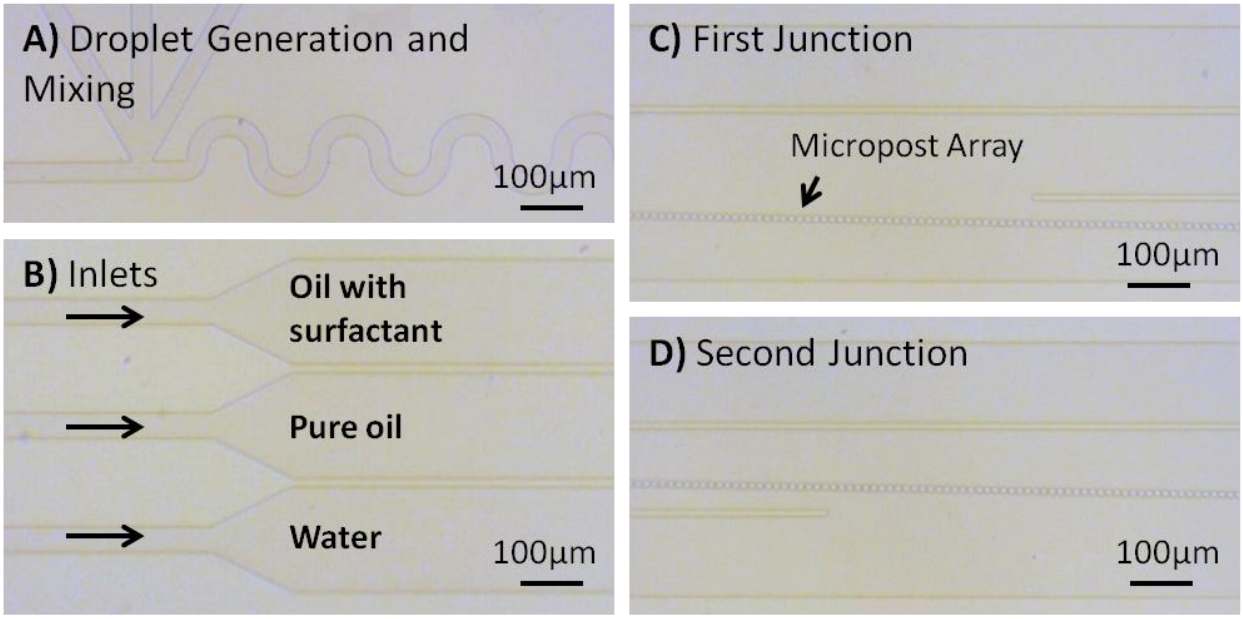

Figure 4.10: Pictures of the fabricated device. A) The droplet generation unit has four inlets; two for reagent solutions, one for buffer solution and one for oil. The mixing channel is sinusoidal to speed up the mixing. B) The system has three independent inlets and outlets for the continuous inputs of droplets with nanoparticles, oil, and water solutions, as well as arrayed microposts for passively guiding the movement of the microdroplets. C-D) There are two junctions for removing surfactant outside of droplets and for merging droplets with water. All scale bars are 100 µm.

4.2.2. Experimental Results

This microfluidic system was used for synthesizing iron-oxide nanoparticles by using the method in [21]. Reagents were delivered by using syringe pumps. Flow rates of reagents and buffer solution were 0.5µm/L while the flow rate of the oil with surfactant was 3 µm/L. As the oil phase hexadecane with Span 80 (2% wt.) was used. As the buffer solution to separate reagents, DI water was used. Figure 4.11 shows the formation of droplets and synthesis of nanoparticles. (Same materials in Section 4.1.2 were used).

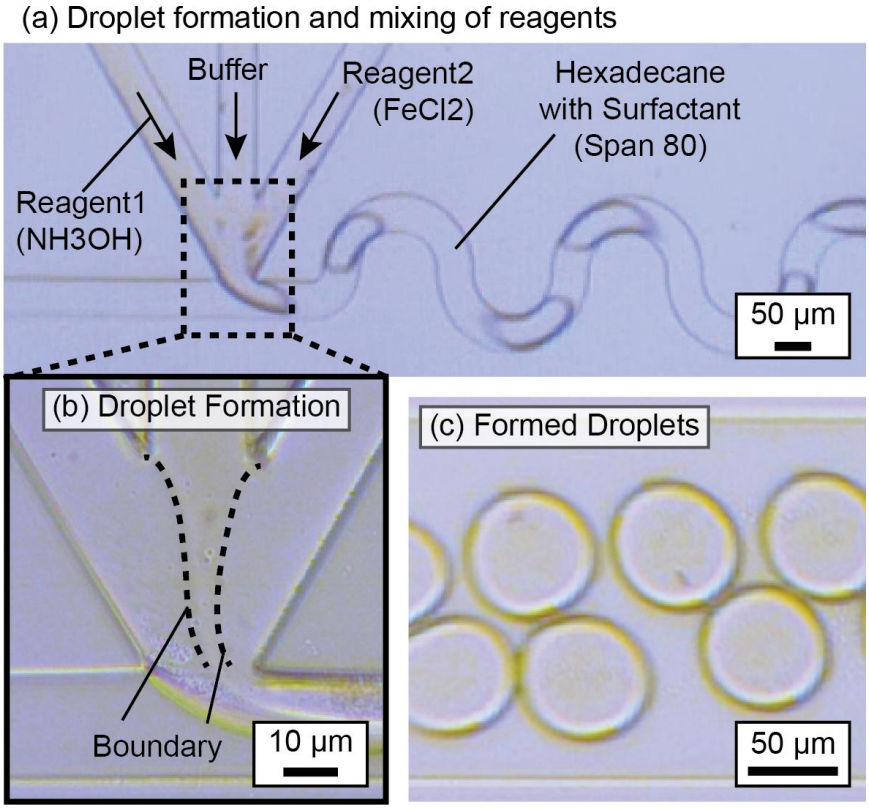

Figure 4.11: Images of nanoparticle synthesis. A) Reagents and the buffer solution form droplets in the channel with the shear rate applied by the oil flow. Reagents mix inside droplets in the winding channel. B) The buffer solution separates reagents until they are inside droplets to prevent clogging. C) The average diameter of droplets formed was 68.5 μm in diameter.

Once droplets were formed and nanoparticles were synthesized, they were guided by micropost arrays to reduce the surfactant on their surface and eventually merge them to the DI water channel. Figure 4.12 shows the experimental results of droplet lysis. Figure 4.12A shows three continuous flow channels and droplets with nanoparticles infused into the top channel. Figure 4.12B shows droplets being guided from hexadecane with surfactant (Span 80) to pure hexadecane at the first junction. After the surfactant on droplet surface is reduced in the pure hexadecane, some droplets merged due to the increased surface tension between droplet phase and hexadecane. At the second junction where pure hexadecane has interface with DI water, droplets were merged into the water flow and nanoparticles were released in the water. (When droplets were directed from the hexadecane with Span 80 to pure water without the washing step, they didn't merge into the aqueous phase). Figure 4.12C shows the merging of droplets and retrieval of nanoparticles into water at the second junction. The DI water was dyed in blue for better visibility. The released nanoparticles were collected at the water flow outlet.

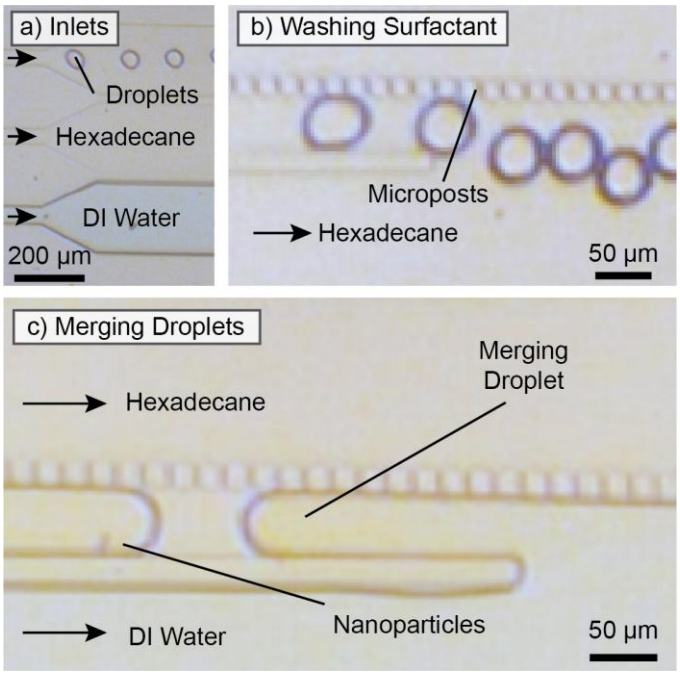

Figure 4.12: Experimental demonstration of the retrieval of nanoparticles from the droplets. A) Droplets, oil, and water solutions are infused continuously. B) Droplets are guided by the micropost array and transferred to the washing flow at the first junction. C) Droplets are lysed into water and the iron-oxide nanoparticles are released into the water flow.

The TEM image of synthesized nanoparticles is shown in Figure 4.13. Average size of the nanoparticles was 5.5±1.5 nm. The synthesized nanoparticles were magnetic (Figure 4.14). These results suggest that the presented microfluidic platform could be used to rapidly synthesize and process a wide range of nanoparticles autonomously, which could be utilized for diverse nanoparticle-based applications.

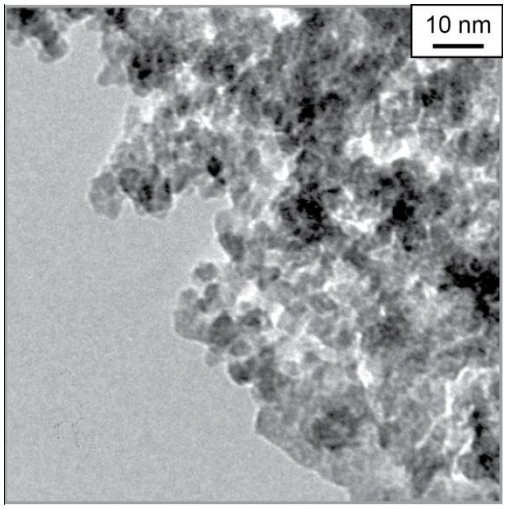

Figure 4.13: TEM image of nanoparticles. Average size of the nanoparticles was 5.5±1.5nm.

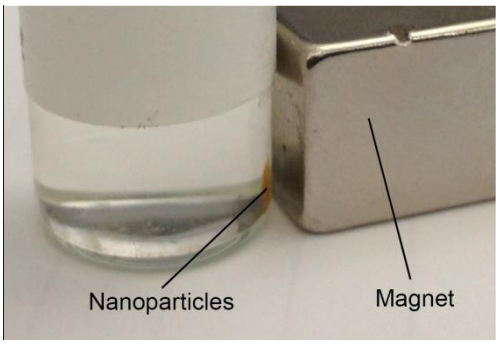

Figure 4.14: Particles were attracted to the magnet showing that they are magnetic.

4.2.3. Conclusion

An integrated microfluidic system is demonstrated for the droplet-based synthesis and retrieval of nanoparticles without having to use centrifuging by utilizing a continuous-flow micropost array railing methodology. Iron-oxide nanoparticles were synthesized inside droplets and they were subsequently released from droplets into water within a few seconds. The micropost array railing technique was used to guide the nanoparticle-containing microdroplets to the washing flow and then to the water flow for the droplet 'lysis' process. This method reduced the post processing time required to remove oil phase from the outputted solution at the end of the synthesis process. The generation of iron-oxide nanoparticles was confirmed via TEM observations and magnetic testing. The average size of the nanoparticles was 5.5±1.5 nm in diameter. It was also observed that the oil was successfully removed and the nanoparticles were suspended in the aqueous solution.

As a future work, this system can be used to synthesize different types of nanoparticles that require elevated temperatures. For this purpose, the substrate material needs to be changed as polymers are not suitable for these types of reactions. A microreactor similar to the multi temperature zone microreactor introduced in Chapter 3 can be used along with the micropost array for a complete system.

4.3. References of Chapter 4

[1] Bai, Y.; He, X.; Liu, D.; Patil, S.; Bratton, D.; Huebner, A.; Hollfelder, F.; Abell, C.; Huck, W., "A double droplet trap system for studying mass transport across a droplet-droplet interface," *Lab. Chip.,* vol. 10, pp. 1281-1285, 2010.

[2] Shi, W.; Qin, J.; Ye, N.; Lin, B., "Droplet-based microfluidic system for individual Caenorhabditis elegans assay," *Lab. Chip.,* vol. 8, pp. 1432-1435, 2008.

[3] Shim, J. uk; Olguin, L. F.; Whyte, G.; Scott, D.; Babtie, A.; Abell, C.; Huck, W. T. S.; Hollfelder, F., "Simultaneous determination of gene expression and enzymatic activity in individual bacterial cells in microdroplet compartments," *J. Am. Chem. Soc.,* vol. 131, pp. 15251-15256, 2009.

[4] Shim, J. -U.; Cristobal, G.; Link, D. R.; Thorsen, T.; Jia, Y.; Piatelli, K.; Fraden, S., "Control and measurement of the phase behavior of aqueous solutions using microfluidics," *J. Am. Chem. Soc.,* vol. 28, pp. 8825-8835, 2007.

[5] Reiner, J. E.; Crawford, M.; Kishore, R. B.; Goldner, L. S.; Helmerson, K.; Gilson, M. K., "Optically trapped aqueous droplets for single molecule studies," *App. Phys. Lett. ,* vol. 89, pp. 013904-013906, 2006.

[6] Hunt, T. P.; Issadore, D.; Westervelt, R. M., "Integrated circuit/microfluidic chip to programmably trap and move cells and droplets with dielectrophoresis," *Lab. Chip.,* vol. 8, pp. 81-87, 2008.

[7] Jeong, J.; Lee, J.; Lee, C.; Teh, S.; Lee, A., "Particle manipulation in a microfluidic chnnel using acoustic trap," *Biomed. Microdevices,* vol. 13, pp. 779-788, 2011.

[8] V. Chakarov, "On the condensation of water on hexadecane," *Colloid & Polymer Sci.,* vol. 261, pp. 452-457, 1983.

[9] N. Tripathi, "Densities, viscosities, and refractive indices of mixtures of hexane with cyclohexane, decane, hexadecane, and squalane at 298.15K," *Int. J. Thermophys.,* vol. 26, pp. 693-703, 2005.

[10] Shestopalov, I.; Tice, J. D.; Ismagilov, R. F., "Multi-step synthesis of nanoparticles performed on milisecond time scale in a microfluidic droplet-based system," *Lab. Chip.,* vol. 4, pp. 316-321, 2004.

[11] Iwai, K.; Tan, W. -H.; Ishihara, H.; Takeuchi, S., "A resettable dynamic microarray device," *Biomed. Microdevices,* vol. 13, pp. 1089-1094, 2011.

[12] Kantak, C.; Beyer, S.; Yobas, L.; Bansal, T.; Trau, D., "A 'microfluidic pinball' for on-chip generation of layer-by-layer polyelectrolyte microcapsules," *Lab. Chip.,* vol. 11, pp. 1030-1035, 2011.

[13] Sochol, R. D.; Ruelos, R.; Chang, V.; Dueck, M. E.; Lee, L. P.; Lin, L., "Continuous flow layer-by-layer microbead functionalization via a micropost array railing system," in *Proc. of Transducers*, Beijing, 2011.

[14] Sochol, R. D.; Li, S.; Lee, L. P.; Lin, L., "Continuous flow multi-stage microfluidic reactors via hydrodynamic microparticle railing," *Lab. Chip.,* vol. 12, pp. 5051-5056, 2012.

[15] Matosevic, S.; Paegel, B., "Stepwise synthesis of giant unilamellar vesicles on a microfluidic assembly line," *J. Am. Chem. Soc.,* vol. 133, pp. 2798-2800, 2011.

[16] Iwai, K.; Sochol, R. D.; Lin, L., "A continuous flow microdroplet 'lysis' system," in *Proc. MicroTAS*, Okinawa, 2012.

[17] Iwai, K.; Sochol, R. D.; Lin, L., "A bead-in-droplet solution exchange system via continuous flow microfluidic railing," in *Proc. IEEE MEMS*, Taipei, 2013.

[18] D. J. Shaw, Colloid & Surface Chemistry, Burlington: Elsevier Science Ltd., 1992.

[19] Peltonen, L.; Hirvonen, J.; Yliruusi, J., "The behavior of sorbitan surfactants at the water-oil interface: straight-chained hydrocarbons from pentane to dodecaneas an oil phase," *J. Colloid and Interface Sci.,* vol. 240, pp. 272-276, 2001.

[20] Duffy, D. C.; McDonald, J. C.; Schueller, O. J. A.; Whitesides, G. M., "Rapid prototyping of microfluidic systems in poly (dimethylsiloxane)," *Anal. Chem.,* vol. 70, pp. 4974-4984, 1998.

[21] Karaağaç, Ö.; Koçkar, H.; Beyaz, S.; Tanrısever, T., "A simple way to synthesize superparamagnetic iron oxide nanoparticles in air atmosphere: iron ion concentration effect," *IEEE Trans. Magnetics,* vol. 46, pp. 3978-3983, 2010.

Chapter 5

PRINTING OF NANOPARTICLES

Nanoparticles have unique properties that can be used in applications such as chemical sensors or biodetection. Microreactor technology currently focuses on synthesizing nanoparticles in a very controlled environment such that they are monodisperse and at the desired size. This controlled synthesis provides the advantage of synthesizing desired nanoparticles for a specific application with a uniform size distribution which increases the sensitivity, therefore the sensor quality. In order to produce these sensors that are composed of nanoparticles, techniques for printing and patterning of nanoparticles on substrates were developed. This chapter describes a study on printing nanoparticles synthesized in the polyurethane microreactor (described in Chapter 2) by using the patterning technique developed by Dr. Michael Demko. The work described here is a collaborative work and the details of the printing technology are explained in the PhD dissertation of Dr. Demko [1]. In this chapter the basic principles of this technique are reviewed and the experimental results are discussed.

5.1. Basic Principles

There are several methods developed for the patterning and printing of nanoparticles on substrates. The traditional methods are the ones that require photolithography whereas the alternative methods are ink-jet printing and template based printing techniques [1]. The technique used in this work was an open template based printing where a physical boundary is provided such that the nanoparticle 'ink' is confined in the desired areas. It is a simple and material independent method that does not require chemical modification of the surface. The schematic of the steps of the patterning process is shown in Figure 5.1. In this method, first a micropatterned polymer mold is fabricated out of polydimethly siloxane (PDMS), which is a vapor-permeable material. This mold is used to create *in situ* micropatterned cellulose acetate polymer template which will be used for printing the nanoparticles. A clean solvent (acetone) is coated on a silicon substrate and the PDMS mold is pressed on the substrate. The cellulose acetate polymer dissolved in acetone is dispensed around the edges of the mold. As the acetone naturally evaporates through the vapor

permeable mold; the cellulose acetate in acetone replaces the clean solvent. Eventually all acetone evaporates and only dried polymer template with patterns is left under the mold. The mold is removed and the surface of the template is treated with oxygen plasma to increase its hydrophilicity for uniform wetting of the nanoparticle ink. After the oxygen plasma treatment a droplet of nanoparticles that were synthesized in the polyurethane microreactor (Chapter 2) is placed on the template and left for evaporation at room temperature. Nanoparticles fill in the patterned structures by the induced corner flow and electrostatic attraction between nanoparticles and the substrate [2]. After the solvent is evaporated completely, an adhesive tape is used to mechanically lift off the cellulose acetate polymer template. No residual particles were observed between the patterned features.

This method is a very simple and versatile way to pattern discrete features composed of nanoparticles. It is independent of the substrate and nanoparticle ink chemistry and it can be used for patterning a wide variety of materials. By using more than one template, it would be possible to print multiple different materials on the same substrate as well; however a study on this was not performed.

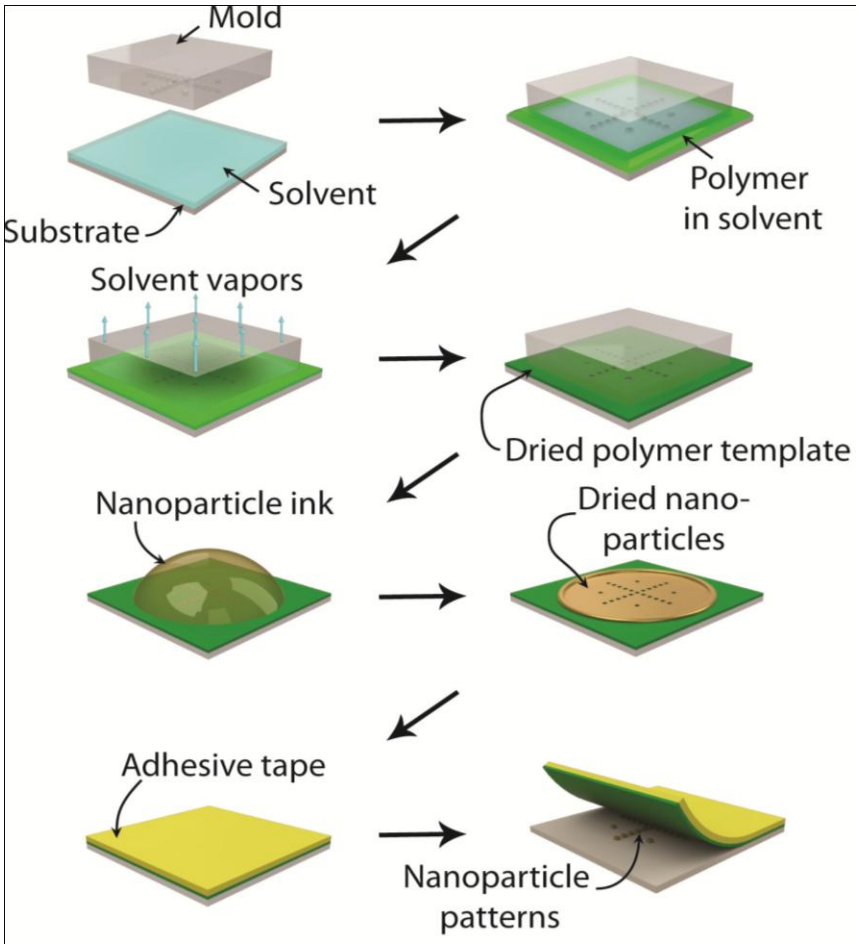

Figure 5.1: Schematic of the nanoparticle printing process [1].

5.2. Results and Discussion

Iron oxide nanoparticles that were synthesized in the polyurethane microreactor (Chapter 2) were patterned by using the cellulose acetate polymer template. The SEM images of the template before and after the printing are shown in Figure 5.2. The empty template has 20μm × 20 μm square features. The iron oxide nanoparticle ink had low concentration (lower than 0.01%) and the nanoparticles had a tendency to agglomerate as was seen from the TEM images in Chapter 2. Therefore in order to achieve uniform nanoparticle coverage of features, the ink deposition and solvent evaporation was repeated multiple times. Also to reduce the agglomeration, the substrate was kept in an ultrasonic bath during the deposition and evaporation steps of the nanoparticle ink. However due to the low concentration, the thickness of nanoparticle features were non uniform and defects such as cracks were observed as shown in Figure 5.3. Defects and non uniform thickness are due to the agglomeration of nanoparticles. This can be improved by modifying the ink such that the particles are not agglomerated and the concentration is high enough to fill the structures uniformly.

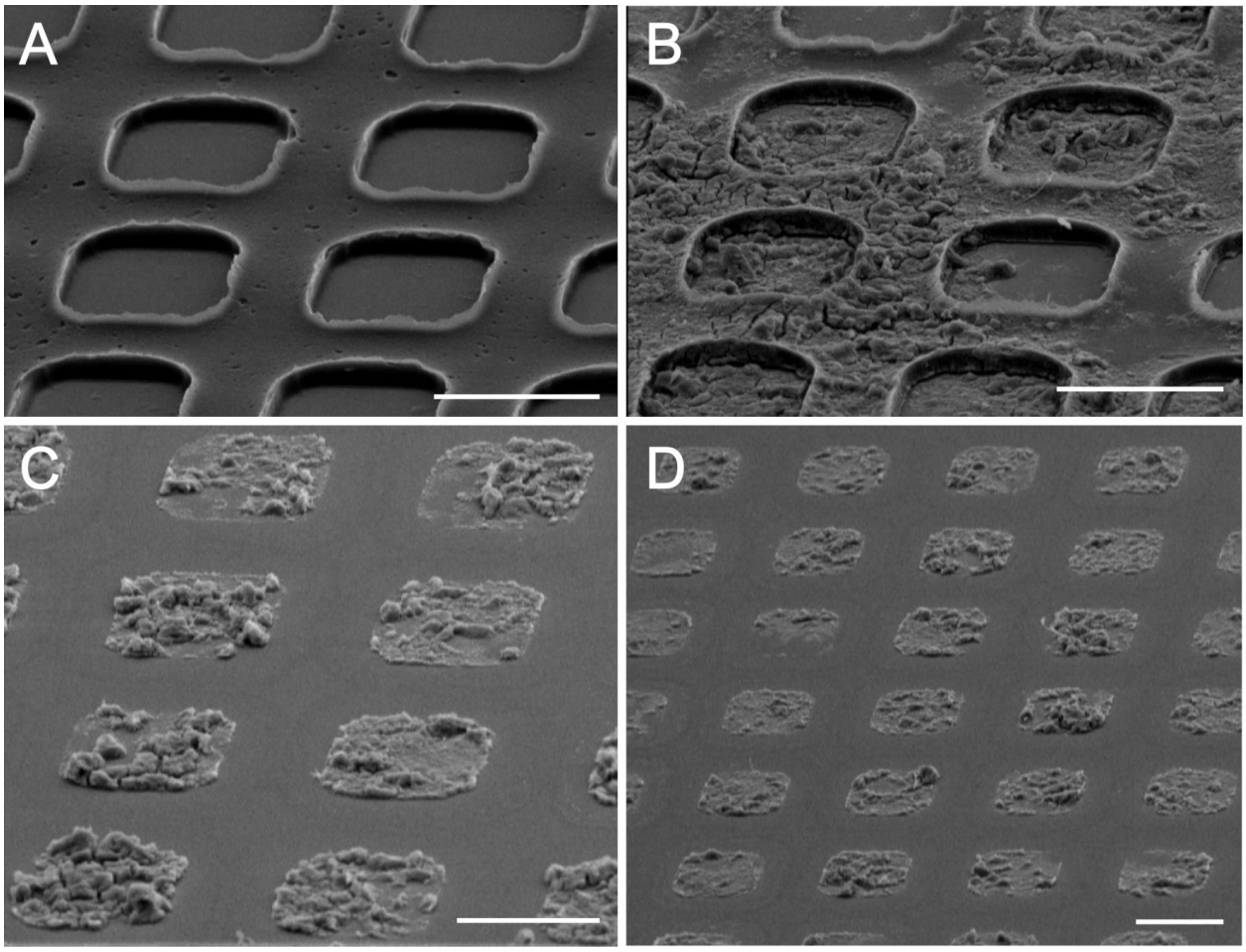

Figure 5.2: SEM images of A) empty template, B) template after nanoparticle deposition, C-D) printed nanoparticles after template is removed with the adhesive tape. All scale bars are 20 μm.

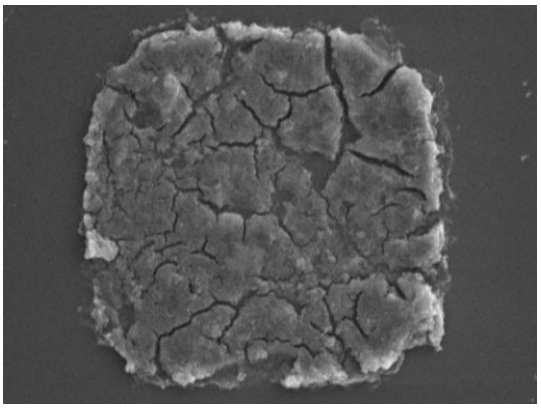

Figure 5.3: SEM image of printed nanoparticles after template removal. The size of the printed feature is 20μm × 20 μm.

5.3. Conclusion

In this chapter, printing of nanoparticles synthesized in the microreactor by using the technique developed in [1] is demonstrated. The printing process was successful; isolated structures composed of nanoparticles did not have any residual layers between them. However printed structures had cracks and uneven thicknesses. This could be due to the low concentration and agglomeration of nanoparticles. The process could be improved by increasing the concentration of particles as well as reducing their agglomeration by using ligands during the reaction.

The quality of printing is also dependent on the attachment of nanoparticles to the substrate. In this method, particles were attached to the surface physically and there was not any chemical modification on the surface. This decreases the strength of printing as some particles can be removed when encountered with another surface or when washed with other solvents. Even though a formal adhesion testing was not performed; adhesion was good enough as particles stayed on the surface during the template removal step. Additional modifications on the surface or chemistry can be made to increase the adhesion of particles. For the purpose of this thesis, only the proof of concept study of printing nanoparticles synthesized in the microreactor was performed. However improvement of the adhesion quality would be a great future work study. Especially it would be interesting and very useful to be able to print nanoparticles such that these surfaces can survive high temperatures or wet environments.

5.4. References of Chapter 5

[1] M. T. Demko, "High resolution additive patterning of nanoparticles and polymers enabled by vapor permeable polymer templates," University of California, Berkeley, 2012.

[2] Demko, M. T.; Choi, S.; Zohdi, T. I., Pisano, A. P., "High resolution patterning of nanoparticles by evaporative self-assembly enabled by in situ creation and mechanical

lift-off of a polymer template," *App. Phys. Lett.,* vol. 99, pp. 253102-253104, 2011.

Chapter 6

CONCLUSION AND SUGGESTED FUTURE WORK

There are several advantages of using microfluidic devices for the synthesis of nanoparticles. Some of these advantages are the possibility of maintaining controlled reaction environments, uniform reaction conditions and applying rapid changes on demand. These properties lead to the uniform synthesis of nanoparticles eventually improving their size distribution compared to conventional batch wise methods.

In this thesis two different microreactor designs were discussed and the results of nanoparticle synthesis were presented. The first microreactor presented was a droplet-based system made out of a polymer material and was designed for room temperature reactions that required fast mixing times. In literature, there are several polymer based microreactors for this purpose however they have low chemical resistance to solvents used in nanoparticle synthesis. In this microreactor, polyurethane was used as the building material of the reactor which has higher chemical resistance to many solvents. Also an alternative method of fabrication by using a CO_2-laser on polyurethane substrate was demonstrated. This fabrication technique decreased the time spent and made it easier to try different designs rapidly. Iron oxide nanoparticles were synthesized by mixing two reagents inside a droplet in the microreactor. The resulting nanoparticles had a standard deviation of size of 10%. This result was better than the result obtained by batch techniques. Nanoparticles were magnetic and crystal planes were observed. This reactor can also be used for synthesizing other types of nanoparticles with similar synthesis methods. One limitation of this reactor was in achieving longer residence times of nanoparticles inside the channel. Due to leaking at high pressures, longer microfluidic channels were not possible to be made. For this purpose, the bonding mechanism can be improved as a future work. However for the purpose of iron oxide synthesis the residence times obtained in this reactor were sufficient.

The second microreactor presented in this thesis was a droplet-based, silicon substrate reactor and it was designed for reactions that required heating. This microreactor had thermally isolated heated zones that had different channel lengths. This property of having

different zones makes it possible to separate nucleation and growth processes of particles; which is a requirement for achieving monodisperse sizes. The smaller zones were designed for nucleation and the longer zone was designed for growth. Using this microreactor, TiO_2 nanoparticle synthesis was demonstrated. This study exemplifies the utility of the microfluidic device for studying the evolution of nanoparticles. In addition, the device shows significant promise for generating uniform sized nanoparticles. It was shown that the temperature of nucleation and growth steps plays a key factor in the formation of nanoparticles. The nanoparticles synthesized in this reactor had a standard deviation of size less than 10% which was better than that achieved in previous methods. There is still a lot of future work that could be done by utilizing this microreactor. Studying the synthesis of various other nanoparticles including quantum dots would be interesting. A detailed study on the effect of various temperatures and concentrations can be also performed to understand the kinetics of the reactions. In addition to, ligand or extra reagent addition during the synthesis would be interesting to try. Ligand addition could reduce the agglomeration of particles. Also this microreactor can be modified to have an extra unit where nanoparticle surfaces can be functionalized after being synthesized. By this way, final product without any further processing would be obtained.

In both of the microreactors, nanoparticles were synthesized inside droplets for the purpose of maintaining uniform reaction conditions and avoiding contact with channel walls. Therefore samples collected at the outlet of the reactors had both the carrier fluid (oil) and the droplets (aqueous) with nanoparticles. In order to collect nanoparticles, the oil had to be removed; therefore centrifuging was performed to achieve that. Centrifuging is an effective way of demulsifying droplets and separating different phases; however it takes a lot of time and effort. Also the result was not always successful, in TEM imaging sometimes it was observed that there were some coating on nanoparticles due to poor centrifuging and the process had to be repeated. In order to address these issues, two microfluidic techniques of retrieving nanoparticles were discussed in this thesis. The first method was based on trapping the aqueous droplet phase inside the microchannel and the second method was utilizing a micropost array to direct droplets from the oil solution to the pure water. Only the trapping mechanism was demonstrated in the first technique but collection was not tested. The second method was shown to work very well to collect nanoparticles in the water and remove oil phase.

As a final work, the printing of nanoparticles synthesized inside the polyurethane substrate microreactor was demonstrated by using the method developed by Dr. Michael Demko. Printing was successful however there were cracks and non uniform thicknesses on the printed features. This could be due to the low concentration of nanoparticles inside the solution used in printing and it requires improvement of the nanoparticle ink being used. This printing mechanism can be used to sensors with sensitivities by using the nanoparticles synthesized uniformly and on demand inside the microreactors.

In conclusion, two different types of microreactors were discussed in this thesis. In addition to these microreactors, microfluidic methods for retrieving nanoparticles from the reactors were demonstrated. In the final part, as an application, the printing of nanoparticles synthesized inside the microreactor is shown. As a future work, it would be

interesting to use these microreactors to functionalize their surface as well as to create core shell nanoparticles. Synthesis of different chemistries would also be interesting to study.

As a future work, various other types of nanoparticle synthesis can be performed in the silicon microreactor. More specifically it would be interesting to look at reactions that require higher temperatures such as quantum dots or other metal nanoparticles such as gold and silver. It would also be interesting to look at the use of ligands in the synthesis to prevent the nanoparticle agglomeration. The third inlet can be used to deliver these ligands to the system. In this work the silicon microreactor was used as a 'closed' environment, where additional reagents were not added during the synthesis. Therefore, in some cases it was observed that increasing the growth time did not make changes in the particle size as there were no reagents left. As a future work, the microreactor can be used as an 'open' system, where extra reagents were delivered right before the growth region. In addition, this microreactor can be integrated with the droplet lysis system discussed in Chapter 4 in order to obtain a fully integrated nanoparticle generation and collection system.

Finally for the nanoparticles synthesized in microreactors to be used in printing of sensors, the nanoparticle ink obtained from the reactor should be improved in terms of the appropriate concentration and solvent to obtain uniform thickness of printed features. The quality of printing is also dependent on the attachment of nanoparticles to the substrate in addition to the ink. Additional modifications on the surface or chemistry can be made to increase the adhesion of particles. For the purpose of this thesis, only the proof of concept study of printing nanoparticles synthesized in the microreactor was performed. However improvement of the adhesion quality would be a great future work study. Especially it would be interesting and very useful to be able to print nanoparticles such that these surfaces can survive high temperatures or wet environments.